Meteorological Analysis of the 22 June 2007 F5 Tornado in Elie, Manitoba

by

Justin J. Hobson

A thesis submitted to the Faculty of Graduate Studies of
the University of Manitoba
in partial fulfilment of the requirements for the degree of

MASTER OF SCIENCE

Department of Environment and Geography

University of Manitoba

Winnipeg

Abstract

During the early evening of 22 June 2007, a violent tornado impacted the western edge of Elie, Manitoba. This was Canada's first documented F5 tornado. Three primary research questions were posed: (1) What were the pre-storm environmental conditions on 22 June 2007? (2) How did the storm and associated tornado evolve? (3) How does this event compare to other major tornadic events in Canada and the U.S.? The tornado passed in close proximity to a fixed-location Environment Canada Doppler radar at Woodlands, Manitoba. This allowed for a detailed examination of local mesoscale boundaries that were present prior to and during the event. The Elie tornado was rare in the fact that it looped three times within the main track and it moved approximately 5 km during its 40 minute lifetime causing F5 damage to homes and structures when it was an estimated 50 m wide.

Remarks & Acknowledgements

I want to thank John Hanesiak, my advisor, for providing me with help and feedback. I also want to thank Ron Stewart (Head, Environment and Geography Department) and Neil Taylor (Environment Canada) for being a part of my graduate committee; Neil also assisted in the radar analysis of the event. Special thanks also goes out to Dave Patrick for providing me with the radar imagery and a thank you goes out to Environment Canada for providing me the time to work on my thesis. Finally, I want to thank Dave Carlsen and Heather Rombough for assisting in quick edits and grammatical corrections.

Dedication

This thesis is dedicated to everyone who gave me moral support and by teaching me that the large undertaking of a master's degree can be accomplished one step at a time. I want to thank my parents Margaret and Bob, and my girlfriend Tristin Arcouette who kept my spirits high even though I thought at times that I could no longer continue.

Table of Contents

List of Figures

List of Tables

CHAPTER 1 - INTRODUCTION

1.1 - Background and Theory

Tornadoes occur in Canada during the warm season with 50-80 tornadoes reported to Environment Canada's weather offices annually (McCarthy et al., 2008). More tornadoes likely occur, touching down in areas not covered by the radar network, where there is sparse population, or where they are difficult to see visually (e.g., heavily treed areas or in areas of steeper terrain). Environment Canada relies on public reports of tornadoes to maintain an accurate record of these events. Major tornadoes are reported to a greater degree around towns/cities and highways due to the fact that more people are located within these areas and the reporting of severe weather in general is related to infrastructure (King, 1997). Tornado spotting and reporting practices have changed over the past decades due to education, population increases, and popular media that has created more awareness. The first chapter will focus on the convective initiation processes of severe thunderstorms and tornadogenesis followed by the introduction to the objective of the thesis.

1.1.1 - Convection Initiation Processes

Features on the synoptic scale are routinely examined by meteorologists. This scale involves atmospheric systems that affect a large area over a period of time from 200 km or more (Stull, 2000). Severe thunderstorms and tornadoes are common in most areas of the planet and occur on the mesoscale. The term "mesoscale" applies to systems that affect a small region (2 – 200 km) over a short amount of time (minutes to hours). Mesoscale and synoptic features are analyzed to determine how conducive the environment is for storms to develop in. For severe thunderstorms to occur, four main ingredients are required:

1. **Instability**
2. **Low-level moisture**
3. **Vertical wind shear**
4. **A method to trigger convection**

Convective available potential energy (CAPE) is a parameter used to quantify the instability required for thunderstorms to develop. CAPE is the integrated buoyant energy that exists where the parcel of air (when lifted from the surface or some other height) remains warmer than the environment. The area between the lifted air temperature and the environmental temperature is representative of the available energy available to be converted to kinetic energy within the updraft if it develops (Figure 1.1).

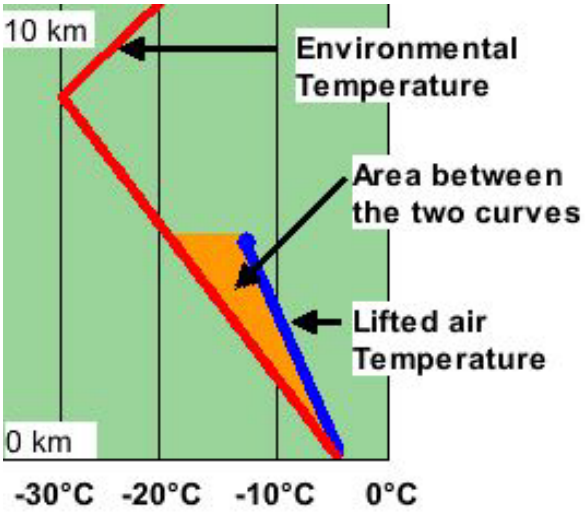

Figure 1.1: Diagram showing how CAPE is determined based on an environmental sounding. Area between the environmental temperature curve (Red) and the lifted air temperature curve (Blue) is the available energy that a storm could use (University of Illinois Meteorology, 2010).

Updrafts in thunderstorms are determined by the amount of energy (or CAPE) being released; although for supercells (mentioned later) pressure gradients associated with atmospheric perturbations can also affect the updraft strength. Updraft speeds can be estimated (Equation 1) once CAPE has been assessed (Stull, 2000). It is assumed that frictional drag, water loading and entrainment are neglected when using this equation to calculate **ω** (updraft speed in m s^{-1}).

$$\omega = [2*CAPE]^{\frac{1}{2}} \quad (1)$$

Instability

Forecasters look at two aspects of CAPE when diagnosing severe thunderstorm potential. The size and distribution of CAPE is important because the same CAPE values could originate from an environment characterized by either having a large temperature difference over a shallow layer or it could come from a small temperature difference over a deeper layer (Figure 1.2). The shallow layer CAPE in sounding A shows that the difference in temperature between the environment and the rising air is greater than what

is found in sounding B. This rising air in sounding A is therefore more buoyant than the surrounding environment and this indicates that stronger updrafts and more severe storms are possible for sounding A than for sounding B. Areas of convective inhibition (CIN) can also exist on the environmental sounding (Figure 1.2). These areas indicate the amount of energy that prevents an air parcel from rising. An area of high CIN is considered stable and prevents updraft development.

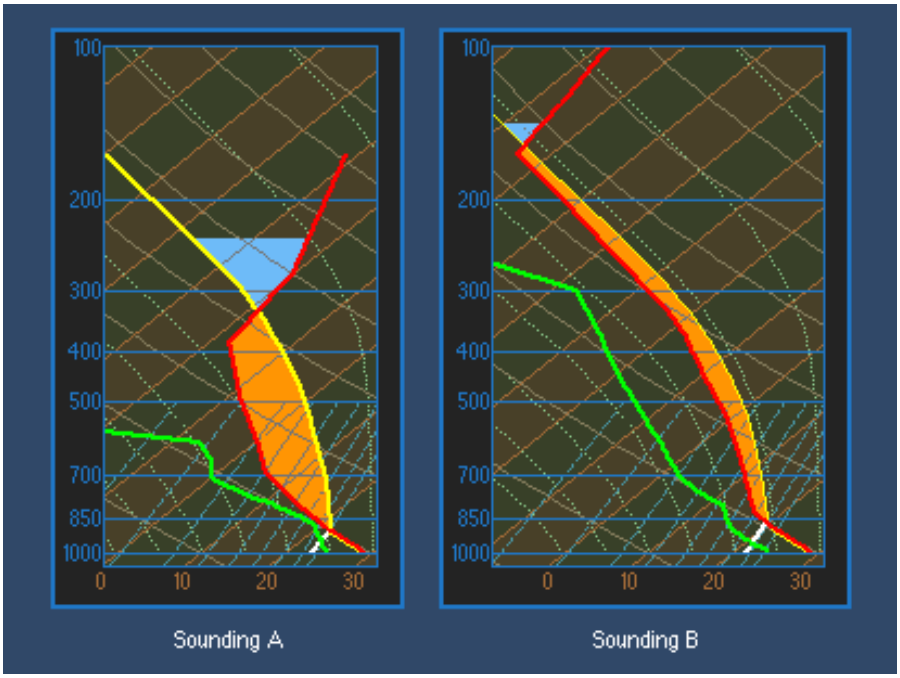

Figure 1.2: Soundings indicating shallow layer CAPE (sounding A) vs. deep layer CAPE (sounding B) with orange area showing the distribution of CAPE and the blue area showing the distribution of CIN (COMET).

CAPE values of 1000 J kg^{-1} indicate weak instability, CAPE values between 1000-2500 J kg^{-1} indicate moderate instability, and CAPE values exceeding 2500 J kg^{-1} indicates strong instability (Vasquez, 2002). The values of CAPE deemed as moderate or strong are location specific but are the most common range of values that a forecaster would see in the US Plains when assessing the potential for severe weather among other parameters. Severe thunderstorms can occur with lower values of CAPE in other areas,

such as Alberta for example, where freezing levels are lower and drier air is more prevalent meaning that larger values of CAPE are not required for severe thunderstorms to develop.

Low-level moisture

Moisture availability can be determined by the dewpoint temperatures in the lower levels of the atmosphere. Dewpoint refers to the temperature the air must be cooled to for the air to become saturated while moisture content and pressure are constant. When this point is reached, water droplets will begin to condense in the air, forming clouds and precipitation. Larger values of dewpoint temperatures can result in larger values of CAPE. Local evapotranspiration is a source of boundary layer water vapour (up to 30% of the daily amount; Raddatz, 2005) and leads to increased dew point temperatures. Evapotranspiration is the combination of two processes where water is lost from the surface by evaporation and a plant by transpiration. Sources of evapotranspiration can be from vegetation that is present over the prairies such as forests, and crops. Evapotranspiration can also be advected in from other upstream areas.

Vertical wind shear

An important factor in controlling the mode of severe thunderstorms is the deep-layer (0-6 km) wind shear, that is, the vertical change in wind speed and horizontal wind direction (Potter and Colman, 2003). During the initial growth of a convective cloud or convective cell, if the wind shear is too strong such that the updraft can not be maintained due to turbulence and mixing, then the convective cell will not persist or be maintained, and the cloud dissipates (Markowski and Richardson, 2010). On the other hand, if there is no wind shear or very little wind shear, the updraft will persist into a mature

thunderstorm (provided there is sufficient buoyant energy) that may lead to precipitation and associated downdrafts being generated within the cloud. The precipitation loading and downdraft energy will eventually overcome the updraft energy, essentially suffocating the cloud from further moisture and buoyant energy, and thereby inhibiting further cloud growth. Hence, there has to be somewhat of a balance between wind shear and buoyant energy for the convective cloud or thunderstorm to persist (Markowski and Richardson, 2010). As wind shear increases in the vertical, the convective cloud gets tilted so the updraft and downdraft are separated, increasing the lifetime of a storm and its potential severity (Markowski and Richardson, 2010). The tilting and stretching of horizontal vorticity associated with the vertical shear can lead to the development of supercells (explained in 1.1.2) (Holton, 2004).

Method to trigger convection

The first three ingredients are important; however sufficient lift is needed for convective initiation (CI) to occur. CI is sensitive to the amount of deep moisture, the amount of instability, and the strength of convergence; which together cause the low-level rising of air. Boundary layer convergence zones are precursors to convective development and can act to locally deepen the moist layer and created conditions favourable for deep convection (Weckwerth and Parsons, 2005). Fronts, horizontal convective rolls within the boundary layer, outflow boundaries from previous thunderstorms, or lake breeze convergence regions allow air to rise at the low-levels (Potter and Colman, 2003). Using Doppler radar (explained later), fine lines of enhanced reflectivity can be seen using reflectivity imagery, and are indicative of boundary layer convergence zones. Radar data is therefore important in detecting boundaries and

identifying likely regions for CI (Weckwerth and Parsons, 2005). It will be discussed later what critical lift mechanisms took place for the Elie, Manitoba storm.

Horizontal convective rolls (HCRs) are defined as counter-rotating horizontal vortices within the planetary boundary layer that originate from a combination of shearing instability and daytime heating (Yang and Geerts, 2005). HCRs are typically aligned with the vertical shear vector and between the rolls upward or downward motion is present. The conditions required for HCR development and maintenance involve a surface layer heat flux, minimal low-level vertical wind shear, and uniform surface characteristics. They are a common form of boundary layer convection and often intersect larger synoptic-scale boundaries (Weckwerth and Parsons, 2005). Areas in which HCRs intersect large-scale boundaries are preferred locations for lift and the air that is forced upward can enhance updrafts and promote cloud development. HCRs can be seen on Doppler radar scans at the lower elevations in close proximity to the radar (see Chapter 3 for examples).

Lakes are powerful generators of boundaries which have been shown to be linked with convection in many areas (King et al., 2003). Lake breezes result from a thermally direct circulation that blows from the surface of a body of water to the shore. Lake breeze boundaries create local areas of convergence and may play two roles by locally increasing both moisture convergence and low-level shear (Weckwerth and Parsons, 2005). Lake breeze fronts can also intersect HCRs to enhance updrafts and develop clouds due to increased lifting at the intersection regions (Weckwerth and Parsons, 2005). Lake breeze boundaries have been further linked to tornadogenesis in addition to convection alone (King et al., 2003). When winds are oriented onshore, there is an

absence of tornado occurrences, while the concentrations of tornado occurrences are found along the apparent convergence lines. This implies that tornadoes do not occur in regions with lake modified air but may be enhanced at the lake-breeze boundaries (King et al., 2003).

Gravity waves exist due to a stable layer of the atmosphere under gravity. Perturbations to the balanced state can result in the excitation of atmospheric gravity waves with a range of spatial and temporal scales (Wang and Geller, 2003). Gravity wave characteristics include wavelengths that can range from a few to thousands of kilometres, occurrence at all altitudes in the atmosphere, and importance because they can trigger convection (Wang and Geller, 2003). Balaji and Clark (1988) also suggest that the interactions of gravity waves propagating along the stable layer at the top of the boundary layer with HCRs can initiate deep convection. Displaced air is forced to rise within a stable layer and eventually sink back to a lower level with time due to the restoring force of gravity. One example of how they develop is air flow over terrain creating waves that crest higher than the terrain the wave originated from. The crest of the waves can eventually saturate to produce clouds and precipitation. Gravity waves, if occurring, can be assessed on a tephigram (see Chapter 3) in terms of their frequency of oscillation and wavelength based on calculating the Brunt-Vaisala frequency. This is the frequency at which an air parcel will oscillate when displaced from its equilibrium height in a statically stable environment (Stull, 2000). The formulas for calculating the oscillation frequency and wavelength follow:

$$\textbf{Frequency of Oscillation: } N_{BV} = \sqrt{(|g|/T_v * \Delta\Theta_v/\Delta z)} \quad (2)$$

$$\textbf{Period of Oscillation: } P_{BV} = 2\Pi/ N_{BV} \quad (3)$$

$$\textbf{Wavelength: } \lambda = 2\,\Pi * M / N_{BV} \quad (4)$$

g = gravity = 9.8 m s $^{-1}$, z = height of inversion (meters), M = wind speed (m s $^{-1}$), temperatures are in Kelvin, T_v (virtual temperature) = T (air temperature) and Θ_v (virtual potential temperature) = Θ (potential temperature) {assuming dry air}

Moisture convergence can occur in areas where moisture cannot advance further horizontally and is forced to move vertically. The moisture is forced to pool if it is blocked by terrain or another feature such as a front or boundary. Near the surface, the air is warmed and moistened by the surface fluxes generated from sunshine and evapotranspiration. It then rises to the top of the boundary layer where it can mix with the air from the capping stable layer that is usually drier. The air then sinks back toward the surface inducing a circulation. This causes the boundary layer to expand in depth as mixing continues with time (Fabry, 2005) and a capping inversion that is present may be slowly eroded away allowing for convection to occur. Areas of moisture convergence are important and can act as lifting mechanisms and eventually promote thunderstorm development (Fabry, 2005). Raddatz and Cummine (2003) and Kellenbenz and Grafenauer (2007) have shown linkages between evapotranspiration and tornadoes. Local evapotranspiration aids in enriching the boundary layer with moisture which can lead to sufficient increases in CAPE and lower cloud bases making it easier for tornadoes to reach the surface.

1.1.2 - Supercell Thunderstorms

Thunderstorms (or Cumulonimbi) are deep convective clouds. There are three types of thunderstorm: single cell, multicell, and supercell (Dunlop, 2002). Strong tornadoes are usually associated with supercells. This thesis will focus on supercell thunderstorms as that is the type of storm that spawned the tornado in Elie, Manitoba on 22 June 2007.

Supercells occur in environments with strong deep-layer vertical wind shear (introduced in the previous section). Supercells can produce the most violent types of severe weather such as intense lightning, large hail, damaging winds (not associated with a tornado), and tornadoes (Dunlop, 2002). Horizontal wind in the boundary layer creates vertical wind shear which creates horizontal vorticity. This vorticity is responsible for creating mid-level rotation in a supercell when it gets tilted into the vertical by the updraft (Stull, 2000). Vertical wind shear allows supercells to develop rotation and be long-lived due to the updraft and downdraft being separated, and unlike single-cell thunderstorms, to persist for hours (1-4 hours are common, and some have been observed to persist as long as 8 hours) (Markowski and Richardson, 2010). Dynamically induced vertical pressure gradients arising from the interaction of the updraft with the vertical wind shear can also strengthen the updraft (Markowski and Richardson, 2010). The rotating updraft of a supercell along with its associated downdraft is referred to as a mesocyclone (Figure 1.3). A mesocyclone is a region of rotation that is 10-15 km in diameter (Stull, 2000) and is located on the rear flank of a supercell thunderstorm.

The lowest region of a mature mesocyclone is where a wall cloud is observed (Figure 1.3). A wall cloud is a lowering that extends below the base of the mesocyclone.

The sighting of a wall cloud precedes the development of a tornado. A rotating wall cloud develops in the rain-free updraft area towards the rear of the thunderstorm. It occurs in the region of the strongest updraft where cool, moist air is entrained from the nearby downdraft (Bureau of Meteorology, 2011). This cool, moist air condenses at a lower height then does the air feeding into the rest of the storm (Bureau of Meteorology, 2011). Funnel clouds and tornadoes form when a narrow, rapidly rotating vortex emerges from the base of a wall cloud. Once a funnel cloud touches the surface, or if debris is noted at the surface, it becomes a tornado. A tornado is not always visible, but usually the intense low pressure and rapid rotation enables the water vapour in the air to condense into a condensation funnel that can be seen (Church et al., 1993).

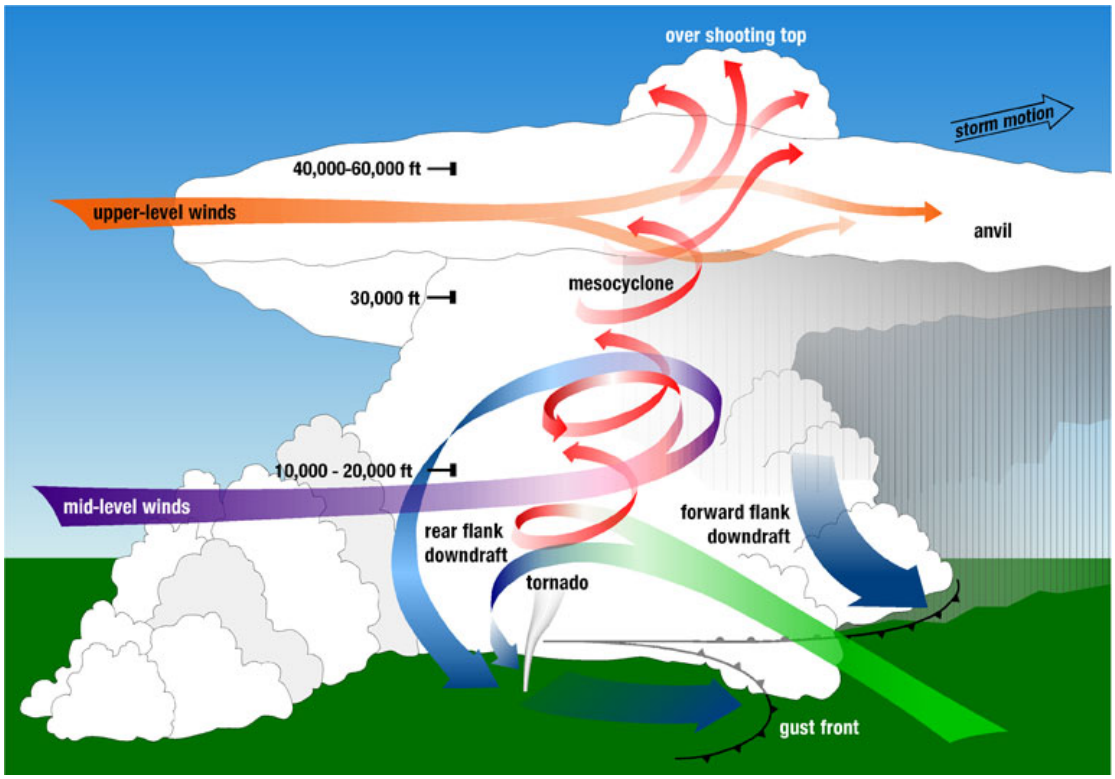

Figure 1.3: Diagram of a supercell showing updraft (red) and downdraft (blue) along with other important features: mid-level winds (purple), upper level winds (orange), low-level winds (green), rear flank downdraft, forward flank downdraft, wall cloud location with tornado, the heavy precipitation core, the overshooting top, and the flanking line (NOAA).

Great attention is given to supercell thunderstorms by operational meteorologists due to the severe weather they produce (see Chapter 2 for tornado forecasting techniques). Heavy rain and hail show large dBZ values on a radar reflectivity image and appear as a hook echo around the lighter precipitation. The hook echo is associated with the region of subsiding air wrapping around the lighter precipitation in the region of rising air (Figure 1.4) (Markowski, 2001). The rear-flank downdraft (RFD) of a supercell is associated with the hook echo, and is suspected to play a key role in tornadogenesis (Fujita, 1975). The RFD is a region of subsiding air that develops on the rear side of the main updraft of supercell thunderstorms (Markowski, 2001). The precise origins of the RFD are unclear, however, it is thought that precipitation loading and evaporative cooling located in this area can further enhance the RFD.

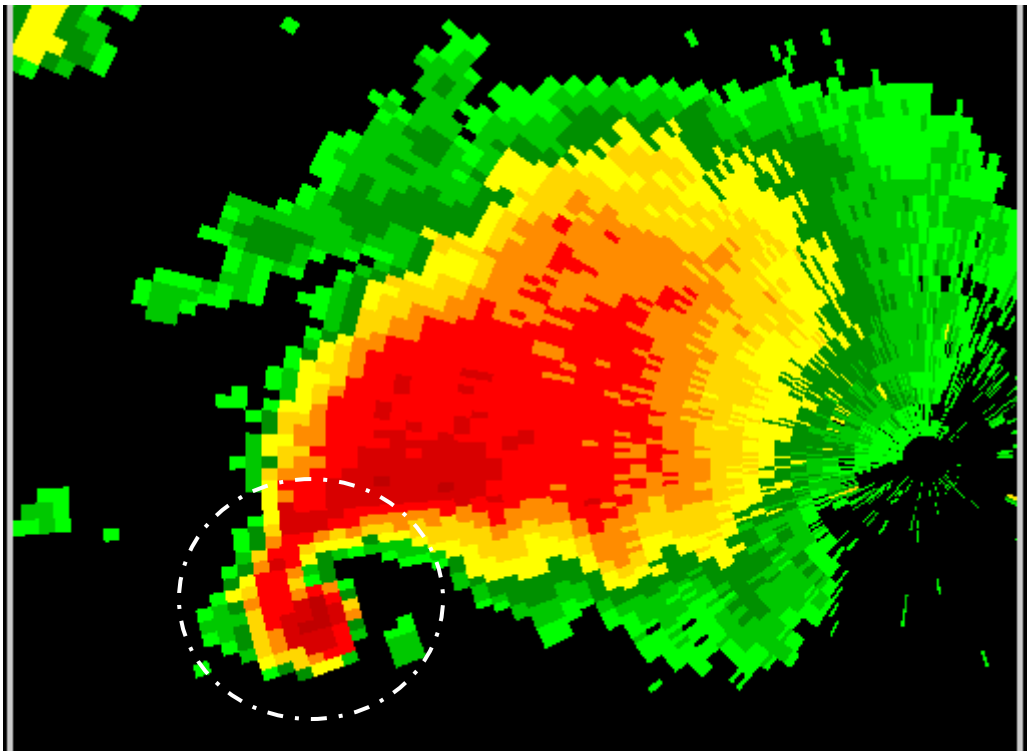

Figure 1.4: Hook echo (white circle) 0.5 degree radar reflectivity example from 3 May 1999 (NOAA).

A bounded weak-echo region (BWER) or vault is also identified by using Doppler radar. This region is where the inflow of warm moist air enters the supercell thunderstorm and goes up into the updraft core (Aguado, 2004). The air that enters the storm rises and the water vapour condenses to form a dense concentration of water droplets. The new droplets in the vault are too small to scatter enough microwave energy back to the radar indicating an area of little to no radar returns (Figure 1.5) (Aguado, 2004). The identification of a BWER using Doppler radar is indicative of a very strong updraft and can also aid in identifying where the hook appendage is found. Thunderstorms exhibiting these features can produce severe weather events (tornadoes, large hail, strong wind gusts) and have longer lifetimes (Potter and Colman, 2003).

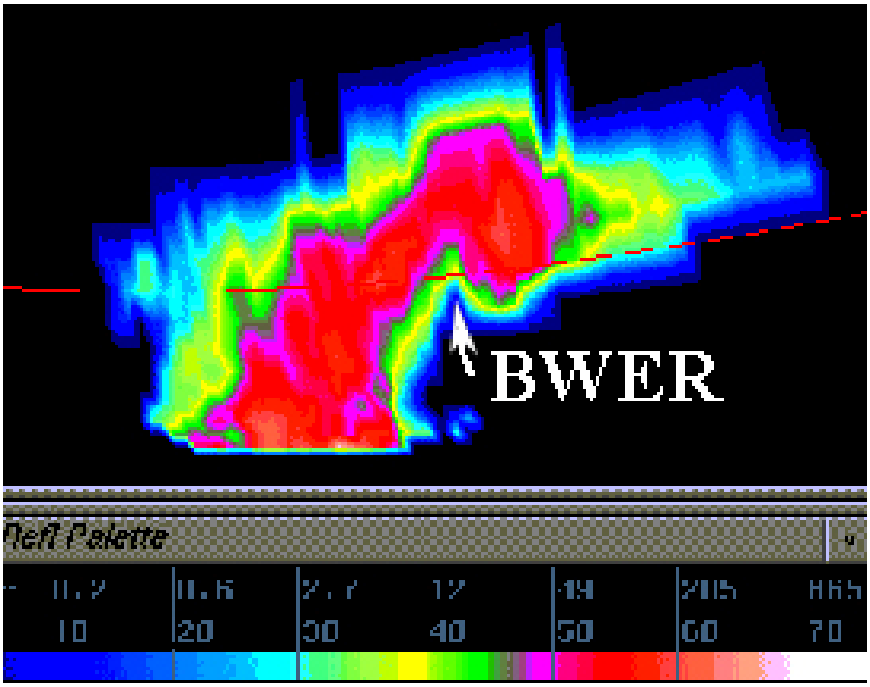

Figure 1.5: BWER location after storm cross-section image was generated within a supercell thunderstorm (METED UCAR).

There are three main types of supercell thunderstorms; Low-Precipitation (LP), Classic (CL), and high precipitation (HP) (Doswell, 1993). LP supercells produce little

precipitation and show clear visual signs of rotation. They occur most often near a surface dryline (boundary separating moist and dry air masses) and develop in relatively dry environments (Doswell and Burgess, 1993). An LP supercell may cause strong RFD winds due to the higher amounts of evaporative cooling that occurs as precipitation evaporates into the lower drier air. Large hail can sometimes occur along with weak to strong tornadoes.

The type of supercell that spawned the Elie tornado was a CL supercell. CL supercells exhibit most, if not all, of the traditional radar echo morphology such as a hook echo, BWERs, and heavy precipitation (Potter and Colman, 2003). A classic supercell can harbour varying degrees of hail size, tornado strength, and strength of straight line winds.

An HP supercell is noted as having a kidney bean shaped appearance on Doppler radar. This type of supercell is also referred to as a rain-wrapped supercell. Tornadoes are not as common in HP supercells as in classic supercells, because the downdrafts are stronger and continuously undercut the updraft with cold outflow that prevents the storm from producing a tornado (Markowski and Richardson, 2010). Tornadoes that do develop in this type of storm are considered to be more dangerous because the tornadoes are usually shrouded in rain (Potter and Colman, 2003). Updraft velocities in an HP supercell are generally lower than other supercell types because of the intense water loading in the thunderstorm. Strong winds associated with the RFD are not as common with an HP Supercell when compared to an LP Supercell because evaporative cooling is lower due to higher moisture content in the lower and middle troposphere.

1.1.3 - Identifying Supercell Environments

Tephigrams are thermodynamic diagrams that assess the behavior of a parcel of air in relation to the surrounding environmental temperature (e.g. Figure 1.6). An atmospheric sounding records pressure, temperature, moisture observations, and wind data (Markowski and Richardson, 2010). This atmospheric profile is obtained when a balloon is launched on the two main synoptic hours (1200 UTC and 0000 UTC). Sounding data is available twice a day at several locations across Canada. Over the prairies, there are only two regular sounding locations (Stony Plain, Alberta and The Pas, Manitoba) that are over 1000 km apart and, in most cases, not representative of the southern portion of the Prairies. There are intermediate sounding locations that can launch balloons at different times during the day. The Prairie and Arctic Storm Prediction Center (PASPC) in Winnipeg is one location that is able to perform balloon launches whenever it is necessary; typically at 1800 UTC. Other atmospheric profile data may be available from airplanes as they ascend and descend through different heights of the atmosphere. These extra data are usually available at major international airports and can help fill in the gaps of missing data between the fixed sounding sites.

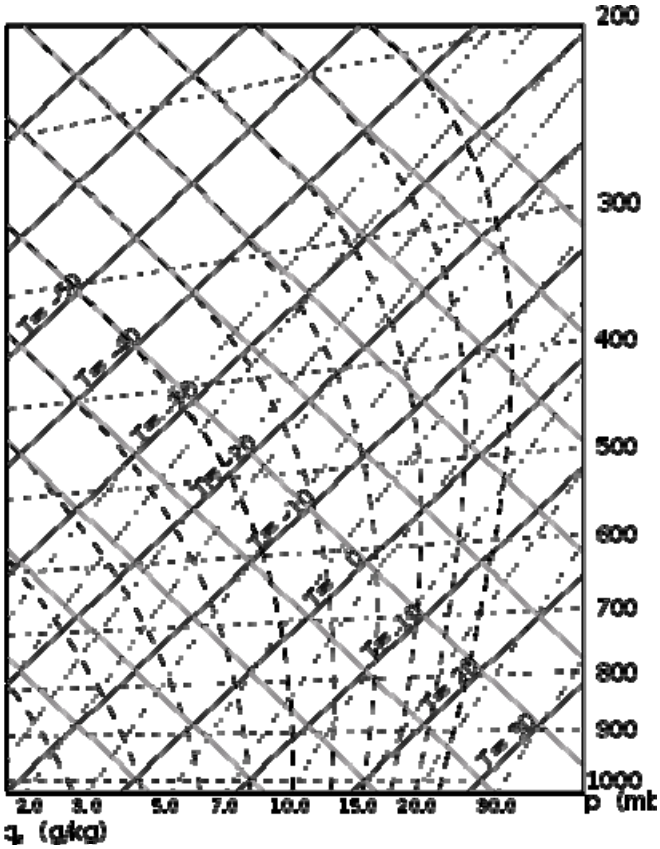

Figure 1.6: Example tephigram showing temperatures along the X-axis, pressure along the Y-Axis, along with mixing ratio and dry/saturated adiabatic curves.

Upon analyzing a tephigram it can be determined with greater confidence if severe thunderstorm development will occur. Instability, moisture, lapse rates, wind profiles, and capping inversions are some examples of what can be analyzed from a tephigram. The evolution of the boundary layer and the stability of the atmosphere can be monitored throughout the day.

For this thesis, assessing the potential for convective initiation was critical. One important feature that was monitored on 22 June 2007 was the capping inversion. A capping inversion is a thermal inversion that works to inhibit deep convection (Church et al., 1993). A capping inversion can be determined and monitored by assessing the sounding data on a tephigram and following the evolution of the temperature/moisture profile by launching balloons at different times throughout the day. The strength of the

cap is strongest earlier in the day and changes throughout the day as daytime heating works to erode the cap via ascent in the column. For example, a capping inversion can be eroded as cold air associated with a cold front approaches. This will steepen the temperature profile and enhance vertical motion enough to erode the cap. A capping inversion can also strengthen throughout the day, as sinking air and warming temperatures aloft can reinforce the cap. If a cap is present, how it evolves determines if surface-based convective initiation will occur on that particular day. Forecasting the strength of a capping inversion and when the capping inversion may be overcome is challenging. Small changes in the strength of the cap can, and usually do, go unnoticed due to the lack of real-time upper-air data. Sometimes, very small changes in cap strength can influence whether storms will develop or not.

Another type of data collected from a weather balloon is wind which can be displayed on a hodograph (Figure 1.7). A hodograph consists of a set of wind speeds and directions at various heights plotted as vectors. The hodograph is created when the tips of these vectors are connected. It provides important information about how the wind changes speed or direction with height. For any two points on the hodograph, the vector wind difference between the two different heights shows the change in wind speed between those two levels. Long hodographs indicate that there is large vertical wind shear. The shape of the hodograph provides important information about how the vertical shear changes with height (Markowski and Richardson, 2010) and can help determine the type of storm that may form. Tornadic supercells are associated with environments that exhibit specific types of wind profiles. A tornadic supercell wind profile is commonly represented by a hodograph that loops or curves in a clockwise direction (Davies, 1994).

Initial storm motions with curved hodographs tend to move with the mean wind velocity averaged over the depth of the environment the storm is developing in. When a storm becomes a supercell, it may deviate from the mean wind (Davies, 1994). This applies to all supercells despite the hodograph shape. Other wind profiles exist that can produce supercells, such as a straight line hodograph. A straight line hodograph can exist if just wind speeds increase with height or if just wind direction changes with height. These wind profiles can favor splitting supercells, left-moving supercells, and right moving supercells and can produce strong tornadoes. Hodographs are important because they allow for an easy interpretation of the shear vector.

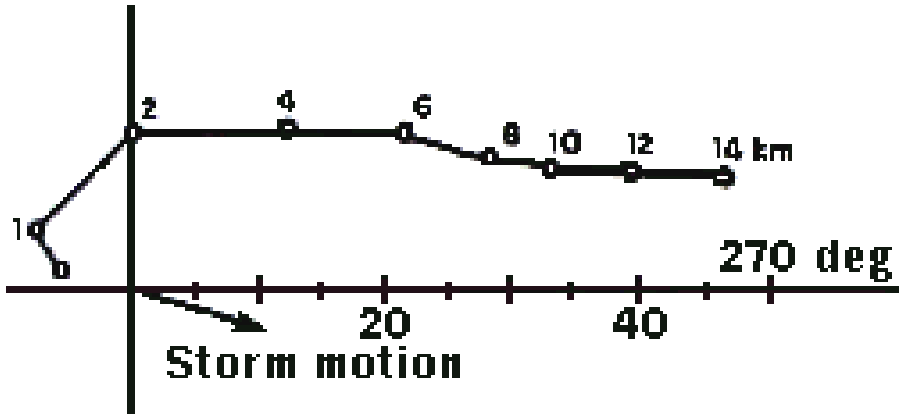

Figure 1.7: Hodograph example showing vertical wind shear for a supercell thunderstorm. Dots along hodograph line show the end point of vectors originating from the origin that reveal wind speed (knots) and direction at the indicated height in kilometres.

As introduced earlier, a supercell is a rotating thunderstorm that can persist for a long period of time and produce a variety of severe weather. In order for the supercell to continue or become increasingly severe, it needs a continued supply of streamwise vorticity. If storm-relative flow is normal to the vertical wind shear vector, the flow is parallel to the horizontal vorticity vector resulting in streamwise vorticity (Doswell, 1991). Streamwise vorticity is equal to the storm relative wind speed multiplied by the

rate at which the storm relative winds veer with height (Markowski and Richardson, 2010). If the horizontal flow is tilted upwards, parcels will spin cyclonically (Figure 1.8).

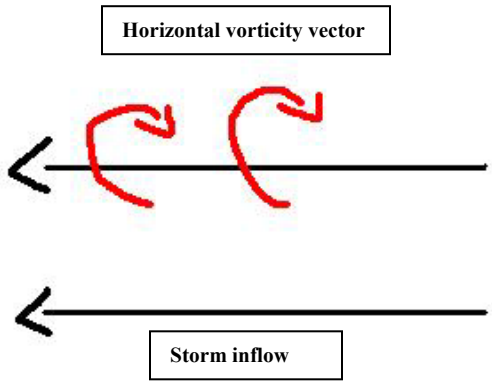

Figure 1.8: Streamwise vorticity showing storm inflow that is parallel to the horizontal vorticity vector.

If storm-relative low-level inflow is in the same direction as the vertical shear vector, this will result in crosswise vorticity (Doswell, 1991). Crosswise vorticity is the rate of increase of the storm relative wind speeds with height (Figure 1.9).

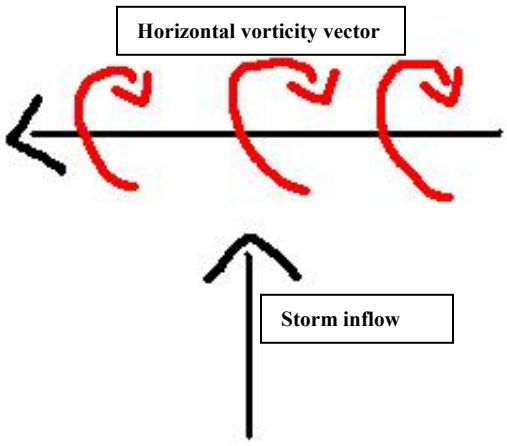

Figure 1.9: Crosswise vorticity showing storm inflow that is normal to the horizontal vorticity vector.

The amount of horizontal vorticity available for tilting to initiate rotation in an updraft can also be computed using a hodograph. This computation is called helicity (Davies, 1994). Helicity values have units of energy and are therefore interpreted as a measure of wind shear energy in $m^2 s^{-2}$. If the hodograph shape turns counter clockwise, then helicity values will be negative and if the hodograph shape turns clockwise, then the helicity values will be positive. Higher positive values increase the potential for right-moving storms to develop rotating updrafts. These values are usually located near frontal boundaries, areas of low pressure, or along outflow boundaries because these are sharply defined regions in which the wind speed and direction change. Negative values of helicity can also occur and these values typically favour anti-cyclonic or left-moving supercells.

Storm-Relative Helicity (SRH) can be determined only when the storm speed and direction is identified or estimated. SRH is therefore proportional to the low-level streamwise vorticity, and it is proportional to the strength of the low-level storm inflow. Hodograph shape identifies whether streamwise or crosswise vorticity are occurring. Davies-Jones et al., (1990) examined the results of 28 tornado cases and determined correlations between 0-3 km storm relative helicity and tornado strength (Table 1.1). In addition, values greater than 100 $m^2 s^{-2}$ at the 0-1 km height suggest an increased threat of strong tornadoes.

150-299 $m^2 s^{-2}$	**Weak Tornadoes (F0-F1)**
300-499 $m^2 s^{-2}$	**Strong Tornadoes (F2-F3)**
450 + $m^2 s^{-2}$	**Violent Tornadoes (F4-F5)**

Table 1.1: 0-3 km storm relative helicity values with corresponding tornado intensities (Davies-Jones et al., 1990).

1.1.4 - Tornadogenesis Processes

Rear Flank Downdraft Theory

As introduced in the previous section, the RFD is said to play a role in tornadogenesis because it can act as an increased vorticity source as the RFD intensifies (Burgess et al., 1977). Amplifications of vertical vorticity are closely linked to the intensification of updrafts due to the stretching and tilting as the storm develops (Markowski and Hannon, 2006). This may allow the storm to produce a tornado because the transition towards tornadogenesis is initiated by the rear-flank downdraft (Lemon and Doswell, 1979). Lemon and Doswell further explained the evolution of the RFD and tornadogenesis as follows:

- Air slows down at the upwind stagnation point and is forced downward to mix with the air below. The air then reaches the surface via evaporative cooling and precipitation drag.
- The initially rotating updraft is then transformed into a new mesocyclone with a divided structure, in which the main area of rotation is situated along the zone that separates the RFD from the updraft.
- The tornado can then develop as the descent of the mesocyclone circulation occurs simultaneously with the descent of the RFD. When the RFD wraps around the low-level rotating updraft, this forces the rotation to become focussed lower to the ground increasing the likelihood of tornadogenesis (Klemp, 1987).

Observers on the ground usually see this process occurring as a clear slot begins wrapping around the wall cloud. Studies of specific tornado events in 1955 and 1959

contain qualitative descriptions of surface temperature within the RFD at close range from a tornado (Markowski, 2001). Tornadoes have been associated with a cold RFD whereas Garrett and Rockney (1962) reported a warm RFD. This may occur if the observation was made south of the tornado wherever forced descent of air is less likely to encounter liquid water associated with the storm. Recent research and simulations have shown that tornadoes are largely composed of air parcels that have passed through the RFD (Markowski, 2001). Results from the Verification of the Origins of Rotation in Tornadoes Experiment (VORTEX) in 1995 did show that most significant tornadoes had relatively warm and moist RFDs, while non-tornadic storms had RFDs that were relatively cold (Markowski, 2001). Based on this research, it can be reasonably concluded that tornadogenesis and longevity requires the RFD to be relatively warm and buoyant (Browning and Bookbinder, 2004)

Three Ingredient Theory

This theory builds onto the RFD theory (mentioned above), and it has been proposed that three ingredients are required before a supercell tornado can begin to develop (Markowski et al., 1998).

- The first ingredient involves the development of a persistent, rotating updraft; a supercell. This is caused by the vertical tilting and stretching of the pre-existing horizontal vorticity that is created by the vertical wind shear.
- The second ingredient includes enhanced boundary layer storm-relative helicity (Chapter 3) as it determines the amount of spin that is present in the storm environment which enables the storm to continue to effectively rotate after it develops. SRH is highly variable both spatially and temporally and the local

enhancement of SRH can result from mesoscale boundaries (mentioned earlier) (Browning and Bookbinder, 2004).

- The third and final ingredient involves the development of a warm and moist rear flank downdraft because in addition to what is mentioned above, the RFD can act as an increased vorticity source that occurs at low-levels.

Vortex Breakdown Theory

Vortex breakdown, a phenomenon that occurs in fluid mechanics, has been documented in tornadoes (Trapp, 1999). The existence of vortex breakdown in supercells has been inferred from observations that have been made of a downdraft near the central axis of the mesocyclone that can lead to tornadogenesis (Brandes, 1978). Trapp explains that vortex breakdown occurs as follows (Figure 1.10):

- As a tornado begins to develop, initially the tornado consists of only an updraft, with an area of low pressure at the center of the tornado near the surface. This one-celled vortex has air that rises throughout the vortex from the surface. (Figure 1.10 A).
- As the area of low pressure deepens, a downdraft forms in the center of the tornado because the vertical jet terminates aloft at a stagnation point along the main center of rotation. This acts to increase the width of the tornado because air is now forced downward as the vortex breaks down which can eventually reach the surface (Figure 1.10 B)
- As the downward forced air reaches the surface, this can result in a broadly rotating, two-celled vortex with downward moving air now occurring at the

main center of rotation. This downdraft occurring at the center of rotation continues to descend which acts to widen the tornado further (Figure 1.10 C).

- Once the tornado widens, smaller vortices can form on the edge of the original tornado as the downward moving air exits the low-levels radially and turns vertically again in separate updrafts at the outer radius of the tornado (Figure 1.10 D).

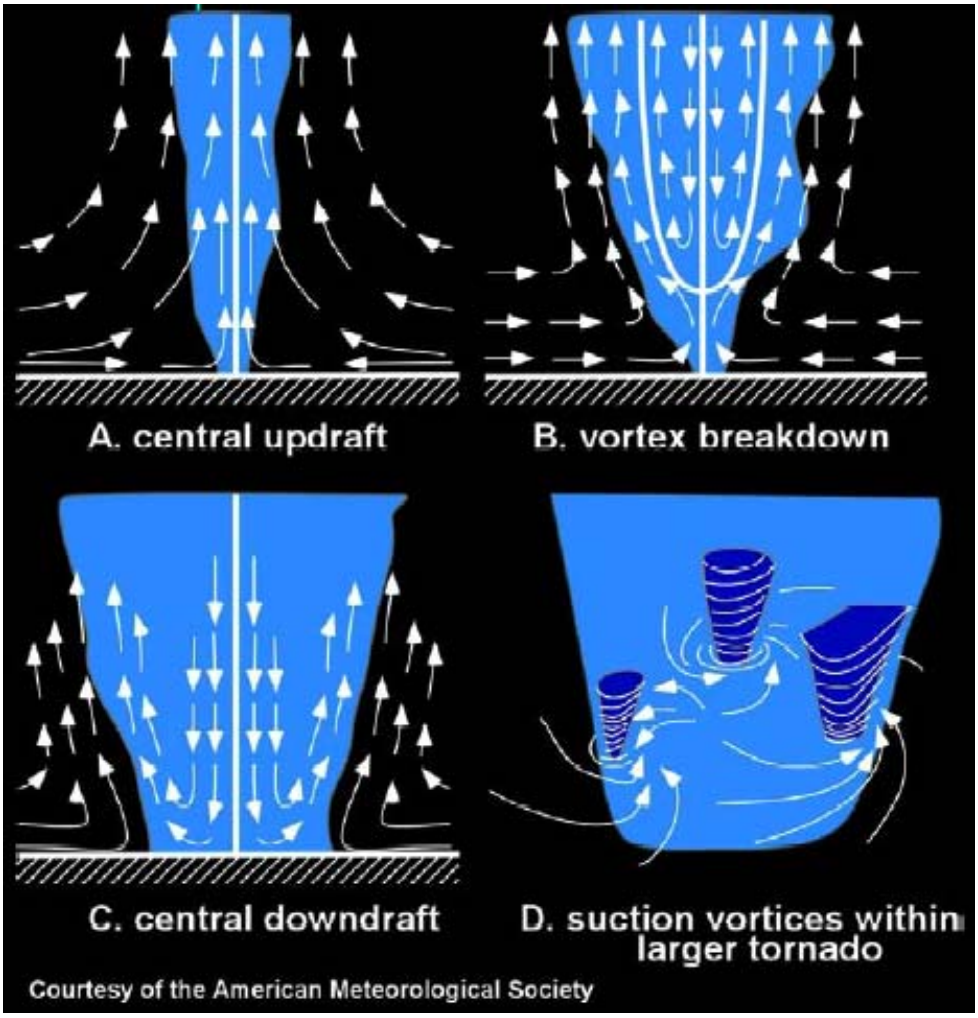

Figure 1.10: Vortex breakdown diagram showing steps A-D referred to from above. Vectors indicate radial and vertical motions (© American Meteorological Society. Reprinted with permission).

Tornado Occurrences Associated with Low-Level Boundaries

Past studies have shown that low-level boundaries are associated with tornadic storms (Markowski et al., 1998). The VORTEX studies, which were comprised of 11 tornado days with over 70 reported tornadoes, involved identifying boundaries through the analysis of surface, radar and satellite observations. To reduce the uncertainties in the analysis, Markowski et al., (1998) considered only the 47 tornadoes reported as strong (F2 or greater) since they were unlikely to be false reports (Figure 1.11). It was found that many of the tornadoes occurred within 20 km of detected boundaries during VORTEX (Markowski et al., 1998).

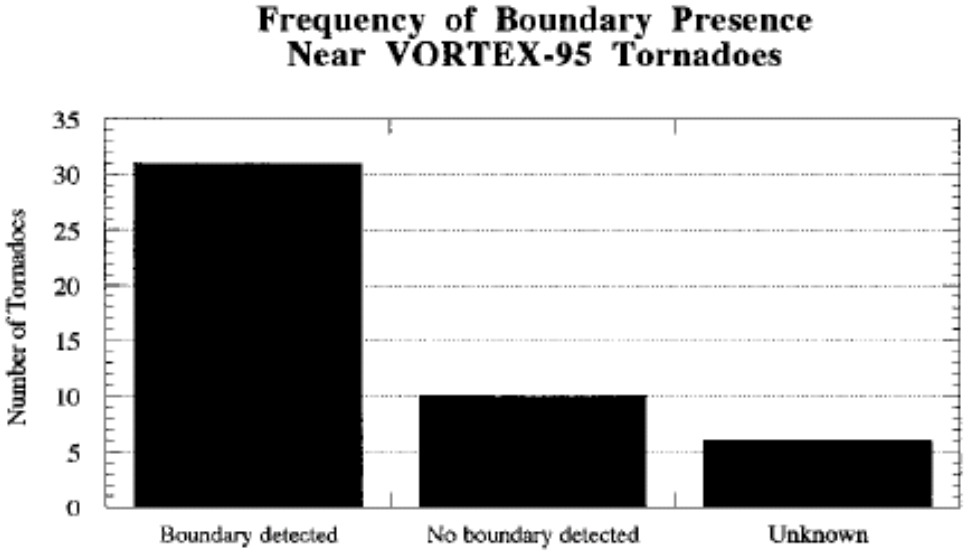

Figure 1.11: Frequency distribution of tornado occurrences in close proximity of boundaries during VORTEX-95 comprised of F2 or greater tornadoes (Markowski et al., 1998).

Strong horizontal vorticity can be produced along baroclinic boundaries such as fronts, pre-existing outflow boundaries, etc. For horizontal vorticity enhancement to be important for a storm, the updraft must draw inflow from the cold side of the boundary (Markowski et al., 1998). This is because boundaries are located on the warm sides of temperature gradients therefore leading us to believe that baroclinic horizontal vorticity

generation occurs on the cold side of a boundary (Markowski et al., 1998). The air parcels that have this enhanced horizontal vorticity must remain buoyant in order to be ingested by the updraft which can then tilt the horizontal vorticity into the vertical (Markowski et al., 1998). Storms that move along a boundary rather than directly across the boundary may have a higher chance of producing a tornado. The greatest tornado potential was found to be located between no more than 10 km into the warm air to roughly 30 km into the cold air. This is important for forecasters to detect and identify boundaries. The importance of boundaries for the Elie event will be discussed in Chapter 4.

1.1.5 - Identifying Tornadic Environments

Research since the mid to late 1990s, has given us a better understanding of the meteorological environments that are conducive to tornadic supercell thunderstorms (e.g., Evans and Doswell, 2002). Studies have shown that analyzing the observations of low level thermodynamic and wind shear profiles can help determine significant tornado days (Miller, 2006). Based on the study done by Miller (2006), two atmospheric conditions in particular are critically important in an environment supportive of significant tornadoes. These are strong low-level vertical wind shear, and moderate to high values of low-level absolute moisture and relative humidity because it is proposed that tornadogenesis and maintenance seems to occur in the lowest levels of the atmosphere, generally less than or equal to one kilometer above ground level (AGL) (Miller, 2006). Miller analyzed several significant tornado days (F2 or greater), and noted the low level wind shear and thermodynamic profiles at or below one kilometer AGL. Some basic conditions that are required in the thermodynamic profile are that the low levels have a mixing ratio that decreases with height, there needs to be a moderate to steep temperature lapse rates (greater then 7 °C km^{-1}) and finally a surface mixing ratio of at least 15 g kg^{-1}. For the hodograph, the observed low-level shear profile should have large bulk shear vectors between the surface and 500 m AGL and the surface to 1 km AGL.

Miller examined fourteen significant tornado days where atmospheric soundings and hodographs had low-level wind shear and thermodynamic profiles similar to the basic conditions mentioned above along with other tornado days that did not. A similarity is noted between the cases in which the hodograph trace has a kink a few hundred meters AGL (Figure 1.8) resulting in the hodograph taking on a distinctive

"sickle" shape (Miller, 2006). Esterheld and Giuliano (2008) hypothesized that a strong (approximately 7.5 m s^{-1} of bulk shear or larger) straight-line hodograph in approximately the lowest 500 m AGL oriented orthogonal to the storm-relative inflow vector at 10 m results in purely streamwise storm-relative inflow. This hodograph shape is proposed to favor significant tornadoes given the occurrence of surface-based supercell thunderstorms. Figure 1.12 from the paper by Esterheld and Giuliano (2008) shows a nearly straight-line hodograph with approximately 11 m s^{-1} of shear from 10 m - 250 m AGL that is approximately perpendicular to the 10 m inflow vector shown by the black line. The presence of a kink in the hodograph is important because it indicates strong near-surface speed shear separated from directional shear at a higher level and this can be a predictor for tornadogenesis since it's the low-level environment which governs if a tornado will develop according to this study.

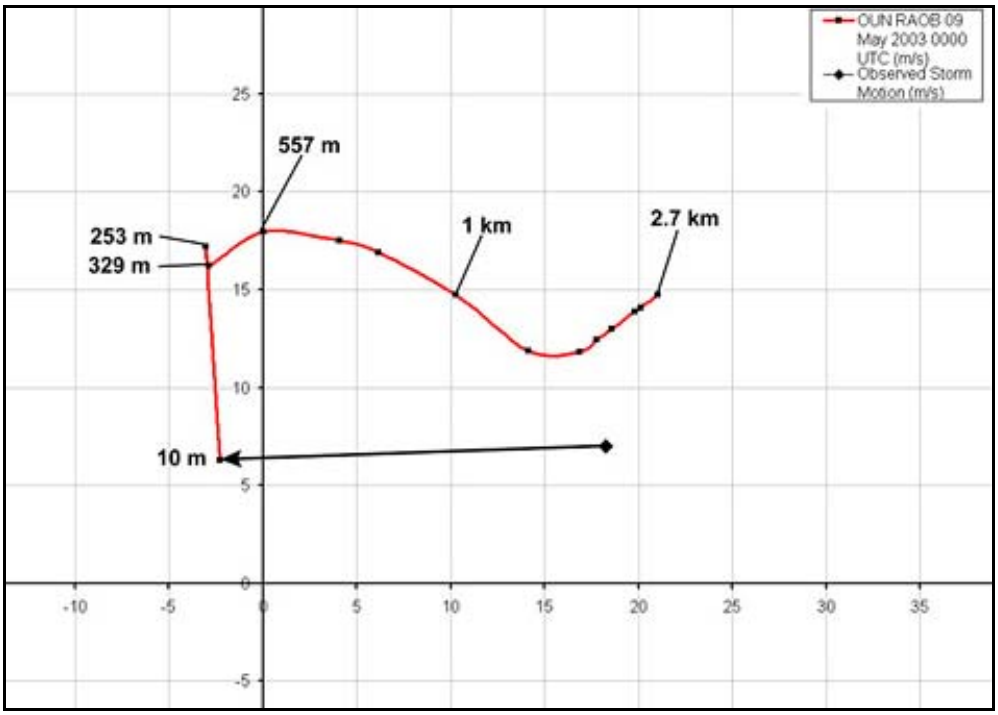

Figure 1.12: Hodograph kink example from OUN showing a notable kink below 500 m AGL on 9 May 2003 with 10 m inflow vector (black line). (Esterheld and Giuliano, 2008).

Miller (2006) went on to gather the mean values of various stability and shear parameters for the cases identified (Table 1.2).

All of the soundings showed significant instability, minimal convective inhibition, a very moist near-surface air mass, low-lifting condensation levels (LCL) and levels of free convection (LFC). Markowski et al., (2002) suggested that a moist near-surface air mass is more conducive to RFDs associated with relatively high buoyancy, which can increase the likelihood of tornadogenesis. A study done by Rasmussen and Blanchard (1998) suggested that relatively low values of boundary layer relative humidity support more low-level cooling through the evaporation of rain which can lead to stronger outflow preventing tornadogenesis. They also stated that half of the soundings in their study that led to tornadogenesis had LCLs below 800 m. All of the hodographs also had large low-level bulk shear vectors, from the surface to the height of the kink, and from the surface to 1 km AGL (Miller, 2006).

Mean Parameters of the 14 Tornado Cases	
Surface Temperature	**25** °C
Surface Dewpoint	**20** °C
Surface Temperature/Dewpoint Spread	**5** °C
Surface relative humidity	**68%**
CAPE	**3445 J kg^{-1}**
CIN	**42 J kg^{-1}**
LCL height (AGL)	**900 m**
LFC height (AGL)	**1628 m**
Height of hodograph kink (AGL)	**418 m**
Shear vector magnitude (sfc-kink)	**10 m s^{-1}**
Shear vector magnitude (sfc-1 km AGL)	**14 m s^{-1}**

Table 1.2: Analyzed case parameters in the study (Miller, 2006).

1.1.6 - How Tornadoes are Rated

The tornado that impacted Elie, Manitoba was rated F5 on the Fujita scale (Fujita, 1971) (Table 1.3). The scale ranges from F0 to F5, with F0 being the weakest and F5 the strongest. It was developed by Dr. Theodore Fujita in order to classify tornadoes based on wind damage. A rating is given based on the damage which equates to a particular wind speed. Tornadoes of F5 intensity cause total destruction to most buildings and trees. Specifically, strong frame houses are lifted off foundations and carried large distances to disintegrate, trees are debarked, vehicles are thrown through the air in excess of 100 m, and steel reinforced structures are heavily damaged (Fujita, 1971). Table 1.4 shows a comparison of the overall percentage of tornadoes with Fujita scale ratings (Grazulis, 2001). 93.9% of all tornadoes are of F2 intensity or lower and cause low-moderate damage. 6% all of tornadoes are between F3-F4 and can cause moderate-major damage. 0.1% of all tornadoes are ranked as F5 causing complete destruction (Grazulis, 2001). Further research into understanding how structures fail during tornadoes is being done at the University of Western Ontario (UWO) led by Gregory Kopp. The UWO is establishing a greater degree of quantification into the estimate of the wind speeds from observed damage caused by a tornado. The research involves looking at houses, primarily roofs and how they fail when tornadic winds impact them. The Fujita scale damage indicators do not mention the shape of the roof and it is the shape of the roof that can play a large role in determining what damage will occur if it is flat or if it is sloped. A sloped roof may not lift during a tornado; the house may be destroyed instead of the roof being blown off because the house may in fact be the weakest link (Gregory Kopp, personal communication, 2011).

The Elie tornado tracked through the south-western edge of the town, devastating three homes and severely damaging a fourth during its 40 minute lifetime. (McCarthy et al., 2008). An Environment Canada damage survey was conducted and the surveyors originally assessed the tornado as having F4 damage. Based on further evidence (McCarthy et al., 2008), it was later rated as Canada's first F5 Tornado. Vehicles were thrown hundreds of meters, two houses were torn from their foundation; with one house disintegrating mid-air, and several trees were debarked. All homes were modern, being built circa 1970, were wood framed and single story. They each had a poured concrete foundation and an attached garage. Three of the four homes had basements. Figure 1.13 shows one of the four homes that was destroyed by the tornado. There were no sill plates remaining on the poured concrete foundation and there was no evidence that anchor bolts were used. The main cross beam that supported the floor joists appeared to have been attached to the basement walls. The attached garage sill plates were bolted to the garage concrete pad and only some of the plates remained after the tornado hit. The remaining plates showed evidence of the washers becoming recently recessed. The damage to this home was initially rated F4 and later upgraded to F5. The upgrade to F5 occurred due to further video evidence that revealed that the structural failure occurred quickly and that one of the homes that was destroyed when the tornado impacted it directly met all of the requirements for the highest damage rating (McCarthy et al., 2008).

Figure 1.13: Storm damage survey picture taken on 23 June 2007 in Elie, MB showing foundation remaining after house was lifted and led to disintegrate in mid-air (PASPC Image Archive, 2007).

The United States has recently adopted the Enhanced Fujita Scale (Marshall et al., 2004). The main differences in the two scales are the level of detail found in each of the damage indicators and the strength of the wind speeds that cause the damage. Between the two scales, the rank of the tornado damage is virtually equivalent despite the somewhat different wind speeds found in each of the scales.

There have been no documented F5 tornadoes in Canada prior to 22 June 2007. Nine tornadoes have been officially recorded as F4. The majority of Canadian tornadoes occur in sparsely populated areas so the likelihood of more historic F4 or F5 tornadoes is high; it's just that no structures were in the path of the tornado to be destroyed.

Fujita Scale		Enhanced Fujita Scale	
F Number	3 Second Gust mph (km/hr)	EF Number	3 Second Gust mph (km/hr)
0	45-72 (72-115)	**0**	65-85 (105-137)
1	73-112 (116-180)	**1**	86-110 (138-177)
2	113-157 (181-253)	**2**	111-135 (178-217)
3	158-207 (254-333)	**3**	136-165 (218-265)
4	208-260 (334-418)	**4**	166-200 (266-322)
5	261-318 (419-512)	**5**	Over 200+ (323+)

Table 1.3: Fujita vs. Enhanced Fujita Scales (SPC, 2007).

Fujita Scale	Percent of All Tornadoes
F0	**38.9**
F1	**35.6**
F2	**19.4**
F3	**4.9**
F4	**1.1**
F5	**0.1**

Table 1.4: Comparison of Tornado Numbers with Fujita Scale Ratings (Grazulis, 2001).

1.1.7 - Prairie Tornado Climatology

Tornadoes can occur anywhere in Canada during the warm season (May through August) but the focus of this thesis is on the eastern Prairie Provinces. The tornado season refers to the time of the year when a region receives most of its tornadoes. The peak period for tornadoes in Western Canada is from mid-June through July (Raddatz, 1998).

The four main ingredients required for severe thunderstorms frequently occur simultaneously during the summer season. Due to the Prairies' geographic location, moisture can advect into the region from the Pacific Ocean at mid-levels and, more commonly, the Gulf of Mexico at low and mid-levels. Local evapotranspiration is also a key source of boundary layer moisture (Raddatz and Cummine, 2003).

The Prairies are separated from the West coast by the Rocky Mountains. The protection from the West coast allows heat and boundary layer moisture to pool in the Prairie regions contributing to the instability needed for thunderstorms to develop. This mountain chain also sets the stage for lee cyclogenesis (low pressure development) which in turn enhances the vertical wind shear as the jet stream interacts with the mountains. The air that flows over the mountains is compressed on the windward side and then stretched as it descends on the leeward side of the mountains. This stretching of the air can increase the relative vorticity promoting convergence at low-levels and divergence at upper-levels (Stull, 2000).

Figure 1.14 shows the distribution of confirmed tornadoes that have occurred over the Prairie Provinces from 1970-2009. They were plotted by rating within the prairie region. This distribution results from a combination of climatology and population

density because tornadoes that occur in unpopulated areas tend to go unreported (Etkin, 1994). Before 1980, there was no effort to develop a tornado database, and in order for an event to be reported, it had to be reconstructed through a variety of search techniques such as searching through newspaper archives (Etkin, 1994). After 1980, Environment Canada put a severe weather program in place, which provides a much better dataset that includes real-time data gathered by regional weather centers.

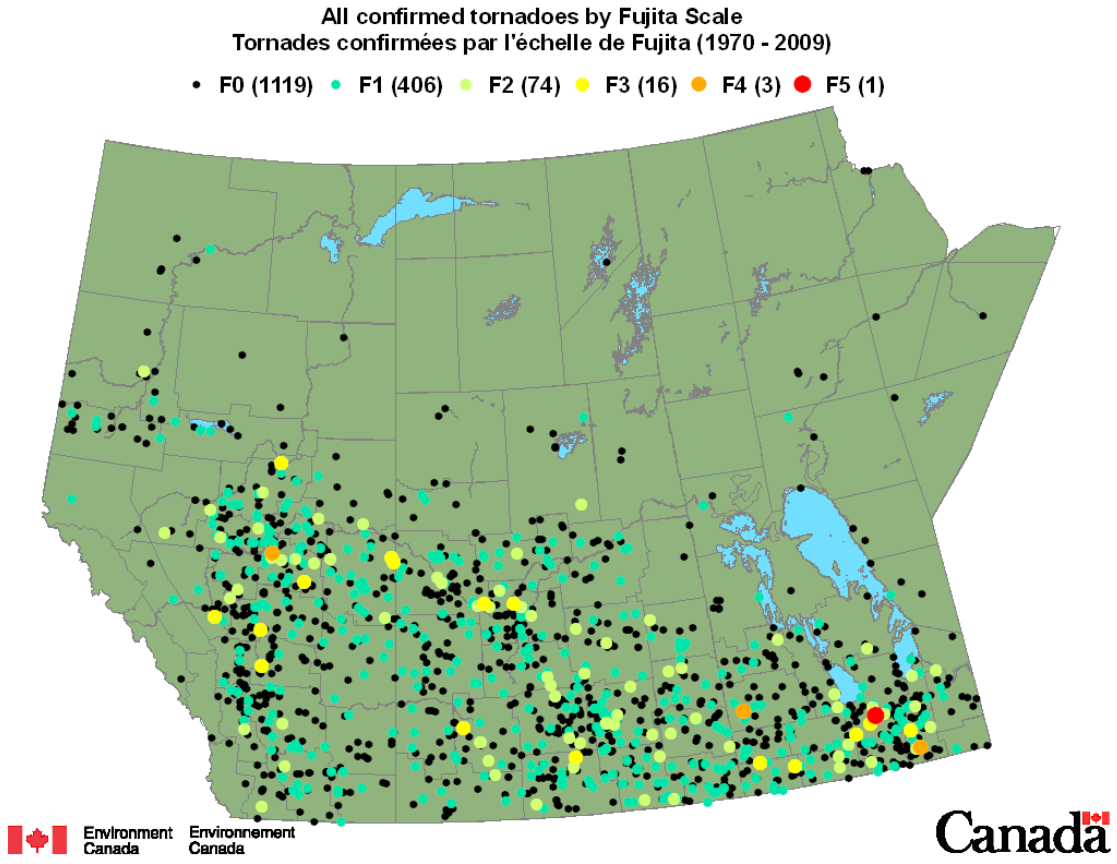

Figure 1.14: Confirmed tornadoes over the Prairies from 1970-2009 showing the individual occurrences and their rating (Environment Canada).

The tornado that impacted Elie, Manitoba in 2007 was one of several significant tornadoes that have occurred in North America in recent years. Some examples include: (1) an F4 tornado that devastated the eastern side of Edmonton, Alberta in July of 1987,

(2) an F5 tornado that impacted the cities of Moore and Oklahoma City, Oklahoma in May of 1999, (3) an F2 tornado in Gull Lake, Manitoba August 2006 and (4) an F3 tornado that destroyed a house and several outbuildings near Pipestone, Manitoba in June of 2007. A comparison between these events and the Elie tornado will be highlighted in Chapter 5.

1.1.8 - Manitoba Geography

Elie, Manitoba is a community in the rural municipality of Cartier. Elie resides approximately 30 km west of Winnipeg, Manitoba, along the Trans-Canada Highway. Lake Agassiz, a vast shallow inland sea covered the areas of Eastern Saskatchewan, Manitoba, and Northwestern Ontario and was formed by a glacier called the Laurentide Ice Sheet that retreated 12,000 years ago (Bone, 2005). The lake water eventually drained into Hudson Bay, the Mississippi river, the Great Lakes, and Mackenzie basin, leaving behind an exposed lakebed (Thorleifson, 1994). The retreat of the Laurentide Ice Sheet did not completely flatten this area and Elie is situated to the east of the Manitoba Escarpment and to the south of the Gunton Bedrock Escarpment. The Manitoba Escarpment peaks at 490 m ASL and the Gunton Bedrock Escarpment rises approximately 24 meters as you progress 47 km northwest from Winnipeg (Figure 1.15).

Figure 1.15: Digital Elevation Model (DEM) Map of Manitoba showing location of the Gunton Bedrock Escarpment that rises 24 m as you progress 47 km northwest from Winnipeg (green circle) and the Manitoba Escarpment that peaks at 490 m ASL (orange circle) with Elie denoted by red star and Winnipeg denoted by blue star (Manitoba Government, 2010).

This thesis will show the importance of the Manitoba Escarpment and the Gunton Bedrock Escarpment in triggering convective initiation. An understanding of local topographical and meteorological effects is critical in understanding thunderstorm development.

Elie sits at the base of two major lakes; Lake Winnipeg and Lake Manitoba. Temperature and wind direction changes can occur to the east and south of these lakes and these lake breezes can potentially aid in providing the focus for severe weather. Lake breezes can be seen periodically on Doppler radar as they originate from the south basin of Lake Manitoba and these can sometimes trigger thunderstorm development.

1.2 - Thesis Objective

The Elie tornado was unique in the fact that it didn't behave like most tornadoes. Most tornadoes move in a relatively straight line from point A to point B due to the upper level winds that steer the storm and can cover a large distance during the storm's lifetime, developing and dissipating as the storm propagates. Tornadoes typically cause significant damage after they impact communities in which people live. Most significant tornadoes are also large in size. As shown by Brooks (2003), historic major tornado widths tend to increase with intensity as they enter and impact a community. Most tornadic storms cycle while producing tornadoes. A tornado may be on the ground but as the storm encounters changing environmental conditions, the tornado may occlude or dissipate. As the storm strengthens again in the low-levels, another tornado may develop. This is the typical behaviour of strong tornadic storms in their mature phase.

The Elie tornado impacted a small area and caused no fatalities. Only minor injuries occurred with the worst being a twisted ankle from a truck driver who tried to get ahead of the tornado before it crossed the Trans-Canada Highway. The storm itself did not cycle as most tornadic storms do. The tornado remained on the ground for nearly 40 minutes and tracked approximately five kilometers, changing size and reaching its maximum width of approximately 140 meters (size of condensation funnel on the surface) before decreasing to 50 meters as it moved over the town of Elie, Manitoba. The Elie tornado was small in size meaning that this tornado had a highly concentrated wind field over a small area that contributed to the localized damage in Elie.

No previous study has been done for this event, and it is important because it was Canada's first documented F5 tornado. The three main scientific questions being asked in the thesis are:

1. What were the pre-storm environmental conditions on 22 June 2007?
2. How did the storm and associated tornado evolve?
3. How does this event compare to other major tornadic events in Canada and the U.S.?

This thesis will address each of the three primary research questions in separate sub-sections in Chapter 4 and Chapter 5. This work will provide new insight into severe storm initiation processes and tornadic storm evolution in Manitoba.

1.3 - Thesis Structure

This was Canada's strongest documented tornado; therefore the main emphasis will be placed on obtaining a better understanding of the pre-storm and storm environment before and during the tornado. Chapter 2 will provide background information on the roles of professionals and the public with respect to forecasting and identifying tornadoes. This will then lead into Chapter 3 which will highlight the data and methods used to determine the results in the chapter that follows. Chapter 4 will focus on analyzing and interpreting the pre-storm conditions leading up to the development of the tornadic storm. A more thorough step-by-step analysis completed at specific time intervals will show how the storm evolved. With radar imagery, satellite imagery, boundary layer observations, and images of the storm, one will achieve a better understanding of the 22 June 2007 event as a whole. Chapter 4 will end by focusing on the post-storm impacts which will include a tornado track/width analysis. Chapter 5 will be comprised of small case study analyses of other significant North American tornado events that have occurred in recent years and will be compared to the Elie event. Finally, Chapter 6 will cover the conclusions and recommendations.

CHAPTER 2 - TORNADO FORECASTING AND DETECTION TECHNIQUES

2.1 - Role of professionals in forecasting and detecting tornadoes

Severe weather outlooks and severe thunderstorm and tornado watches are issued by forecasters based on statistical and numerical forecast models, detailed surface mesoanalyses, real-time satellite imagery, and radar data (Mogil & Groper, 1977). Watches, warnings, and statements are sent via internet, commercial radio, television stations and cable television companies for broadcast to the public. Lead times for tornado watches are up to three hours before storms develop, and warnings are given up to 10 minutes prior to a tornado impacting a region. A tornado watch is issued by the Meteorological Service of Canada (MSC) when severe thunderstorms are forecast and conditions are favourable for one or more tornadoes to develop from those thunderstorms within a defined watch area. A watch is designed to inform the public, and activate storm spotter groups to be prepared to act in case a warning is issued (Mogil & Groper, 1977). A tornado warning is issued by the MSC when at least one tornado is imminent or occurring, as indicated by reports or radar. Some radar indicators of severe storms that a meteorologist may observe (* - tornadoes) are:

1) **hook echo*** – when rain, hail or even debris is wrapped around the supercell
2) **tornado vortex signature (not seen on Canadian Radar)*** – detected rotation algorithm showing strong mesocyclone through differing heights of the thunderstorm (term used in thesis analysis, however it is not based on algorithm)
3) **line echo wave pattern** – squall line oriented in wave like pattern
4) **bounded weak echo region** – often associated with supercells showing a strong updraft which can produce severe weather

5) **merging or splitting cells** – depending on environment one storm can become more severe after it splits from the other cell
6) **cells with hail shafts** – can produce large hail
7) **intense thunderstorm ahead of an instability line** – has a higher likelihood of becoming severe because it is not competing with other storms within the same environment
8) **attenuation** – a strong thunderstorm core may block the radar beam from detecting targets beyond the core that is between the radar and the target that is further away

The Meteorological Service of Canada (MSC) has a National Doppler Radar Network that is comprised of 31 WSR-81 C-band Doppler radars to support the weather forecast and warning production programs. Severe weather meteorologists on the Canadian Prairies monitor nine Doppler radars plus three adjacent Canadian radars and four NWS radars (Patrick and McCarthy, 2008).

The beam-width of most of the Canadian radars are 1.1 degrees with the data being recorded and logged in 1 km length bins for every elevation angle for the first 120 km radial range and 2 km length bins for the 120-240 km radial range (Patrick and McCarthy, 2008). Every ten minutes, 360 degree scans of radar reflectivity/velocity are made at 24 different elevation angles ranging from 0.5 degrees to 30 degrees. The reflectivity volumetric data set can be further processed for the user via URP (Unified Radar Processing) software. The output from URP shows important reflectivity/velocity storm-related features (e.g. echo tops, vertically integrated liquid, bounded weak echo regions, mesocyclones, velocity couplets) to help identify which cells are showing severe storm characteristics. The combination of conventional and Doppler radar along with URP can help in forecasting and monitoring the evolution of thunderstorm structure and severity.

2.2 - Role of non-professionals in detecting tornadoes

The Meteorological Service of Canada's (MSC) main responsibility is to prepare and issue severe weather watches and warnings based on conventional tools and meteorological expertise as mentioned in the previous section. Unfortunately, issuing these severe weather bulletins is simply not enough to alert the public. Townships and large urban centers should have individual storm emergency plans set up by local emergency measures organizations as these plans help citizens understand severe weather watches and warnings. Environment Canada has a database of weather watchers that they can contact who relay important information as to what is going on near/under a storm. This provides supplemental information in addition to the information that is provided by conventional radar. The most reliable indicators of severe weather events such as tornadoes are provided by watchers located near the storm (Moller, 1978).

CHAPTER 3 - DATA AND METHODS

3.1 - Methodology

The main focus of this thesis is to present the meteorological conditions that were present over southern Manitoba on 22 June 2007 by going through an in depth analysis of the synoptic scale and mesoscale atmospheric conditions. To perform this analysis, several aspects of meteorological information were investigated:

3.1.1 - Synoptic information

a. 1200 UTC upper air data (250 hPa, 500 hPa, 700 hPa, 850 hPa)

b. 1200 UTC surface data

3.1.2 - Mesoscale information

a. 1200 UTC/1800 UTC/2100 UTC/0000 UTC surface analyses

b. 1800 UTC – 2200 UTC radar analysis prior to convective initiation

i. Lake breeze interactions

ii. Horizontal convective rolls

iii. Moisture convergence

iv. Gravity wave interactions

3.1.3 - Local sounding data

a. 1800 UTC Hodograph from XWI (Winnipeg) and XWL VAD Hodograph

b. 1800 UTC Tephigram from XWI (Winnipeg)

3.1.4 - Radar analysis after convective initiation

a. 22 June 2007 1800 UTC – 23 June 2007 0030 UTC Low level reflectivity/velocity radar analysis

3.1.5 - Tornado Path/Width Analysis

3.1.1 - Synoptic Information

Upper air maps from 1200 UTC were analyzed to identify areas of mid-level moisture, ridges, troughs, deformation zones, vorticity centers and where these features were moving. Standardized heights that are commonly analyzed are 250 hPa (10,000 m), 500 hPa (5,500 m), 700 hPa (3000 m), and 850 hPa (1500 m).

Surface analyses were then completed at 1200 UTC, 1800 UTC, 2100 UTC and 0000 UTC. The surface analysis for each above mentioned time began by contouring areas of equal mean sea level pressure (isobaric analysis). After the isobaric analysis was complete, the surface analysis was completed by analyzing and identifying areas of low pressure, high pressure, pressure gradients indicative of strong surface winds, the orientation of the surface winds, temperature, dewpoint temperature, and differing air masses separated by surface fronts. Once the surface analyses were completed, a four dimensional analysis of the atmosphere could be built in combination with the upper air maps. On days when severe weather is expected, a more thorough mesoscale analysis is completed to supplement the surface analyses to understand what may locally influence a storm if it developed.

3.1.2 - Mesoscale Information

A mesoscale analysis is completed on the surface map that is zoomed in on the order of 1:5 vs. the 1:10 used for the surface map. A 1:5 scaled map means that one centimeter on the map equals 5 million centimeters or 50 kilometers, and a 1:10 scaled means that one centimeter on the map equals 10 million centimeters or 100 kilometers. The pressure, surface temperature, dewpoint temperature, areas of upslope flow, areas of downslope flow, where a dry line might reside, where local convergent boundaries are, and where moisture is pooling can all be identified on a mesoscale analysis. This mesoscale analysis is important because it highlights a specific area that should be monitored throughout the day. An area can only be honed in on after looking after everything from the top of the atmosphere down.

Another approach to analyzing the weather is by doing a Miller (1972) analysis. It involves all of the analysis techniques when identifying a threat area but it is all illustrated on one composite map. By overlaying the mid-level and surface wind data wind maximums, the surface/mid-level moisture, areas of convergence (synoptic/mesoscale), positions of vorticity maximums or any other important feature, a threat area can be .highlighted. The composite map illustrates processes and how they relate to one another to highlight a convective threat area.

During the day, identifying and monitoring the other mesoscale features, such as gravity waves, horizontal convective rolls, lake breezes, and moisture convergence (defined in Chapter 1), on radar can further define the convective threat area.

3.1.3 - Local Sounding Data

More detail is added to the synoptic and mesoscale analyses by analyzing atmospheric sounding data. A balloon was launched at the PASPC in Winnipeg at 1800 UTC on 22 June 2007. The 1800 UTC hodograph and tephigram were analyzed and modified based on surface observations and low/mid-level winds that changed that afternoon prior to convective initiation.

3.1.4 - Radar Data

Radar data from XWL (Woodlands, MB) located northwest of Elie is used in the pre-storm analysis in Chapter 4.1 as well as the storm evolution analysis in 4.2 as it provided the best information to monitor the progress of the tornadic storm since it occurred in close proximity to the radar site. The products used while monitoring the evolution of the tornadic supercells on 22 June 2007 were the corrected log Z (ClogZ) low-level reflectivity/velocity products, 7.0 km constant altitude plan position indicator (CAPPI) product, Cell Viewer, and the Velocity Azimuth Display (VAD).

The ClogZ products apply to the lowest angles of the radar (Figure 3.1). The term CLogZ is short for Corrected Log Z. "Z" is the radar reflectivity, and "Log Z" is the usual scaling factor applied to the "Z" reflectivity data for display. It is essentially a plot of radar reflectivity in "dBZ" units. The "Corrected" means that the reflectivity is corrected to remove ground clutter echoes by using a Doppler clutter suppression technique that eliminates echoes with zero velocity (Dave Patrick, Personal Communication, 2011).

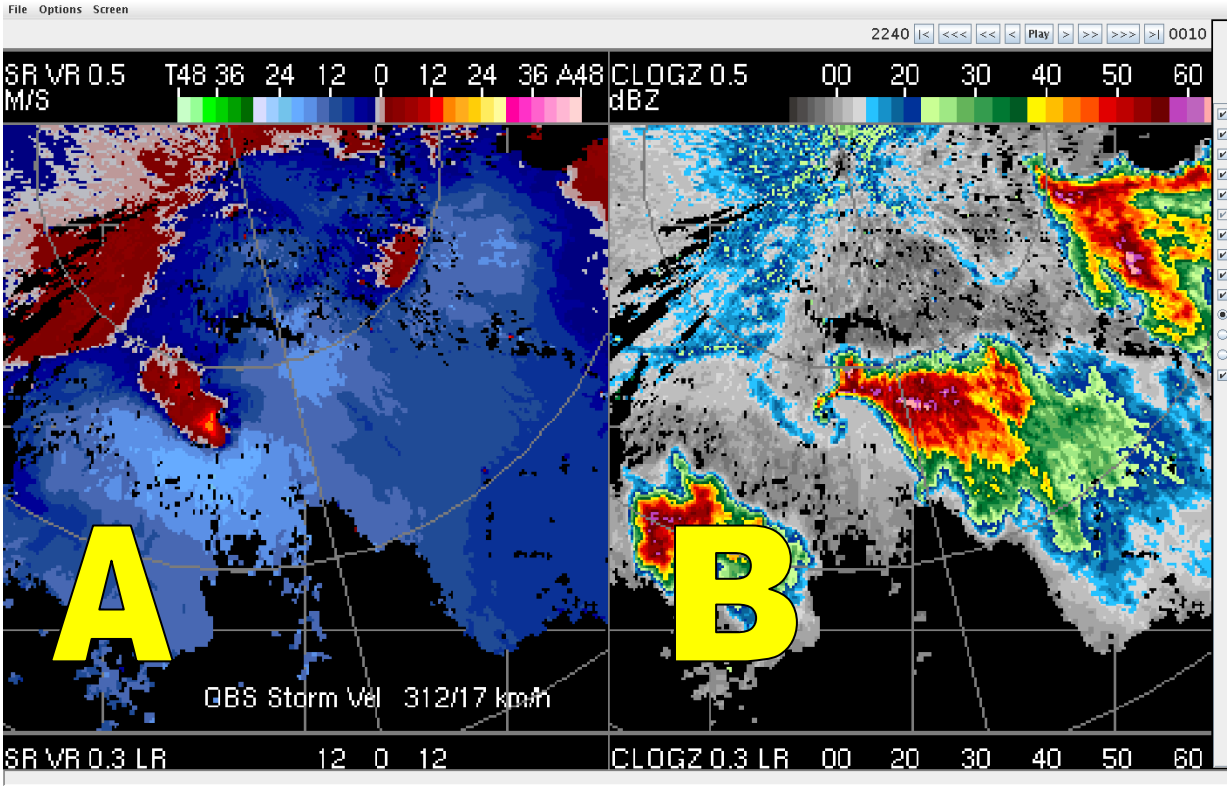

Figure 3.1: ClogZ velocity/reflectivity example showing supercell velocity couplets on the left (A) with their associated hook echoes on the right (B).

LOLAA (lowest local application angle) radar reflectivity data detects hydrometeors at the lowest elevation angle and can only be used properly if hydrometeors are detected close to the radar. It is designed to see as low as possible over areas that are of particular interest. This is critical during the summer months when severe weather, such as tornadic activity, occurs low to the ground. The range of the LOLAA scan extends out 120 km from the radar. The velocity data is equally important because it can identify hydrometeors travelling towards the radar and away from the radar and analyze velocity couplets which indicate that rotation is present in the thunderstorm.

The 7.0 km CAPPI product detects hydrometeors 7 km above the ground (Figure 3.2). It is a common product that is used because it is a good indicator of severe thunderstorm activity in the Prairies because seeing high reflectivities at this height have a high likelihood of producing large hail and/or very heavy rain.

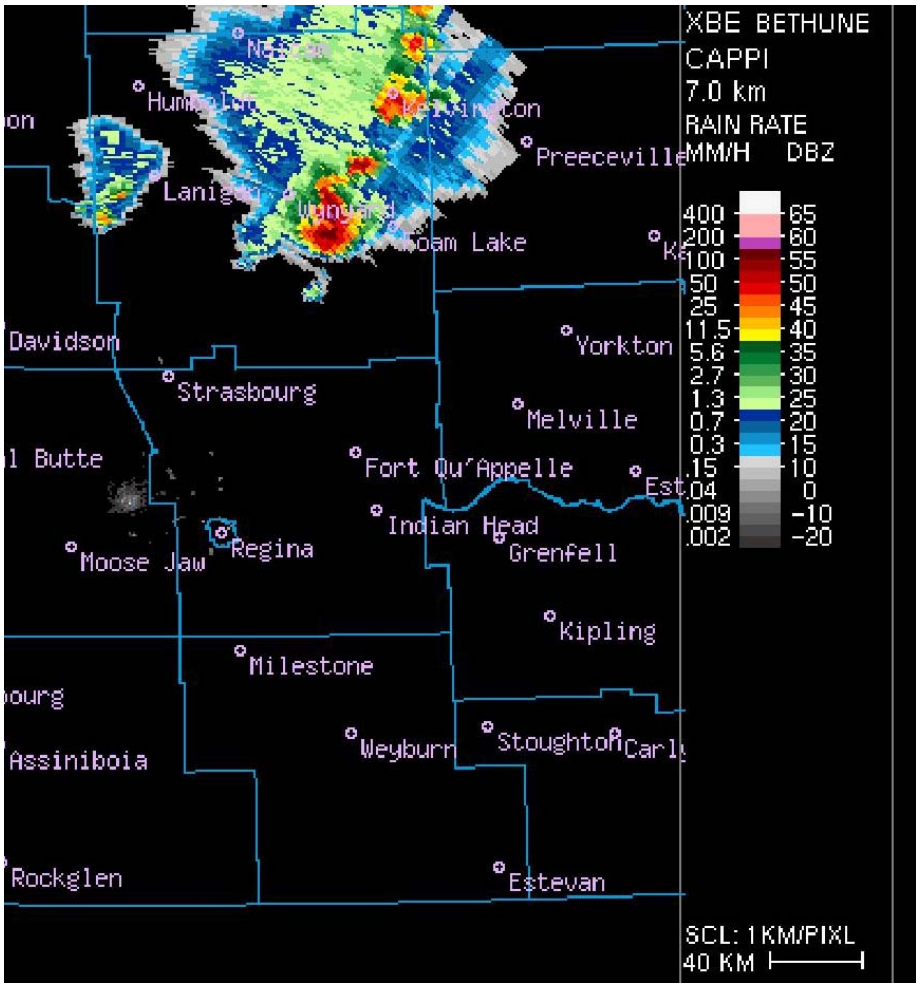

Figure 3.2: 7 km CAPPI image showing thunderstorms extending at or above 7 km into the atmosphere.

The cell view window shows a variety of information (Figure 3.3). The ensemble (Figure 3.3; A) displays the low-level and mid-level reflectivity/velocity patterns of a storm, and shows where various algorithms are triggered with respect to this pattern. It allows for a "quick" comparison to conceptual models of convective storms (Patrick and

McCarthy, 2008). Below the ensemble is where two automatic cross sections are produced (Figure 3.3; B). The centres of the two cross sections are at the storm centroid (geometric center); at the 40 km mark. The automatic cross sections are 80 km long, longer than the arrows shown on the ensemble. The cross section imagery shows where a bounded weak echo region may be located within the thunderstorm. The reflectivity colour scale is shown across the top of the graph indicating the intensity of the thunderstorm. Figure 3.3; C, shows four radial velocity/reflectivity images: The bottom row shows the best angle for long distance angle and includes second trip echoes. Above that is the 0.5 degree scan, then the 1.5-degree scan and finally the 3.5-degree scan. The colour scales corresponding to away and towards velocities are displayed in m s^{-1} and the colour scales corresponding to reflectivity are in dBZ.

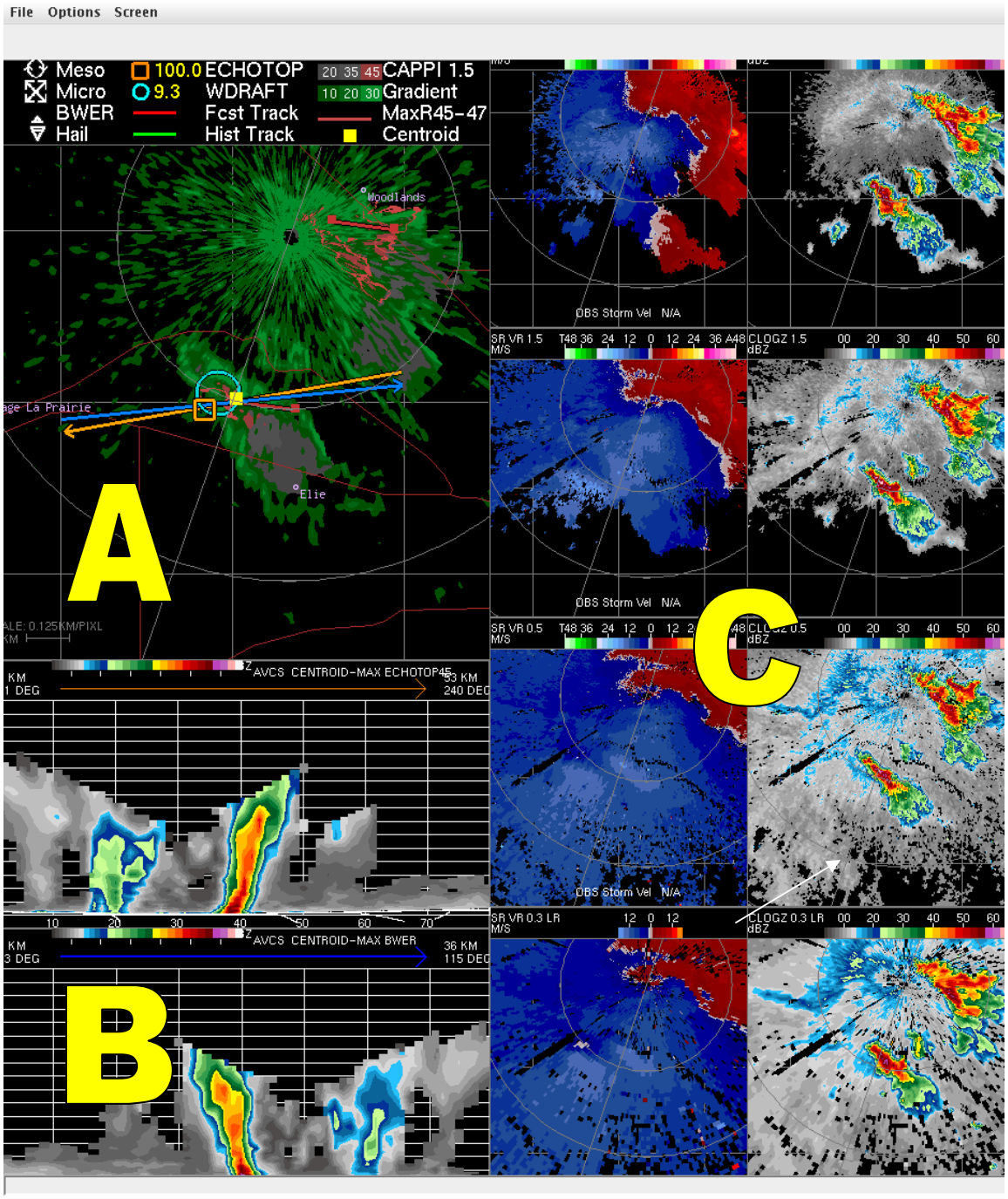

Figure 3.3: Cell view window showing important storm characteristics ranging from the cell (A), cross sections (B), velocity data with scale for different elevation scans (m s $^{-1}$) (C: left), reflectivity data with scale for different elevation scans (C: right).

The Velocity Azimuth Display (VAD) product for each of the 3 Doppler scans (shown in green, yellow and red) are shown with a best fit sine curve that is applied to all the available radial velocity data for each scan (Figure 3.4). From this, an estimate of

wind direction and speed over the radar domain can be produced. Range corresponds to a height for a given elevation angle, therefore plots of wind speed and wind direction with height can be made. Also plotted is reflectivity that is averaged around a range bin that is converted to a height as well as model derived cell motion and helicity parameters. If cells develop, this can contaminate the radar VAD resulting in errors in the calculations of the low level winds. The VAD method is therefore very sensitive to systematic errors caused by velocity ambiguities that can take place once storms develop.

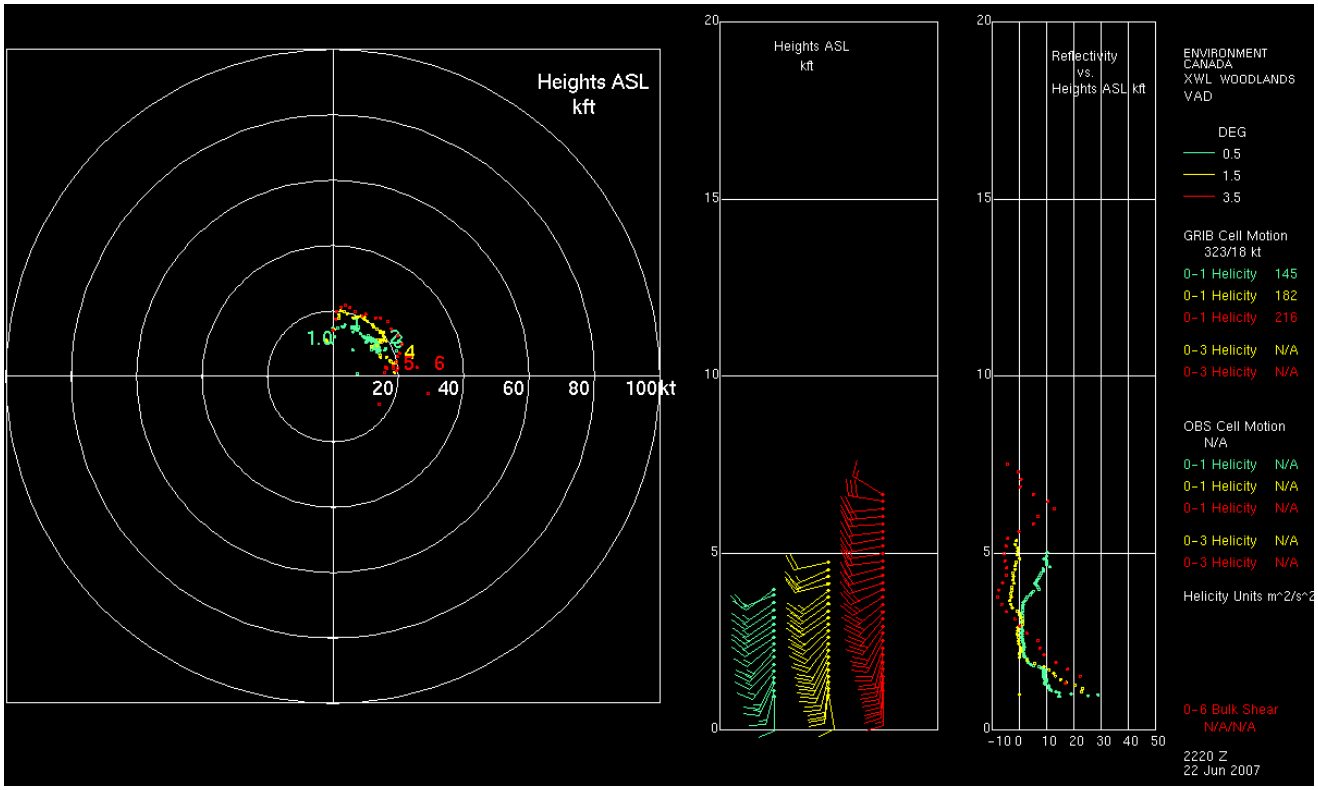

Figure 3.4: VAD Image Example showing hodograph (left), wind speed/direction changes with height (center), reflectivity vs. height trace (right) and radar and model derived helicity values (far right) (Leduc, 2010).

Important boundaries and other features can be detected on radar because of clear air echoes. There are two main categories of radar echoes in the clear air. The first is from insects, dusts, chaff and other particulates in the atmosphere that are large enough to

return some power back to the radar (Rinehart, 1997). The second source of return is from what is called refractive-index gradients (Rinehart, 1997). Particulates that are detected can give an estimate of the wind speed and direction in the atmosphere. Refractive index gradients occur when the refractive index of the atmosphere changes significantly over short distances compared to the wavelength of the radar (Figure 3.5). Rapid changes of temperature and moisture can cause rapid changes in the refractive index which can be detected by the radar. The region that contains these sharp, small-scale fluctuations can return some of the energy back toward the radar (Rinehart, 1997). The refractivity index gradients can also be caused by turbulence in the atmosphere as the energy from the radar is back-scattered (Rinehart, 1997). Turbulence is associated with variations in the density in the atmosphere. When turbulence the size of the radar wavelength (or smaller) mixes warm and cold or dry and moist air, the radar may be able to detect it. This scatter from turbulence in the atmosphere is called Bragg scatter (Rinehart, 1997). Radar echoes in a clear atmosphere will be more common when the lower atmosphere is unstable below an inversion, if the wind increases rapidly with height near the surface, or if there are thermals present (Rinehart, 1997). Clear-air-echoes are important to monitor because they indicate low level mesoscale boundaries which can serve as the focus for severe thunderstorm development and eventual tornadogenesis.

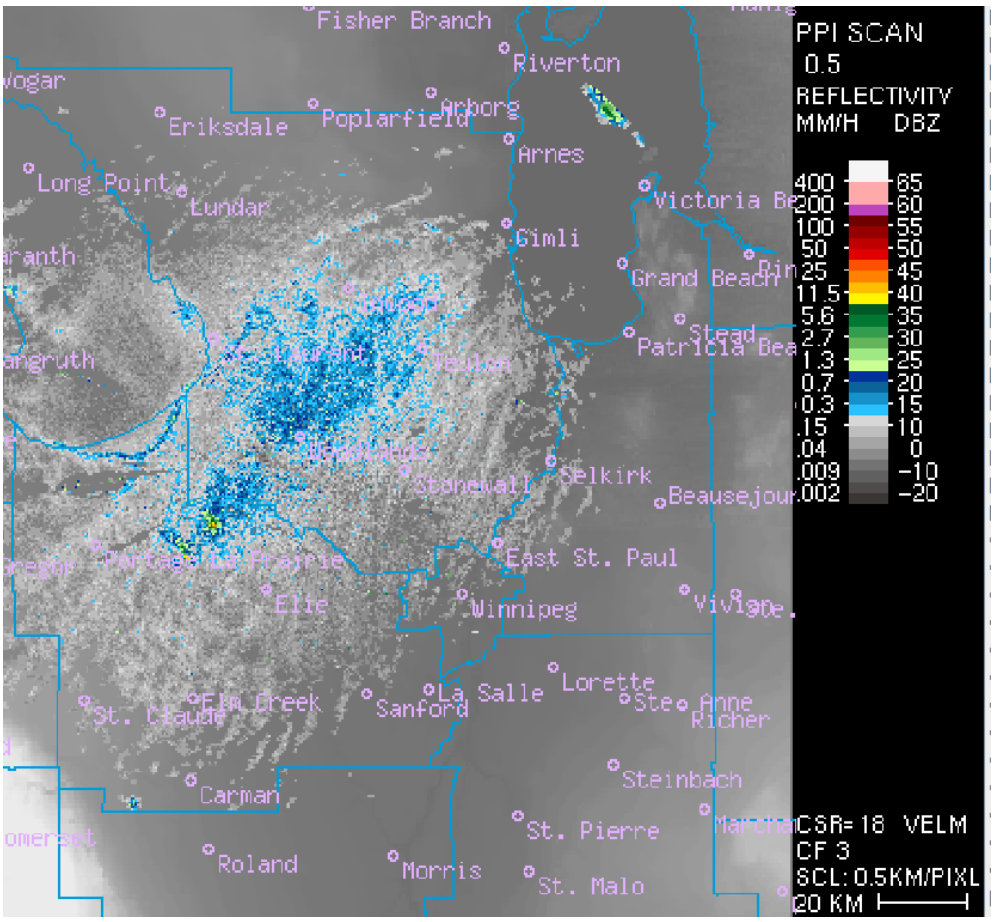

Figure 3.5: CLOGZ LLAA radar image showing clear-air returns possibly caused by refractive index gradients in the boundary layer beneath an inversion. Gradients in the image are likely caused by density fluctuations attributed to turbulence and moisture in the boundary layer.

3.1.5 - Tornado Track Investigation

The relationship of the size of tornadoes to the intensity of their damage may be useful in attempting to forecast intensity (Brooks, 2003). As introduced earlier, longer path lengths mean that there is more opportunity for damage to occur, and in general longer path lengths are associated with longer lived tornadoes (Brooks, 2003). Wider tornadoes will take longer to pass over a specific point, giving more time for damage to occur if peak wind speeds remain constant and we assume the tornado is nearly symmetric. Brooks (2003) states that the F-scale increases with increasing reported tornado size although F5 tornadoes are never the most likely event for any tornado size. Also for most lengths and widths, there is a wide range of F-scale values associated with significant probability of occurrence (Brooks, 2003).

For the tornado that occurred in Elie on 22 June 2007, a track investigation was performed by Environment Canada to determine where the tornado tracked after it touched down. The track was determined by examining video and ground damage photos that was made available to Environment Canada by local storm chasers and a couple of local pilots who provided Environment Canada with aerial images. Detailed video was obtained from a local colony that was filming from a fixed point 2.8 km northwest of Elie and from myself who filmed the entire event (time-coded) from a fixed position 1.6 km south of Elie. In addition to the video, I photographed the tornado several times (also time-coded) as it evolved. For this thesis, I only included the photographs that were deemed important to describe the evolution of tornado itself. A revisit to the site by Environment Canada employees helped fine tune the track based on examining damage to crops and the scouring of gravel roads. After the track was determined, a further

analysis was performed to estimate how wide the tornado was at different stages of its life cycle. This analysis was performed by examining storm photos taken by local residents in the area and the above mentioned videos to determine fixed points. Fixed points included houses, parked vehicles, highway markers, power lines, and agricultural infrastructure. Once the fixed points were determined, they were overlaid on the same track map to determine how far away the tornado was and approximately how wide it was at that time. The time the tornado was located over a certain location was determined by cross-examining the time coded video of the tornado with other tornado photos as well as using the tornado track map determined by McCarthy (2008). The shape of the tornado in the photographs was able to be matched with the shape of the tornado in the time-coded video to identify the approximate time the tornado occurred at one specific location.

CHAPTER 4 - RESULTS

4.1 - Pre-storm Meteorological conditions prior to the Elie Tornado

4.1.1 - Upper Features

1200 UTC 22 June 2007 Data

At 1200 UTC on 22 June 2007, the upper-level height fields revealed a building upper ridge over the southern Prairies. 250 hPa winds (not shown) were analyzed at 31 m s^{-1} from the northwest over southwest Manitoba with the main jet core (46 m s^{-1}) similarly oriented to the 500 hPa winds (Figure 4.1) across the central Prairies. 500 hPa winds (Figure 4.1) were analyzed at 18 m s^{-1} from the northwest over southwest Manitoba with a weak shortwave moving through central Alberta. The main jet core (26 m s^{-1}) was located to the north over the central Prairies. At 700 hPa, the winds (Figure 4.2) were analyzed from the west at 10 m s^{-1} over southern Manitoba on the eastern side of the upper ridge. A thermal ridge could also be seen through southern Saskatchewan suggesting that areas to the east of the thermal ridge were capped for surface based convection due to continued warming at that level.

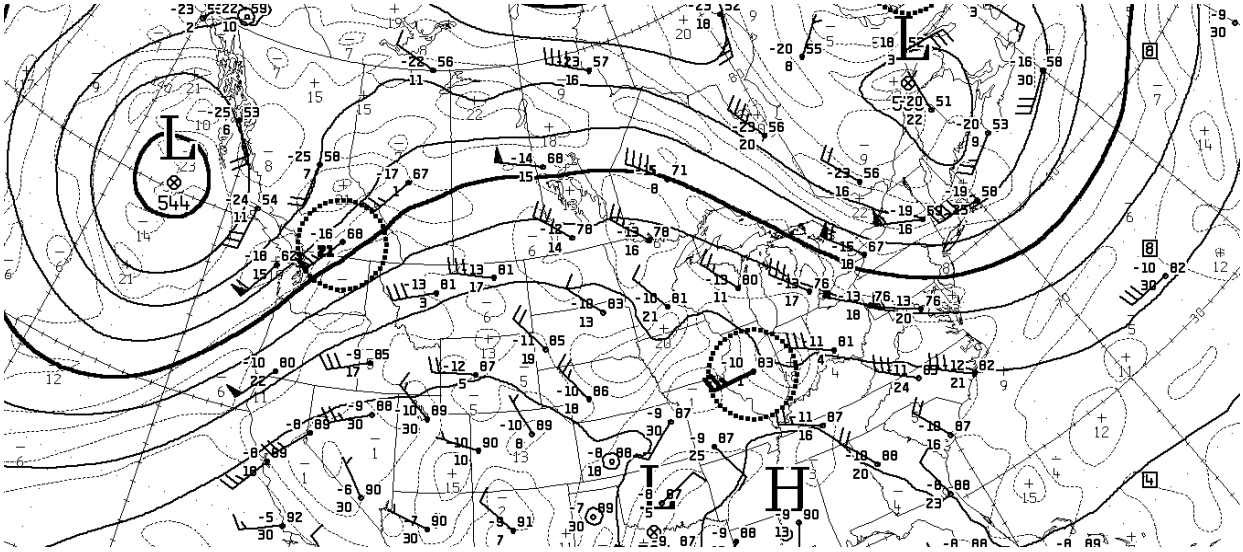

Figure 4.1: 500 hPa 1200 UTC analysis on 22 June 2007 showing wind speed, temperature, vorticity centers, and areas of high and low geopotential heights. Wind barbs are in knots and top left numbers are for temperature in °C and bottom left numbers are for dewpoint depressions (T-Td) in °C. Top right number is the geopotential height value.

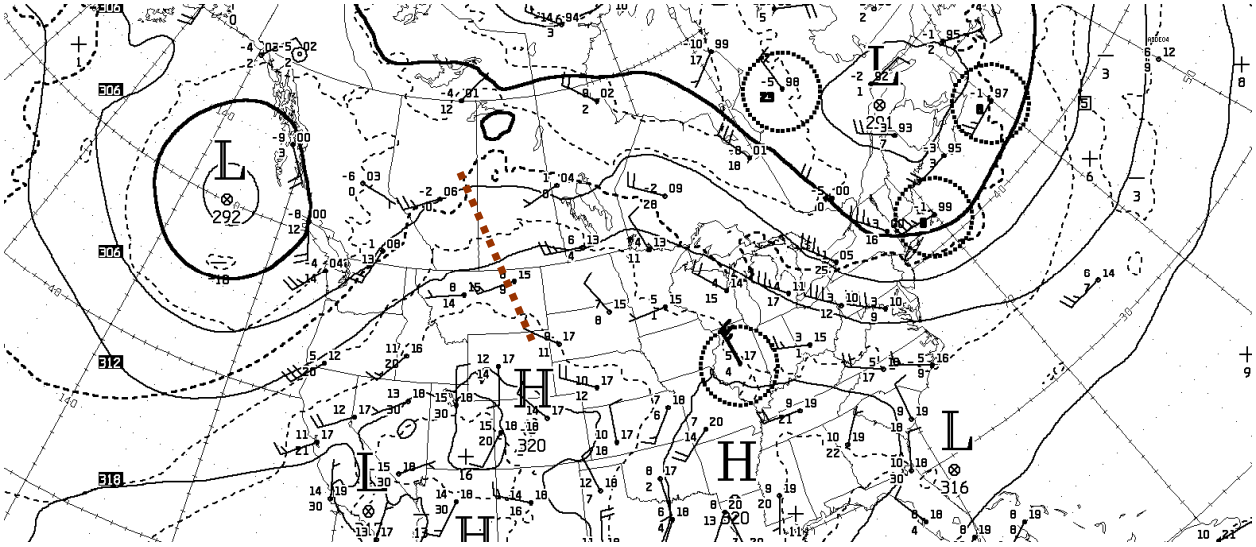

Figure 4.2: 700 hPa 1200 UTC Analysis on 22 June 2007 showing wind speed, temperature, vorticity centers, and areas of high and low geopotential heights. Wind barbs are in knots and top left numbers are for temperature in °C and bottom left numbers are for dewpoint depressions (T-Td) in °C. Top right number is the geopotential height value.

At 1200 UTC, a southwesterly 850 hPa jet max was analyzed over southern Manitoba at 10-15 m s^{-1} that was rounding the western side of the ridge of high pressure situated over the eastern United States with dewpoints of 10-14 °C being advected into

the same region from the central plains (Figure 4.3). A weak thermal ridge was also seen extending from southern Alberta southeast into eastern Montana. This showed that there was warming at 850 hPa to the east of the thermal ridge revealing that there was a warm nose near that height which was confirmed later with the sounding data. This low-level jet cannot be seen in full detail due to the sparse network of upper air sites. However, the orientation of the 850 hPa jet over southern Manitoba shown by the VAD and balloon data (seen later) enabled the storm inflow region to get a continued supply of warm moist air for an extended period of time. This supply of moisture originated from the Gulf of Mexico combined with local and advected evapotranspiration. Due to the ridge that was established at 850 hPa, and the orientation of the southerly low-level jet on the western edge of this ridge with speeds on average of 8 m s^{-1}, it would have taken approximately 90 hours for the moisture from the Gulf of Mexico to be advected into Southern Manitoba. This is based on the assumption that a southerly flow did not already exist in the central plains where the Gulf of Mexico moisture was situated closer to Southern Manitoba.

Based on examining the above mentioned heights, the general wind shear characteristics at 1200 UTC for the 250 hPa, 500 hPa, 700 hPa, and 850 hPa revealed directional and speed changes (estimated at 15 m s^{-1}) with height that were conducive for severe storms and confirmed by the hodograph (shown later).

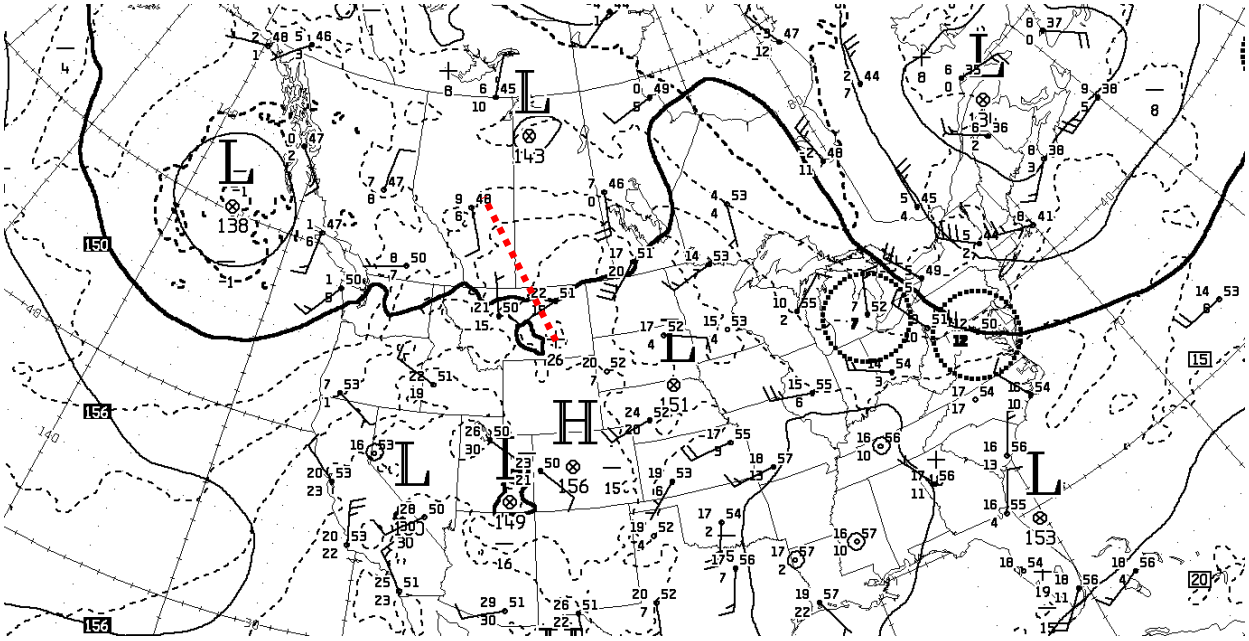

Figure 4.3: 850 hPa 1200 UTC Analysis on 22 June 2007 showing wind speeds, temperatures, vorticity centers, and areas of high and low geopotential heights. Wind barbs are in knots and top left numbers are for temperature in °C and bottom left numbers are for dewpoint depressions (T-Td) in °C. Top right number is the geopotential height value.

4.1.2 - Surface Features

At 1200 UTC on 22 June 2007, a broad area of low pressure was analyzed at 1010 hPa over southeast Saskatchewan with a warm frontal wave extending eastward through the Interlake region as an upper ridge encompassed the southern Prairies (Figure 4.4). Winds were already responding to the area of low pressure coming from the southwest, advecting in warm temperatures and high dewpoint values.

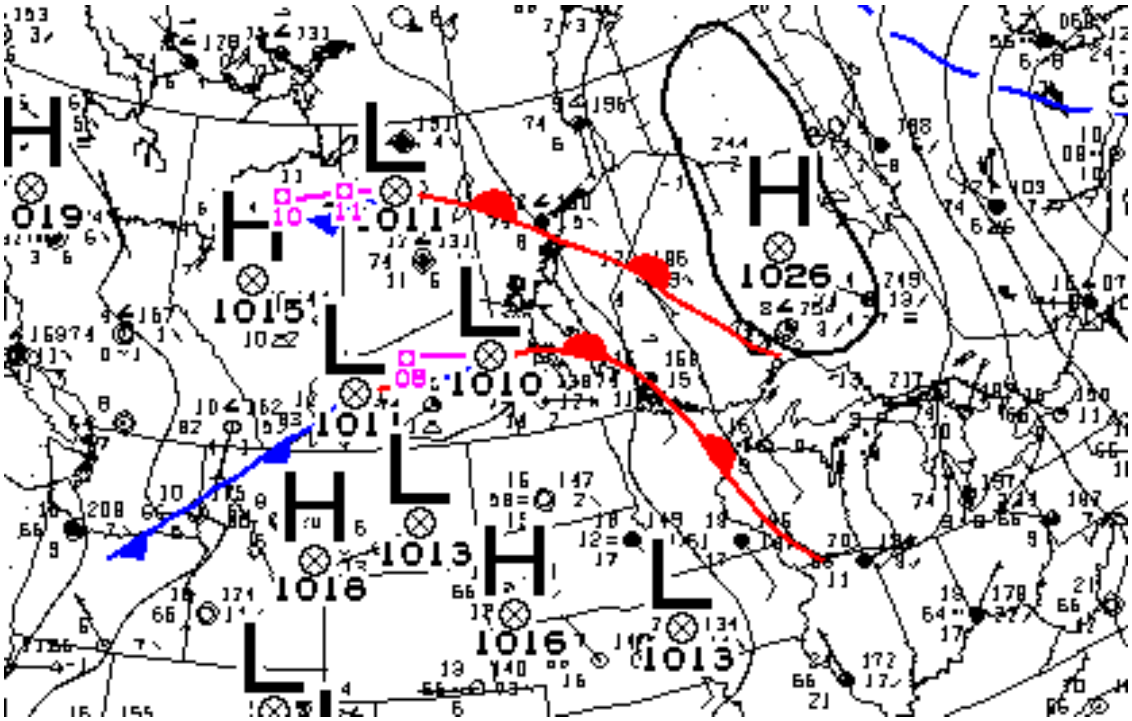

Figure 4.4: June 22nd, 2007 1200 UTC Surface Analysis showing wind speeds (knots), temperatures (°C), dewpoints (°C), pressure tendencies and areas of high and low pressure with fronts added.

At 1800 UTC, the surface low pressure system analyzed at 1008 hPa had moved east to reside over Dauphin Lake (Figure 4.5). Temperatures within the warm sector of the area of low pressure ranged from 26-28 ºC with dewpoints of 18-20 ºC. For the analyses that follow, colored boxes have been inserted to highlight the sites that surround Elie. A summary of surface observations for the sites surrounding Elie is presented in

tables at the end of this section to show in greater detail how the temperature, dewpoint, wind speed and direction changed after 1800 UTC in a tabular format.

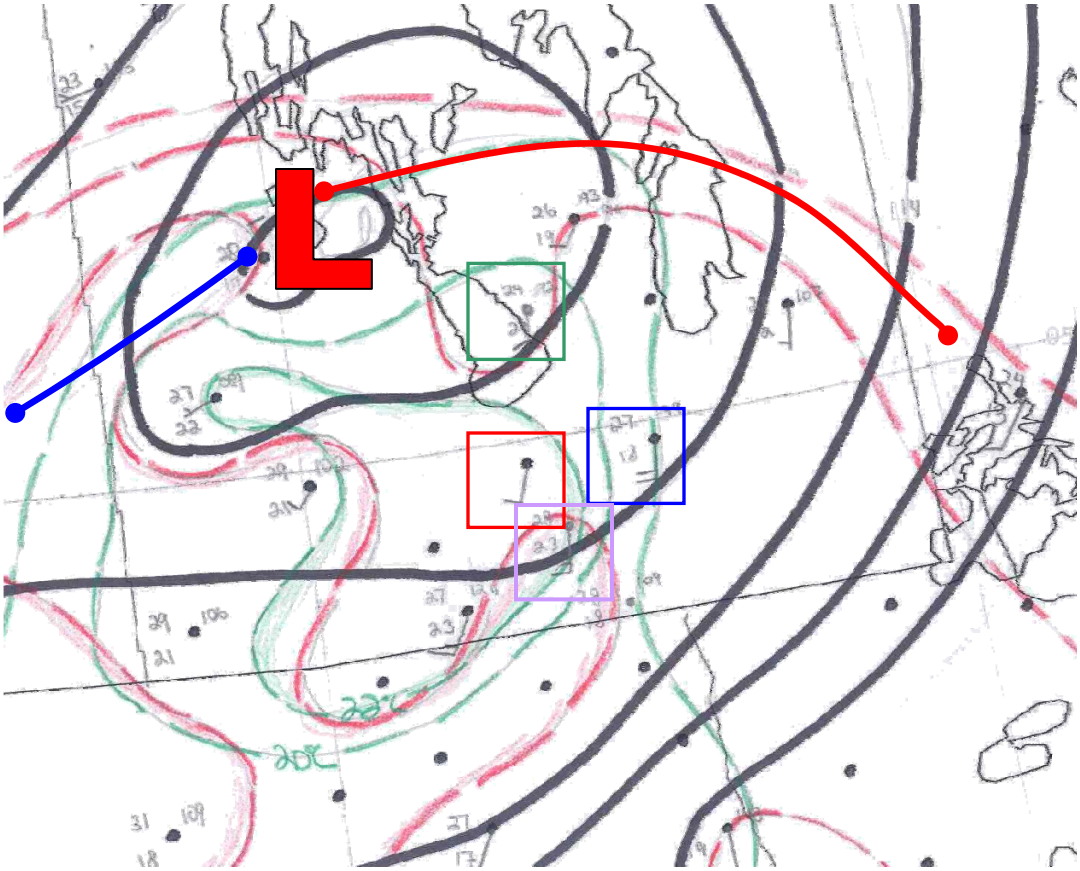

Figure 4.5: 22 June 2007 1800 UTC Surface Analysis showing fronts (warm; red, cold; blue), wind speeds (knots), temperatures (°C), dewpoints (°C), and surface pressure with colored boxes indicating locations surrounding Elie (blue – CYWG:Winnipeg, green – CWOJ:Oak Point, red – CYPG:Portage La Prairie, purple – CWNK: Carman).

The PASPC in Winnipeg launched a weather balloon (station ID CXWI) at 1800 UTC that revealed an unstable atmosphere (1281 J kg $^{-1}$ of CAPE) with a large capping inversion (169 J kg^{-1} of CIN) present at ~920 hPa or roughly 776 m above sea level (ASL) (Figure 4.6).

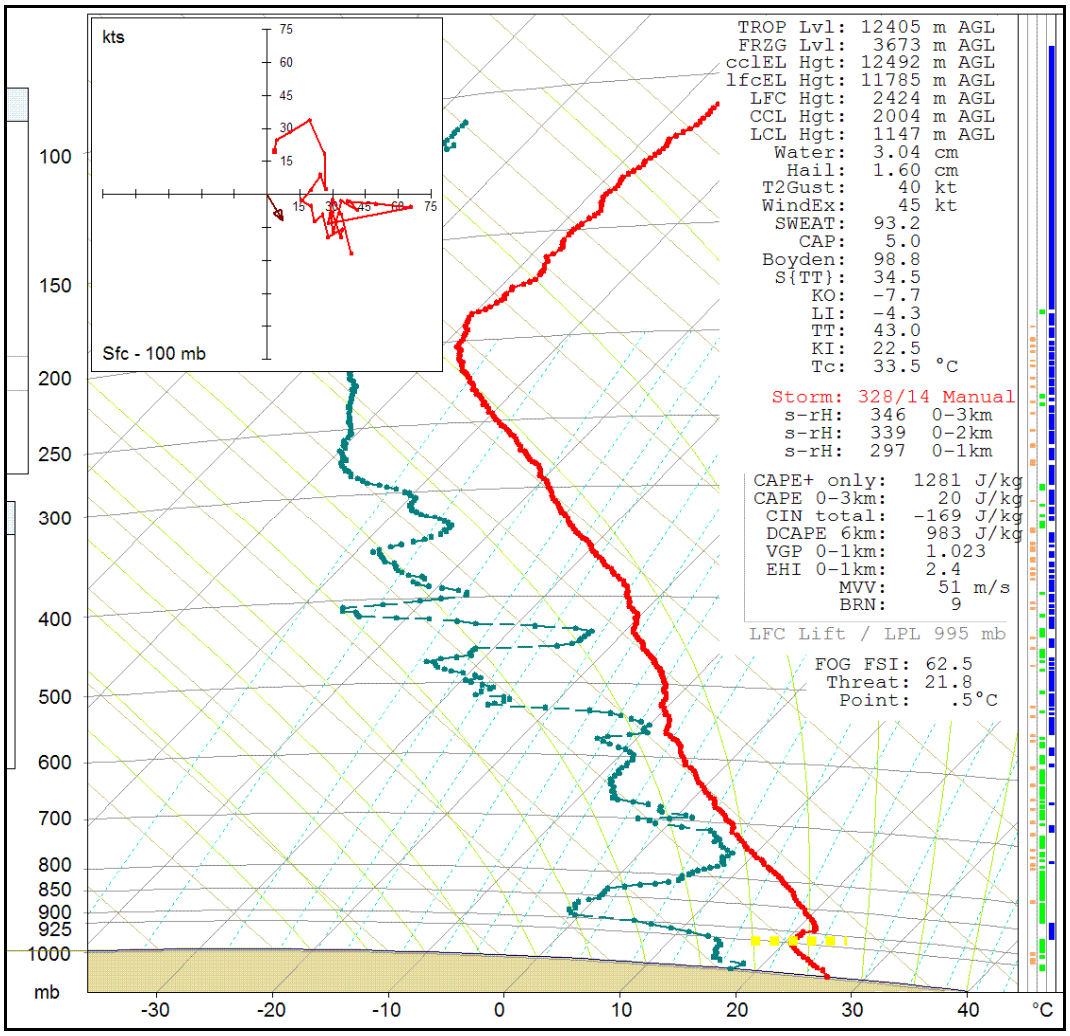

Figure 4.6: 1800 UTC XWI RAOB sounding on 22 June 2007 showing temperature and dewpoint temperature with computed severe weather parameters as the balloon ascended through the atmosphere. Capping inversion highlighted in yellow.

At 2100 UTC, the area of low pressure was analyzed at 1008 hPa and was located over the South Basin of Lake Manitoba with a surface trough extending to the south from the low. Temperatures were 30 ºC within the warm sector and even warmer to the southwest near the Saskatchewan border into North Dakota. An area of higher dewpoint values in excess of 22 ºC was located along the Manitoba Escarpment. These higher dewpoints were advecting north-eastward with the southwest oriented winds that were occurring within the warm sector of the area of low pressure (Figure 4.7).

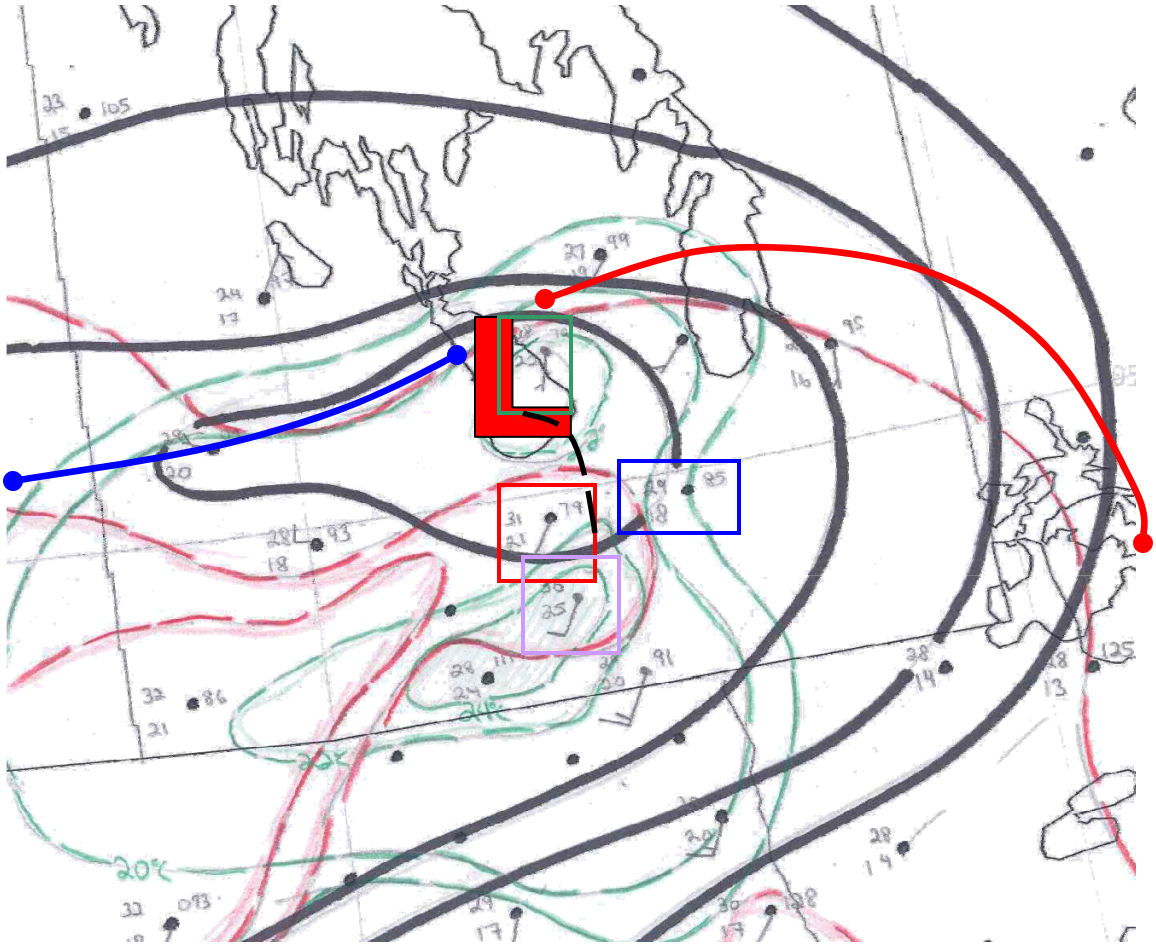

Figure 4.7: 22 June 2007 2100 UTC Surface Analysis showing fronts (warm; red, cold; blue, trough; black), wind speeds, temperatures, moisture, and surface pressure with colored boxes indicating locations surrounding Elie (blue – CYWG:Winnipeg, green – CWOJ:Oak Point, red – CYPG:Portage La Prairie, purple – CWNK: Carman).

At 0000 UTC on 23 June 2007, (after storms were already present) the area of low pressure was quasi-stationary over the Lake Manitoba South Basin with an analyzed surface pressure of 1007 hPa (Figure 4.8). Two tornadoes were now on the ground; one impacting Elie and the other impacting a farmstead near Oakville. Both tornadoes were occurring between Winnipeg and Portage la Prairie. Within the area of low pressure, a surface trough was analyzed denoting a wind shift between Portage La Prairie and Winnipeg. Both tornadoes were occurring very close to this trough. Temperatures had cooled to 23-27 ºC within the warm sector with dewpoint values remaining in the 19-22 ºC range.

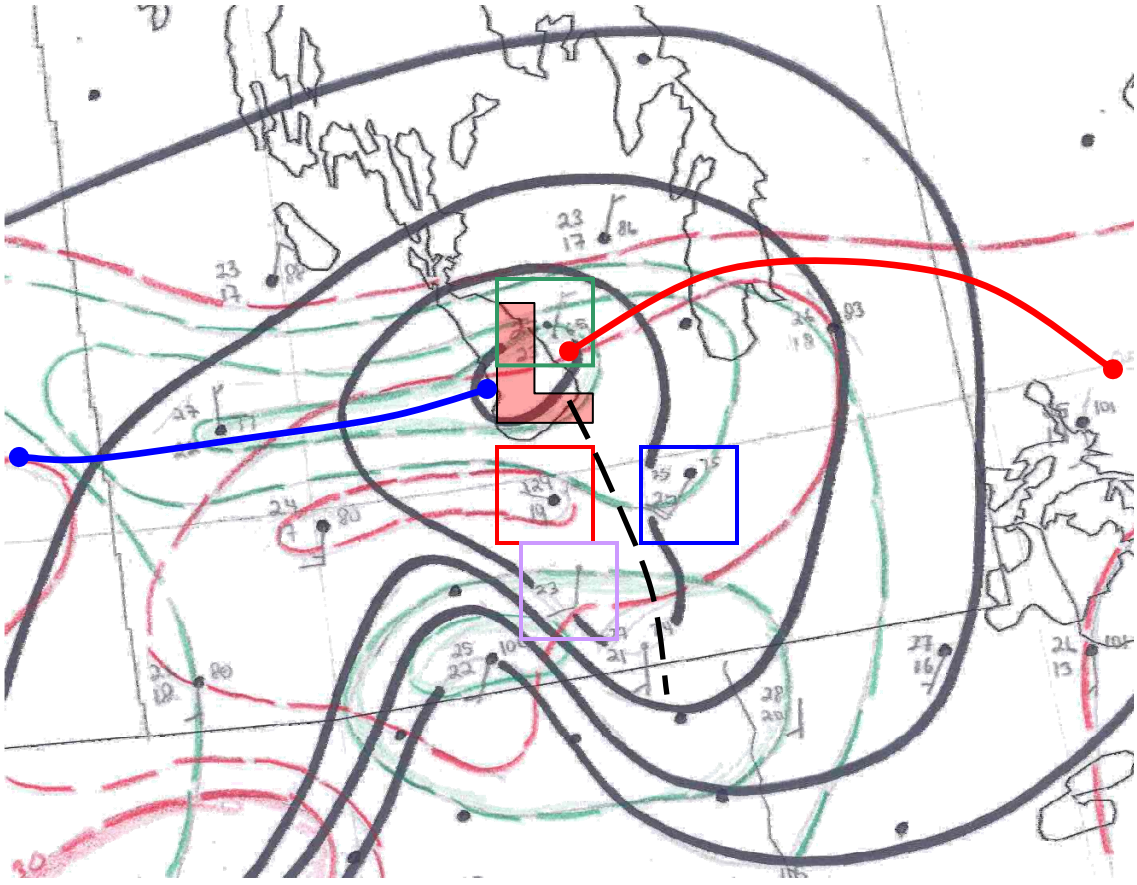

Figure 4.8: 23 June 2007 0000 UTC Surface Analysis showing fronts (warm; red, cold; blue, trough; black), wind speeds, temperatures, moisture, and surface pressure with colored boxes indicating locations surrounding Elie (blue – CYWG:Winnipeg, green – CWOJ:Oak Point, red – CYPG:Portage La Prairie, purple – CWNK: Carman).

In summary, the data mentioned below (Tables 4.1 – 4.5) for the surface observation sites revealed that wind speeds and gusts ranged from 2-12 m s^{-1} within the warm sector of the area of low pressure and the main wind direction was from the south to southwest. Temperature and dewpoint values increased throughout the afternoon with very high dewpoint values occurring upstream of Elie near Carman and along the Manitoba Escarpment.

Oak Point Surface Observations from 1900 UTC – 0000 UTC

WOJ SA 1900 AUTO8 M M M 092**/24/21/1807**/M/ 8016 72MM= **(S Winds at 3.5 m s^{-1})**
WOJ SA 2000 AUTO8 M M M 089/**25/21/2103**/M/ 6017 98MM= **(SSW Winds at 1.5 m s^{-1})**
WOJ SA 2100 AUTO8 M M M 084/**27/22/1804**/M/ 6015 57MM= **(S Winds at 2 m s^{-1})**
WOJ SA 2200 AUTO8 M M M 079**/28/22/1903**/M/ 8011 38MM= **(SSW Winds at 1.5 m s^{-1})**
WOJ SA 2300 AUTO8 M M M 072/**29/22/3203**/M/ 8014 23MM= (**NW Winds at 1.5 m s^{-1}**) **Cold front has moved through**
WOJ SA 0000 AUTO8 M M M 066/**28/23/0208**/M/ 8016 46MM= (**NNE Winds at 4 m s^{-1}**) **A wind shift occurred between 5:00-6:00pm local time probably associated with the cold front that was moving southeast throughout the afternoon**

Table 4.1: Oak Point surface observations showing temperature (°C), dewpoint (°C), wind direction and speed (knots) from 1900 UTC – 0000 UTC on 22 June 2007.

Delta Marsh Surface Observations from 1900 UTC – 0000 UTC

ZUG SA 1900 AUTO8 M M M M/**30/19/2013**+19/M/ PK WND 1919 1851Z M **(SSW Winds at 6.7 m s^{-1} with gusts to 9.7 m s^{-1})**
ZUG SA 2000 AUTO8 M M M M/**31/20/1914**+21/M/ PK WND 1921 1956Z M **(SSW Winds at 7 m s^{-1} with gusts to 11 m s^{-1})**
ZUG SA 2100 AUTO8 M M M M/**32/20/2112**+18/M/ PK WND 2019 2021Z M **(SW Winds at 6 m s^{-1} with gusts to 9.7 m s^{-1})**
ZUG SA 2200 AUTO8 M M M M/**31/20/2808**/M/ PK WND 2017 2100Z M 06MM= **(WNW Winds at 4 m s^{-1} with SSW Gusts to 8.7 m s^{-1}) – *Wind Shift***
ZUG SA 2300 AUTO8 M M M M/**28/20/2906**/M/ M 58MM= **(NW Winds at 3 m s^{-1}) – Cold front has moved through**
ZUG SA 0000 AUTO8 M M M M/**26/16/2313**+23/M/ PK WND 2323 2359Z M **SW Winds at 6.7 m s^{-1} with gusts to 12 m s^{-1} – Winds have switched back again along with a drop in dewpoints. This was probably caused by storm outflow from storms occurring to the South.**

Table 4.2: Delta Marsh surface observations showing temperature (°C), dewpoint (°C), wind direction and speed (knots) from 1900 UTC – 0000 UTC on 22 June 2007.

Carman Surface Observations from 1900 UTC – 0000 UTC

WNK SA 1900 AUTO8 M M M M/**28/23/1912**/M/ PK WND **2017** 1842Z M 44MM= **(SSW Winds at 6 m s^{-1} with gusts to 8.7 m s^{-1})**
WNK SA 2000 AUTO8 M M M M**/29/23/2012**/M/ M 86MM= **(SSW Winds at 6 m s^{-1})**
WNK SA 2100 AUTO8 M M M M/**30/25/2011**+16/M/ M 60MM= **(SSW Winds at 5.5 m s^{-1}) – Very impressive dewpoint values indicative of pooling south of the Gunton Bedrock Escarpment**
WNK SA 2200 AUTO8 M M M M/**30/25/2211**/M/ PK WND 2417 2137Z M 96MM= **(SW Winds at 5.5 m s^{-1} with gusts to 8.7 m s^{-1})**
WNK SA 2300 AUTO8 M M M M/**30/25/2211**/M/ PK WND 2317 2206Z M 79MM= **(SW Winds at 5.5 m s^{-1} with gusts to 8.7 m s^{-1})**
WNK SA 0000 AUTO8 M M M M/**27/24/2106**/M/ M 34MM= (**SSW Winds at 3 m s^{-1}**) **– Pair of tornadoes were occurring North of Carman at this time with wind direction still oriented from the southwest**

Table 4.3: Carman surface observations showing temperature (°C), dewpoint (°C), wind direction and speed (knots) from 1900 UTC – 0000 UTC on 22 June 2007.

Winnipeg Surface Observations from 1900 UTC – 0000 UTC

YWG 1900 Winds SSE at 7.7 m s^{-1}. Temperature: 28 Dewpoint: 19.
YWG 2000 Winds SW at 5 m s^{-1}. Temperature: 29 Dewpoint: 17.
YWG 2100 Winds SW at 5 m s^{-1}. Temperature: 29 Dewpoint: 18.
YWG 2200 Winds SSW at 5 m s^{-1}. Temperature: 28 Dewpoint: 19.
YWG 2300 Winds SE at 2.6 m s^{-1}. Temperature: 27 Dewpoint: 19.
YWG 0000 Winds SW at 10 m s^{-1}. Temperature: 25 Dewpoint: 20.

Table 4.4: Winnipeg surface observations showing temperature (°C), dewpoint (°C), wind direction and speed (knots) from 1900 UTC – 0000 UTC on 22 June 2007.

Portage la Prairie Surface Observations from 1900 UTC – 0000 UTC

YPG 1900 Winds SSW at 7.7 m s^{-1}. Temperature: 30 Dewpoint: 21.
YPG 2000 Winds SW at 5 m s^{-1}. Temperature: 31 Dewpoint: 20.
YPG 2100 Winds SW at 5 m s^{-1}. Temperature: 31 Dewpoint: 21.
YPG 2200 Winds SW at 5 m s^{-1}. Temperature: 31 Dewpoint: 21.
YPG 2300 Winds WNW at 10 m s^{-1}. Temperature: No Data Dewpoint: No Data.
YPG 0000 Winds WNW at 2.6 m s^{-1}. Temperature: 24 Dewpoint: 19.

Table 4.5: Portage la Prairie's surface observations showing temperature, dewpoint, wind direction and speed (knots) from 1900 UTC – 0000 UTC on 22 June 2007.

4.1.3 - Mesoscale Features

Horizontal convective rolls (HCRs) could be seen at 1800 UTC (figure 4.9) on the Woodlands CLOGZ LOLAA Doppler imagery oriented from the southwest to the northeast showing that the boundary layer winds originated from the southwest. The HCRs continued to occur throughout the afternoon. Moisture could also be seen advecting north-eastward on the radar from North Dakota along the Gunton Bedrock Escarpment (GBE) located to the southeast of Lake Manitoba which rises from approximately 248 m ASL to 272 m ASL as you progress 47 km northwest from Winnipeg.

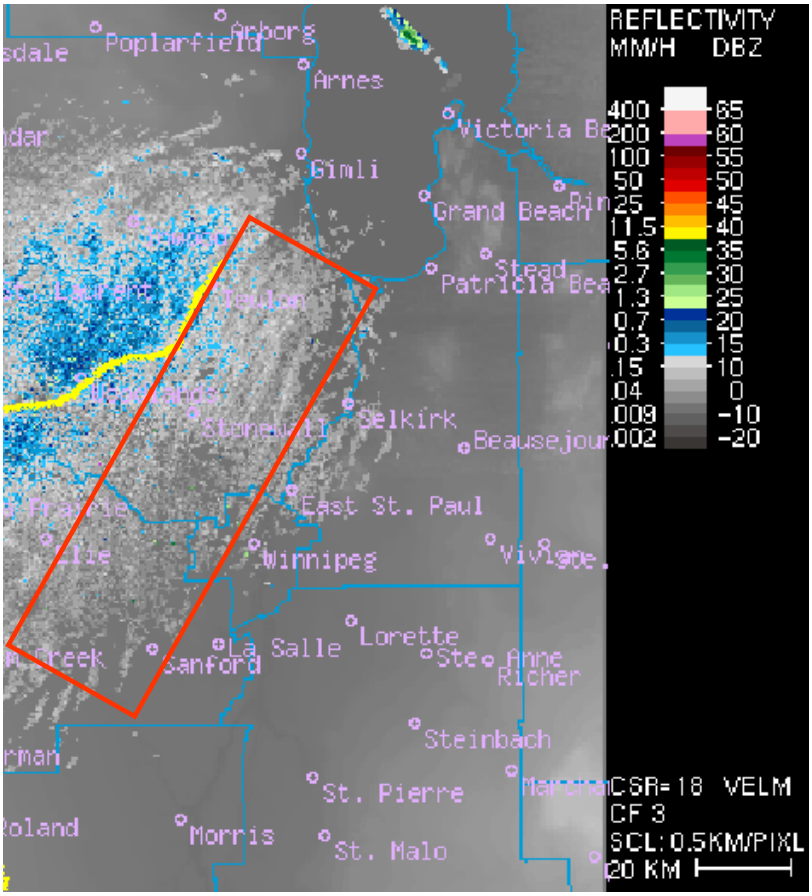

Figure 4.9: CLOGZ LOLAA Imagery showing horizontal convective rolls (red box) and Gunton bedrock escarpment (yellow line) at 1800 UTC.

An elevated thunderstorm developed near Portage La Prairie, MB at 1810 UTC (figure 4.10) that propagated southeast towards St. Malo, MB where it later dissipated at 2020 UTC (not shown). A severe thunderstorm watch was issued at 1828 UTC for most of southern Manitoba.

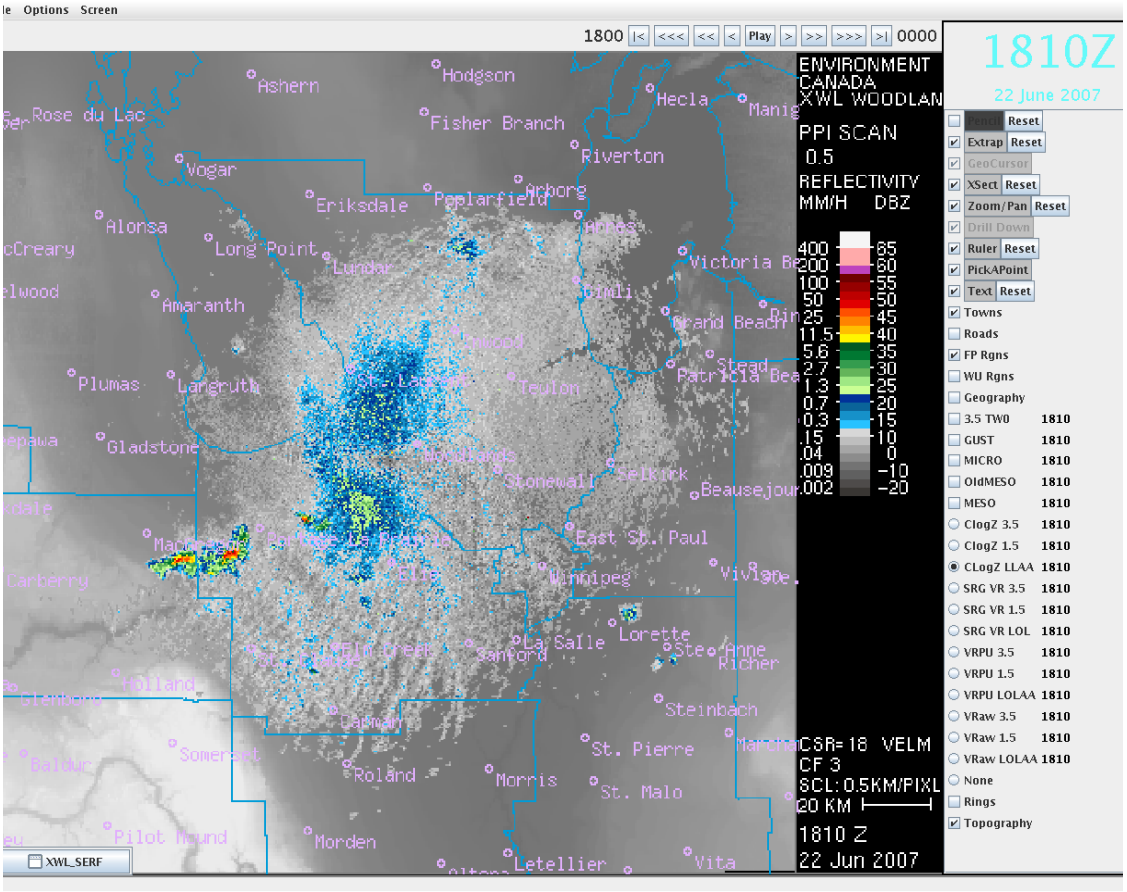

Figure 4.10: CLOGZ LOLAA imagery at 1810 UTC showing elevated thunderstorm developing to the south of Lake Manitoba.

At 2140 UTC, the cold front associated with the area of low pressure and a lake breeze boundary (LBB) moved from Lake Manitoba towards Woodlands, MB to the west of the HCRs (Figure 4.11). The cold front, LBB and HCRs were all occurring within the warm sector of the analyzed area of low pressure shown earlier in figure 4.7.

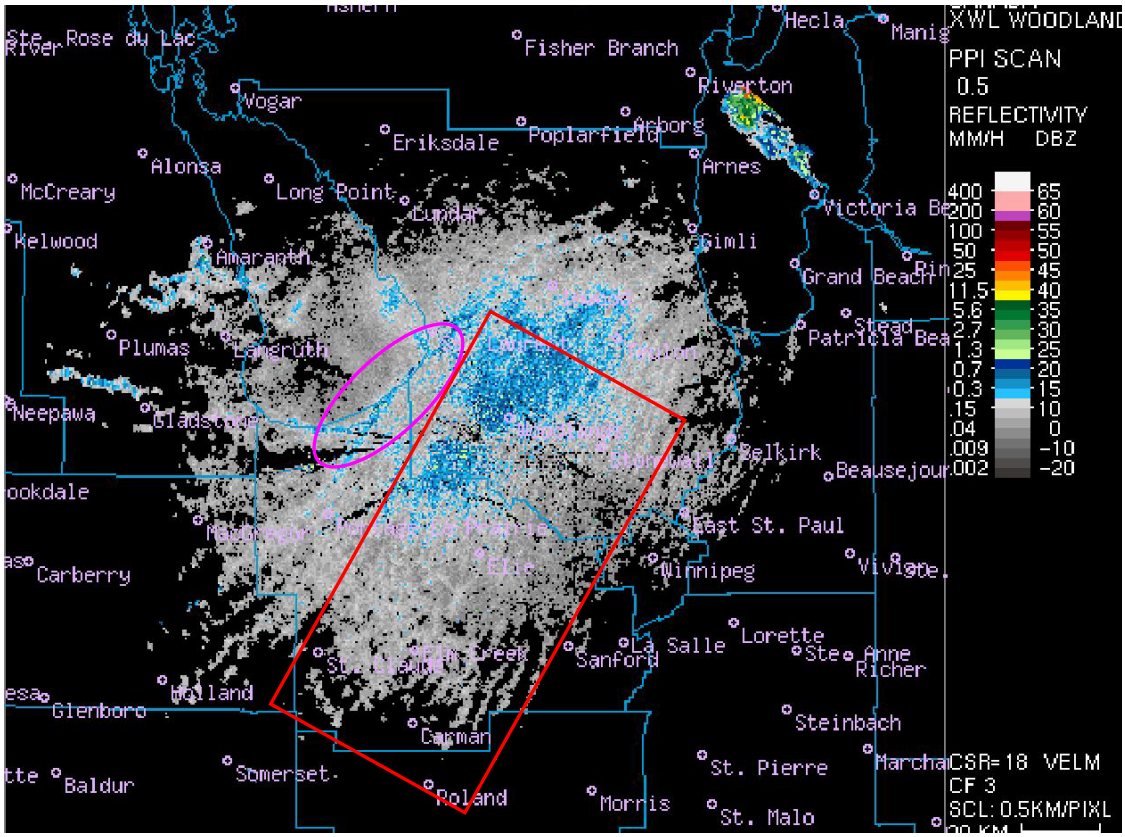

Figure 4.11: CLOGZ LOLAA Imagery at 2140 UTC showing cold front and lake breeze boundary emerging from Lake Manitoba (pink oval) with HCRs occurring within the red box.

At 2150 UTC, low-level convergence was likely occurring within the boundary layer and this could be seen ahead of the cold front, LBB and within the area of HCRs on the radar scan (Figure 4.12). The surface low was located west of Woodlands, Manitoba.

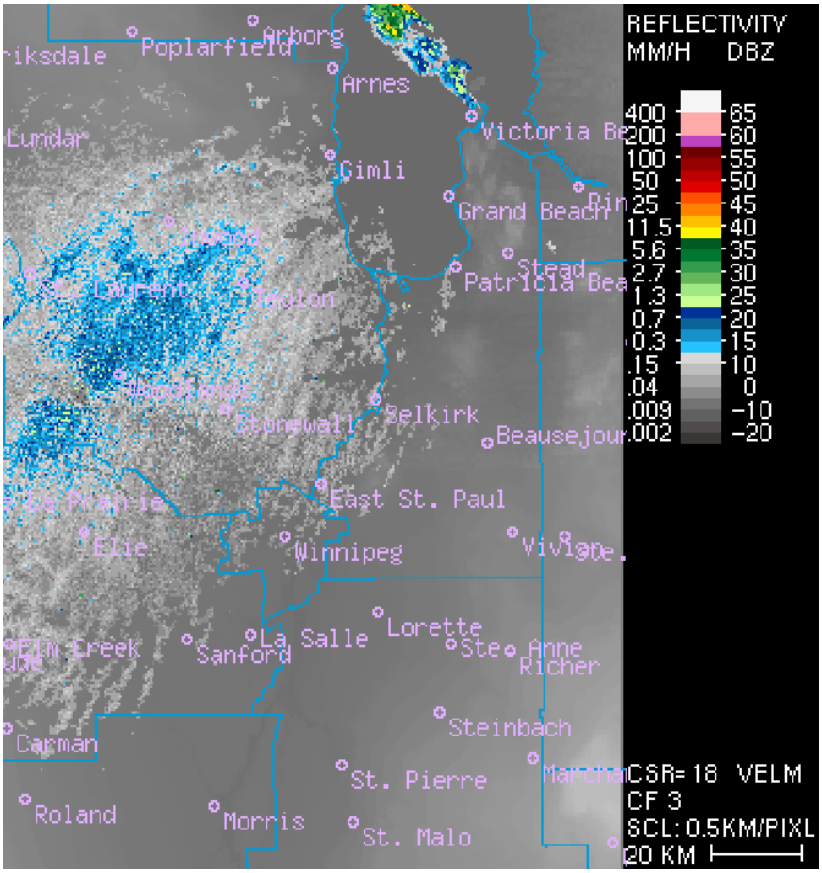

Figure 4.12: CLOGZ LOLAA imagery at 2150 UTC showing low-level convergence along the Gunton Bedrock Escarpment (area of blue).

At 2200 UTC, a gravity wave located 36 km to the southwest of Woodlands, MB was identified on the ClogZ1.5 (Figure 4.13) and ClogZ LOLAA (Figure 4.14) scans moving at 10 m s^{-1} normal to the HCR's and LBB.

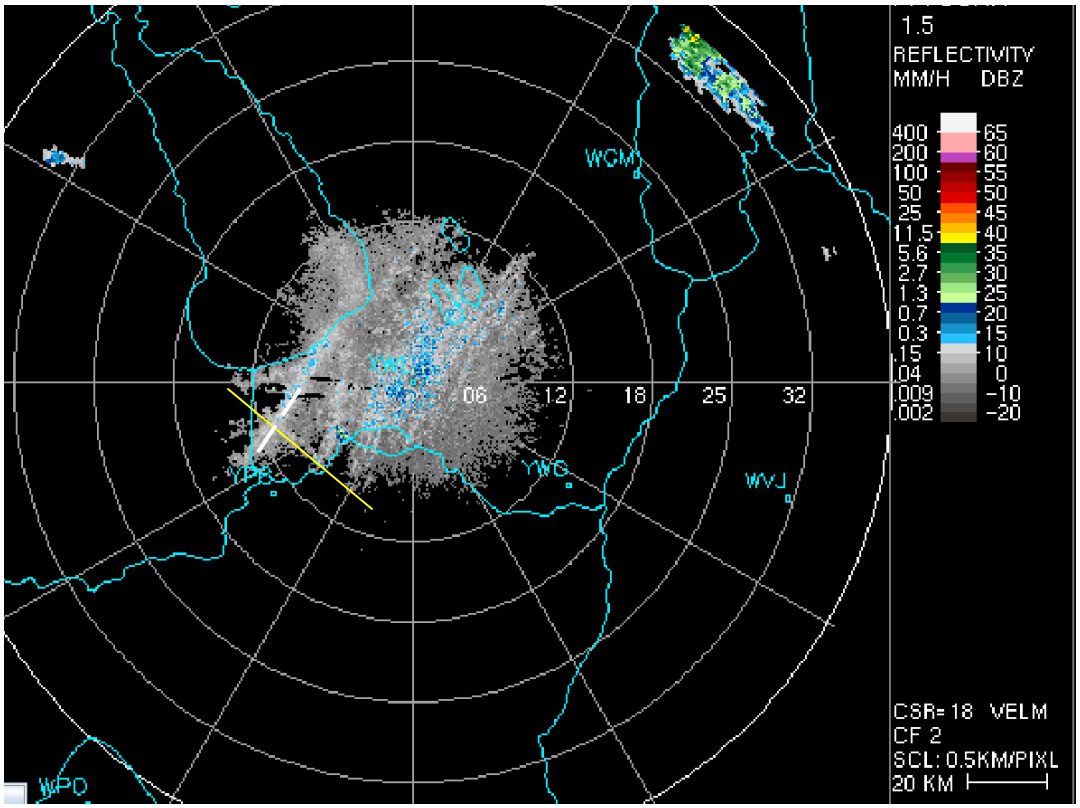

Figure 4.13: 2200 UTC CLogZ 1.5 imagery showing gravity wave (yellow line) moving normal to the HCRs (white dashed line).

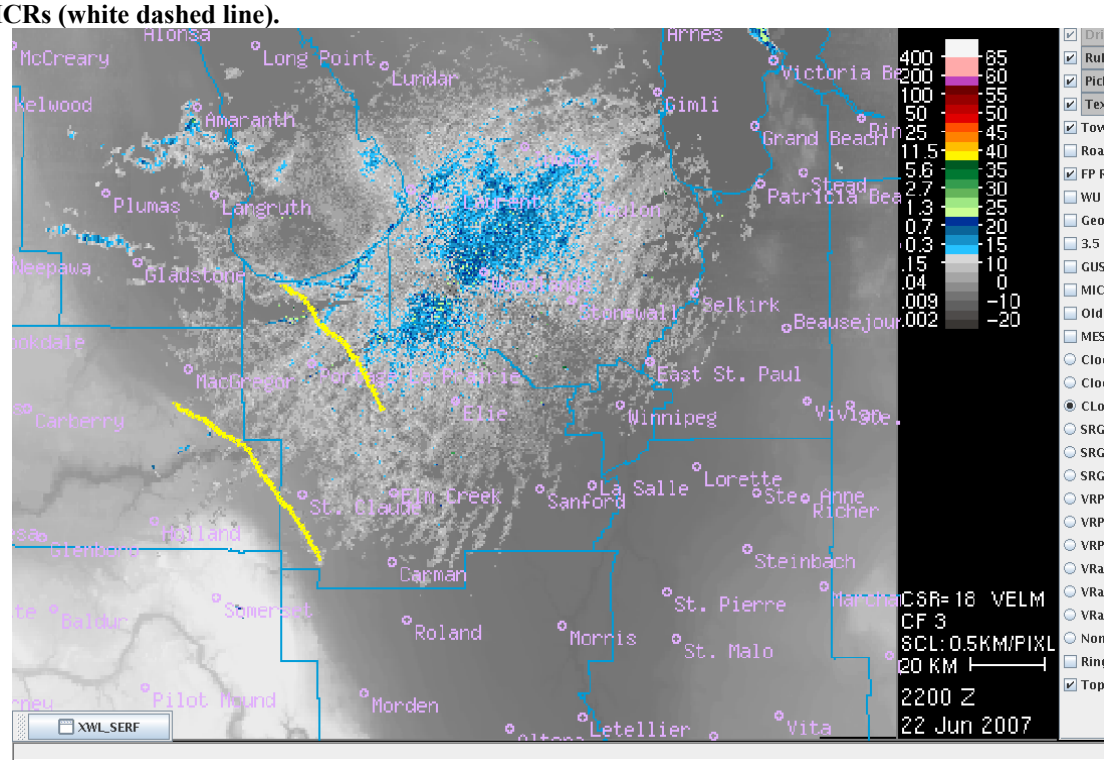

Figure 4.14: 2200 UTC CLOGZ LOLAA Imagery showing gravity waves (in yellow) originating from the Manitoba Escarpment.

The gravity waves were spaced approximately 39 km apart from each other and originated from the Manitoba Escarpment (ME) oriented from the southeast to northwest from Morden to MacGregor, MB where it transitions into the Riding Mountains to the northwest. The Manitoba Escarpment rises to ~490 m above sea level (ASL) over a short distance. The height of the ME adjusted to AGL from the radar site (height of radar at 12 m incorporated) equates to around 208 m AGL near its highest elevation. The height of the gravity waves, by using the elevation angle of 0.5 degrees on the low level Doppler and the range of the waves from the radar at 36 km (Dave Patrick; personal communication, 2010), gave a corresponding height above the ground of 391 m. The height of the gravity waves with its associated crest (391 m AGL) corresponds to the height of the terrain (208 m AGL) in which the gravity wave originated. Based on the Brunt-Vaisala formulas introduced earlier (Equations 2-4), the period of oscillation was calculated to be 445.8 seconds using the 1800 UTC Winnipeg surface observations and the 1800 UTC XWI sounding data to determine the environmental lapse rate below the inversion. The wavelength was calculated to be 33.6 km and is approximately 5.4 km different in terms of what the measured spacing was between the gravity waves on the radar.

At 2210 UTC, the gravity waves continued moving northeast where they began to intersect the HCRs that were present ahead of the LBB and surface trough near the GBE. The combination of lift associated with the gravity waves and the ascending branch of the HCR interacted with the low level moisture that had been located along the GBE during the afternoon. Lift below the capping inversion from the contributions of the mesoscale features (based at 920 hPa or 776 m ASL) aided in triggering convection at 2210 UTC.

4.1.4 – Hodograph Analysis

An analysis of the 1800 UTC XWI hodograph revealed that there was strong low level shear (horizontal vorticity generation) with 0-1 km values of 12 m s^{-1} as well as clockwise curvature with height that extended to 6 km above the surface. The storm motion according to the XWI hodograph was to the southeast at 7 m s^{-1} if a storm developed. The storm motion estimation was made using the Bunkers method (Bunkers et al., 2000) in the universal rawinsonde observation program (RAOB) that was used to analyze the hodographs. There were large 0-1 km SRH values (297 m^2 s^{-2}) along with large 0-3 km SRH values (346 m^2 s^{-2}) which revealed an increased threat of strong tornadoes as Davies-Jones et al. (1990) suggested (Figure 4.15).

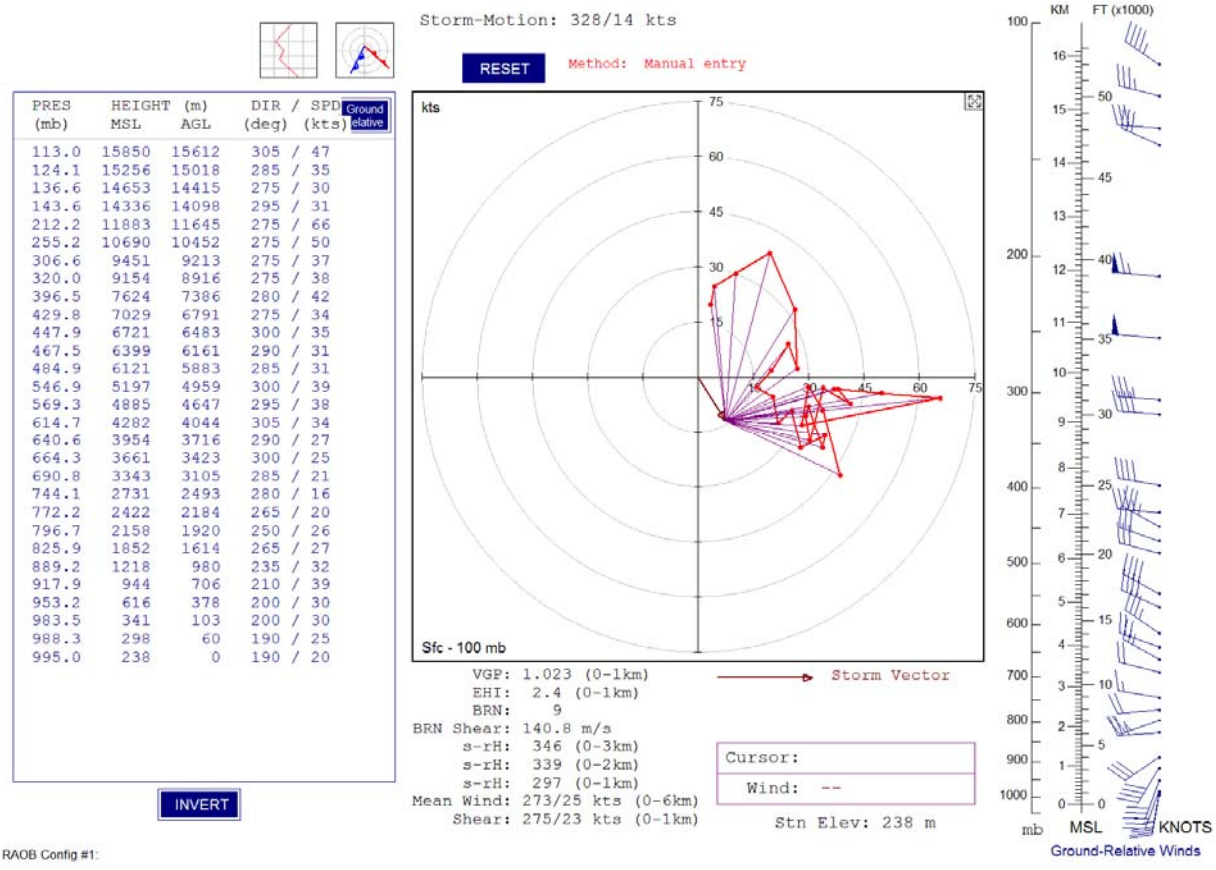

Figure 4.15: 22 June 2007 1800 UTC XWI Hodograph showing wind direction and speed (knots) at different heights in the atmosphere along with calculated storm parameters.

The VAD data from the Woodlands radar site was used and compared to the XWI hodograph at 1800 UTC to illustrate the similarities between the two. The 1800 UTC VAD hodograph (Figure 4.16) revealed that 0-1 km shear values were 14 m s^{-1} and the 0-1 km SRH values (335 m^2 s^{-2}) as well as the 0-3 km SRH values (351 m^2 s^{-2}) were large. The storm motion was to the southeast at 5 m s^{-1} which was similar to the 1800 UTC XWI hodograph. The main difference between the XWI hodograph and the VAD hodograph was that the VAD hodograph had greater helicity values at low levels. This difference can be explained due to the location of the radar site and from where the balloon was launched. The radar is located near Woodlands which is 55 km away from where the balloon was originally launched and the environmental conditions can vary significantly between two sites. When a balloon is launched, it is carried with the upper winds so the hodograph that results is not a true representation of the point from which the balloon was launched. However, examining the wind direction and speed changes with height between the XWI hodograph and the VAD hodograph revealed that the two hodographs were comparable from 850 hPa to 500 hPa at 1800 UTC. After analyzing the 10-minute VAD hodographs from the XWL radar from 1800 UTC up to storm initiation at 2210 UTC, it was decided that the VAD hodograph data was sufficient to use at low-levels for the pre-storm environment since the balloon that was launched at 1800 UTC may not have been representative at the low-levels for times and locations much beyond its launch time.

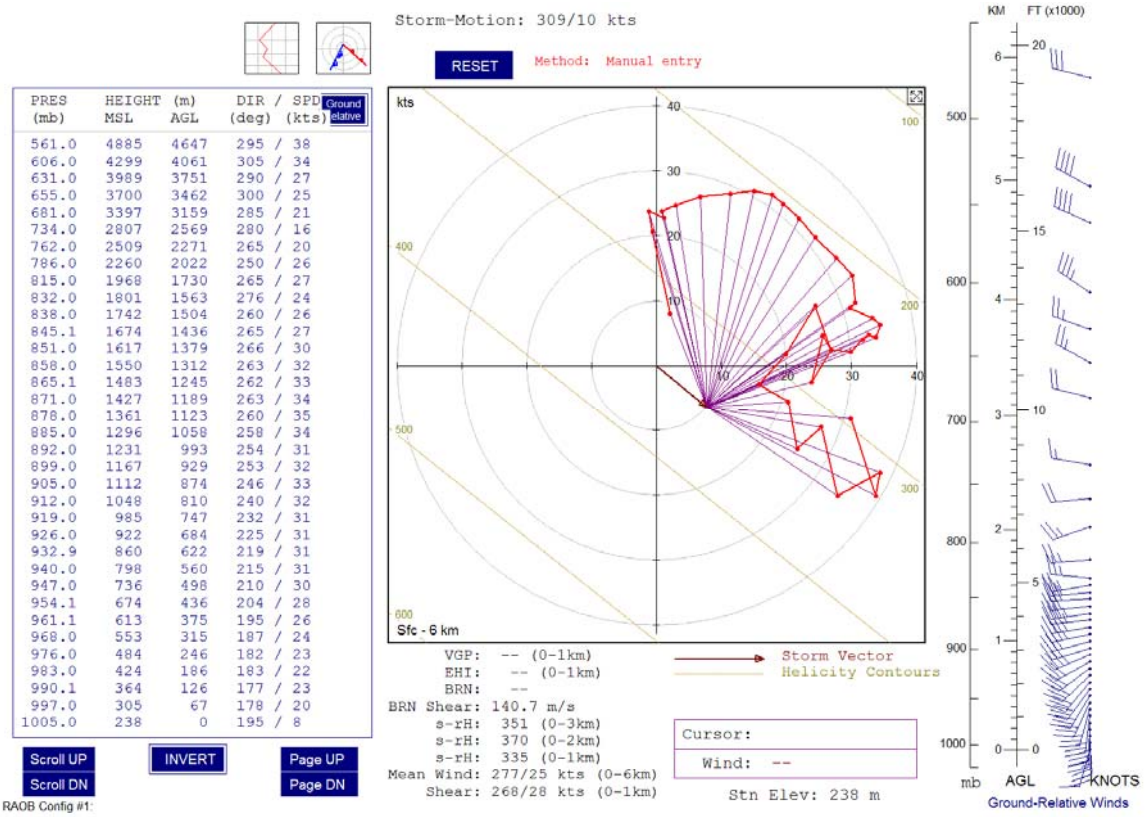

Figure 4.16: 22 June 2007 1800 UTC VAD Hodograph showing wind direction and speed (knots) at different heights in the atmosphere along with calculated storm parameters.

From 1800 UTC until 2210 UTC, a 10-minute hodograph analysis was performed to see how the low level wind field and helicity changed prior to storm initiation at 2210 UTC (Table 4.5).

The 2210 UTC VAD hodograph (Figure 4.17) combined with the XWI sounding mid-level wind data after 1800 UTC is similar to many of the Miller (2006) soundings and hodographs, exhibiting the hodograph kink (see Chapter 1).

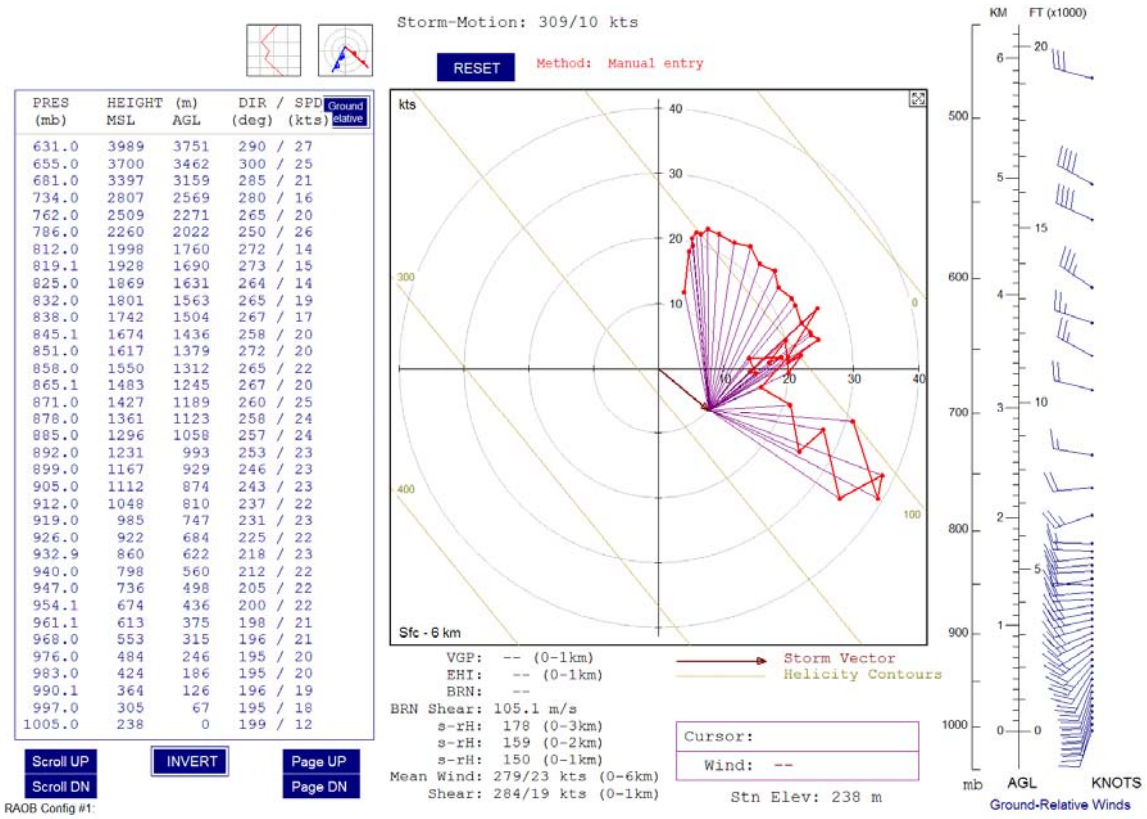

Figure 4.17: 2210 UTC Hodograph showing wind direction and speed (in knots) at different heights in the atmosphere along with VAD-derived storm parameters.

The 2210 UTC XWL VAD hodograph provided the best information for what was occurring at the low-levels because it provided a tracer of the environmental winds just before convective initiation. After 2210 UTC, cells rapidly developed, contaminating the radar VAD (chapter 3) which resulted in deficiencies in the calculations of the low level winds.

Based on the 2210 UTC VAD hodograph, from the surface to 126 m AGL, the hodograph showed increasing shear with the wind direction nearly constant from 195 degrees with an increase in speed from 6 m s^{-1} at the surface to 10 m s^{-1} at 126 m AGL. From 126 m AGL to 500 m AGL, the wind speed remained fairly constant around 10-11 m s^{-1} but there is a directional change from 195 degrees at 126 m AGL to approximately 205 degrees at 500 m AGL. From 500 m AGL to 1 km AGL, the wind speed is nearly

constant around 12 m s^{-1} but there is a greater directional change from 205 degrees at 500 m AGL to 257 degrees at 1 km AGL. From 500 m AGL to 1 km AGL, speed shear is nearly constant, but the directional shear component began to dominate resulting in a hodograph kink. The increased turning with height from the surface to 3 km of greater than 80 degrees in combination with the speed shear showed that once storms developed, there was be a high tendency for them to rotate due to the high helicity values that were present. The 0-1 km shear was 10 m s^{-1}, and the calculated 0-1 km SRH / 0-3 km SRH values (150 m^2 s^{-2} / 178 m^2 s^{-2}) were sufficient for a heightened tornado threat. This environment was characterised as having a significant component of streamwise vorticity below 3 km as the low-level storm relative inflow was mainly parallel to the horizontal vorticity vector and normal to the vertical wind shear vector.

Table 4.5 refers to the VAD hodograph information that was part of the radar analysis in the next section. As mentioned earlier, these calculated values are accurate but the values are probably estimates because of the calculation errors attributed to the storms that were developing on the radar. However, they were important because they provided some information leading up to and after tornadogenesis. The table shows that from 2210 UTC, the 0-3 km SRH values remained nearly constant (178 m^2 s^{-2}) until storms began to mature on the radar. The SRH was calculated with the observed storm motion on radar to the southeast at approximately 5 m s^{-1}. The 0-1 km SRH spiked at 2220 UTC (182 m^2 s^{-2}) but dropped as the storms strengthened. The 0-6 km mean wind remained constant from 2210 - 0000 UTC (12 m s^{-1}) and the 0-1 km shear did not change significantly during the same time. SRH values were higher before cell contamination took place after 2240 UTC. After 2240 UTC, errors in calculations began to increase as

the radar was now detecting several storms and had to now discern between returns heading toward and away from the radar. When comparing the SRH values to what is frequently observed for a significant tornado, it is apparent that these values are substantially lower than what is typically seen for strong tornadoes; but this may be attributed to calculation errors in the VAD winds.

Time (UTC)	0-3 km SRH values in $m^2 s^{-2}$	0-1 km SRH values in $m^2 s^{-2}$	0-6 km mean wind in m s^{-1} (direction in degrees)	0-1 km wind in m s^{-1} (direction in degrees)
2210	178	150	12 (270)	10 (284)
2220	174	182	12 (279)	11 (292)
2230	NO DATA	NO DATA	NO DATA	NO DATA
2240	178	140	12 (281)	6 (232)
2250	78	54	12 (281)	4 (267
2300	86	94	13 (282)	9 (265)
2310	65	68	12 (284)	8 (243)
2320	59	47	12 (285)	7 (264)
2330	84	30	12 (284)	6 (230)
2340	21	42	12 (286)	11 (284)
2350	23	-14	12 (285)	6 (251)
0000	22	-8	12 (285)	6 (258)

Table 4.6: Hodograph Evolution Summary from 2210 UTC – 0000 UTC showing 0-3 km, 0-1 km SRH values along with 0-6 km and 0-1 km wind values and direction.
* Denotes pre-storm and initiation time
* Denotes missing data (Radar had data error and no VAD data was available)
* Denotes storm developing
* Denotes time period when tornado is on the ground

4.1.5 – Thermodynamic Sounding Data Analysis

The 1800 UTC thermodynamic diagram was used with modified surface temperature and moisture observations from Carman, Manitoba at 2200 UTC just prior to convective initiation (Figure 4.18). Using Carman as the representative observation site for temperature and moisture at 2200 UTC in combination with the 1800 UTC XWI mid and upper-level thermodynamic data was decided since the wind direction was from the southwest and Elie was located 45 km downstream from Carman. The air mass surrounding Elie would have therefore been very similar to what was occurring in

Carman. One major change in the near surface level which cannot be accounted for due to data availability is how deep the low-level moisture was. It is therefore assumed that the lifting of the parcel will take place from the surface without the low-levels being mixed. The thermodynamic diagram revealed large values of CAPE (6330 J kg^{-1}) and no CIN when using the Carman surface data. The CIN values (170 J kg^{-1}) that existed earlier on the 1800 UTC XWI thermodynamic diagram were now removed.

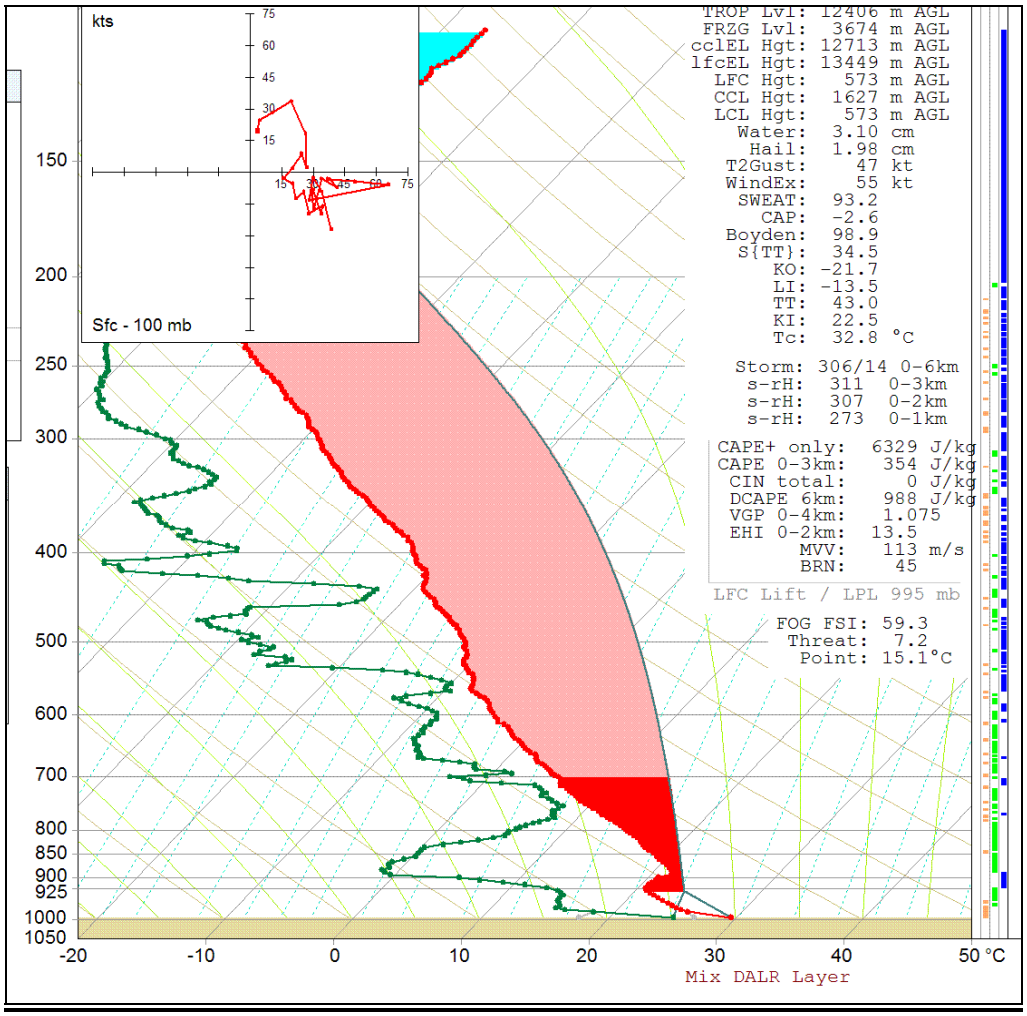

Figure 4.18: 22 June 2007 Carman, Manitoba thermodynamic sounding for 2200 UTC showing temperature (°C), and dewpoint (°C) with computed severe weather parameters as balloon ascended through the atmospheric column.

Using the same levels that were examined in the hodograph at 2210 UTC, we see that from the surface to 126 m AGL there was an exceptionally moist and humid near-

surface air mass with T/Td of 30/25 ºC at the surface to 26/18 ºC at 126 m AGL. As the parcel ascended from 126 m AGL to 500 m AGL the temperatures cooled and the moisture decreased to 22/15 ºC. From 500 m AGL to 1 km AGL the temperature remained constant, but moisture was drastically lower at -1 ºC. It cannot be known for sure exactly how the low-levels changed. However, given the time of the year, we can assume that there was a constant supply of moisture in the lowest couple of hundred meters above the ground from evapotranspiration, and advection. In addition, the low level jet as seen in the previous section had a southerly component in this region for over 3 days which was favourable for moisture transport from the Gulf of Mexico and areas that are moisture rich due to evapotranspiration especially during the latter part of June. The temperature and dewpoint observations at the surface resulted in a low lifted condensation level for a surface parcel of 573 m AGL.

Referring back to the study done by Miller (2006; Chapter 1), the mean values of the parameters used in his analysis were similar to the values seen on the VAD/XWI adjusted sounding on 22 June 2007 which makes the Elie case fit in with Miller's results with what is considered to be a significant tornado day before the tornado even developed. Table 4.6 shows the values from 22 June 2007 compared to Miller's parameters. It can be noted that most of the parameters that were calculated on 22 June 2007 prior to initiation were in fact more exceptional than those required for significant tornadoes suggested by Miller's guidelines.

Parameter Name	22 June 2007 Parameters	Miller Parameters
Surface Temperature	**30 ºC**	**25 ºC**
Surface Dewpoint	**25 ºC**	**20 ºC**
Surface Temperature/Dewpoint Spread	**5 ºC**	**5 ºC**
Surface relative humidity	**75%**	**68%**
CAPE	**6330 J kg^{-1}**	**3445 J kg^{-1}**
CIN	**0 J kg^{-1}**	**42 J kg^{-1}**
LCL height (AGL)	**573 m**	**900 m**
LFC height (AGL)	**573 m**	**1628 m**
Height of hodograph kink (AGL)	**500 m**	**418 m**
Shear vector magnitude (sfc-kink)	**10 m s^{-1}**	**10 m s^{-1}**
Shear vector magnitude (sfc-1 km AGL)	**12 m s^{-1}**	**14 m s^{-1}**

Table 4.7: Elie Parameters compared to Miller's mean guideline parameters (Miller, 2006).

The parameters are important because by having the guidelines established by Miller we can determine which days are more conducive to significant tornadoes. If there is ample instability and deep layer shear for supercells in combination with greatly sheared and moist low levels, then the likelihood of strong tornadoes is increased.

4.2 - During the Storm

4.2.1 - Radar Analysis

Initiation rapidly commenced shortly after 5:00 pm local time or 2200 UTC. Data used in monitoring the storm evolution via URP became available at 5:40 pm local time or at 2240 UTC. A brief analysis is given from 2210 UTC to 2240 UTC, but from that point on, reference to figure 4.19 should be maintained for the storm shape of the three storms (A, B, C) that occurred. Each number represents the storm and its shape at each specific time (1 = 2240 UTC, 2 = 2300 UTC, 3 = 2320 UTC, 4 = 2340 UTC, 5 = 0000 UTC). The storm shapes are supplemented with a range of different shades with the darkest shades being the oldest scans (2240 UTC) and the lightest shades being the newest scans (0000 UTC) to show where the storm was spatially in relation to other scans. The outlined shape of each cell was determined based on radar reflectivities at or above 20 dBZ that were analyzed every 20 minutes. Radar reflectivity, radar velocity, visible satellite, and still photographs will also be incorporated into the analysis at different times when significant changes occurred and therefore required more detailed information. For the radar velocity analysis, gate-to-gate velocities were used to assess the strength of the low-level mesocyclone by identifying a velocity couplet. The velocity couplets were identified where there was a sudden change that occurred that over a small area from targets heading towards the radar and away from the radar. The National Severe Storms Laboratory (NSSL) in the United States uses very low velocity difference thresholds (minimum 11 m s^{-1}) to identify the individual gate-to-gate velocity pairs which indicate that there is relatively high shear; which can classify the circulation as either tornadic, potentially tornadic or non-tornadic (Mitchell et al., 1997). The gate-to-gate

velocities are a cumulative total of the velocity of inbound and outbound targets. Table 4.8 refers to storm B's parameters (Elie storm) that were monitored and analyzed at specific times between 2240 UTC and 0000 UTC. Section 4.2.2 is a more in depth analysis of the tornado itself in terms of the width and how it tracked after it touched down at approximately 2330 UTC.

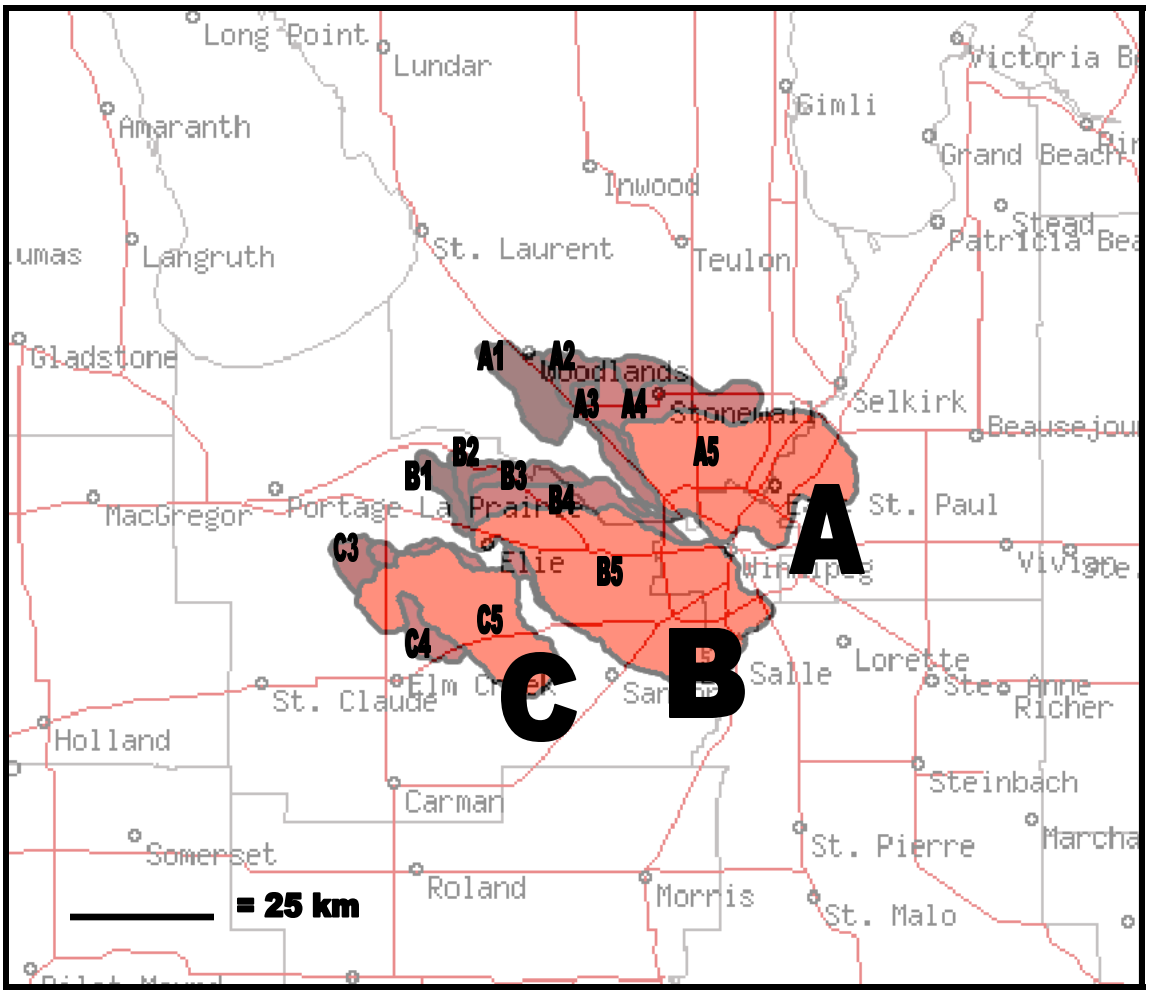

Figure 4.19: Radar map showing the evolution every 20 minutes of three supercells (A,B,C) that occurred on 22 June 2007. Storm outlines drawn where low-level reflectivities were at or above 20 dBZ with darkest shades showing the oldest cells at 2240 UTC and the lightest shades showing the newest cells at 0000 UTC. Numbers also denote the time the cells were occurring (1 = 2240 UTC, 2 = 2300 UTC, 3 = 2320 UTC, 4 = 2340 UTC, 5 = 0000 UTC). Cells were overlaid on the XWL Woodlands URP Doppler radar image.

CELL	Time	Height (km) AGL of BWER (Bounded Weak Echo Region)	Gate-to-gate Velocity (m s^{-1})
B1	**2240**	N/A	no couplet
	2250	N/A	no couplet
B2	**2300**	7.6	20
	2310	N/A	20
B3	**2320**	N/A	36
	2330	8.1	32
B4	**2340**	7.8	30
	2350	6.2	42
B5	**0000**	10.8	44
	0010	9.2	no couplet

Table 4.8: Storm B parameters from 22 June 2007 analyzed from 2240 UTC to 0000 UTC.

At 2210 UTC, rapid storm development was occurring 45 km northwest of Winnipeg or 18 km northwest of Elie (Figure 4.20). This was probably occurring in the vicinity of the Gunton Bedrock Escarpment (GBE) and an upward branch of a horizontal convective roll phasing with a gravity wave originating from the Manitoba Escarpment (ME) (Figure 4.20). At that time, satellite imagery revealed convergence occurring along the GBE and low-level radar reflectivity imagery was indicating that deep convection was occurring (Figure 4.21). At this time, URP did not detect this new development.

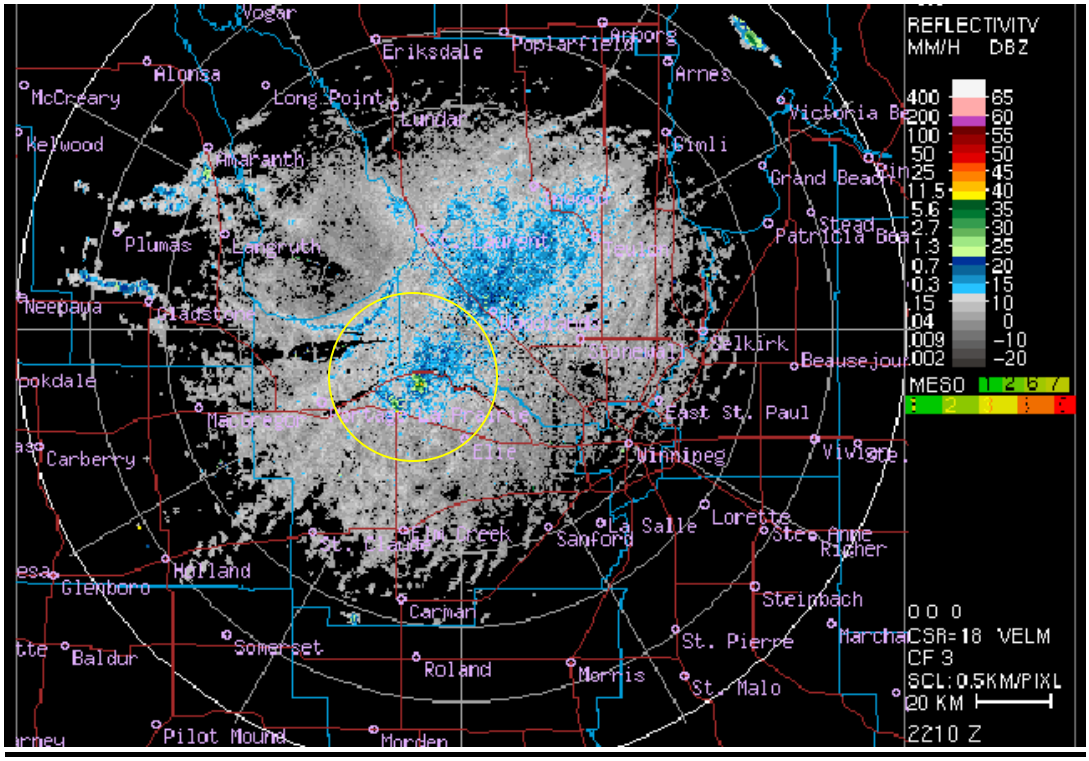

Figure 4.20: 0.5 km CLOGZ LOLAA Imagery at 2210 UTC showing storm formation due to mesoscale interactions (yellow circle).

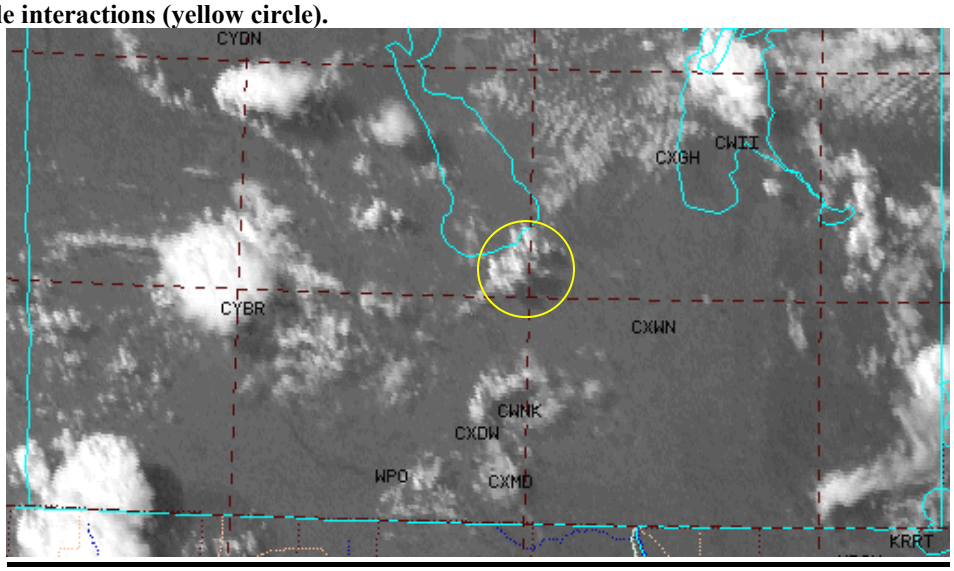

Figure 4.21: 2201 UTC GOES Visible Satellite Imagery showing surface based convection south of Lake Manitoba (yellow circle) (College of DuPage, 2007).

At 2220 UTC, the low-level reflectivity radar scan continued to show two storms rapidly developing in a region where moisture convergence, horizontal convective rolls and a gravity wave likely came together to remove the capping inversion 10 minutes earlier (Figure 4.22). **Storm A** was approximately 10 km southwest of Woodlands, MB and **Storm B** was 20 km northwest of Elie, MB.

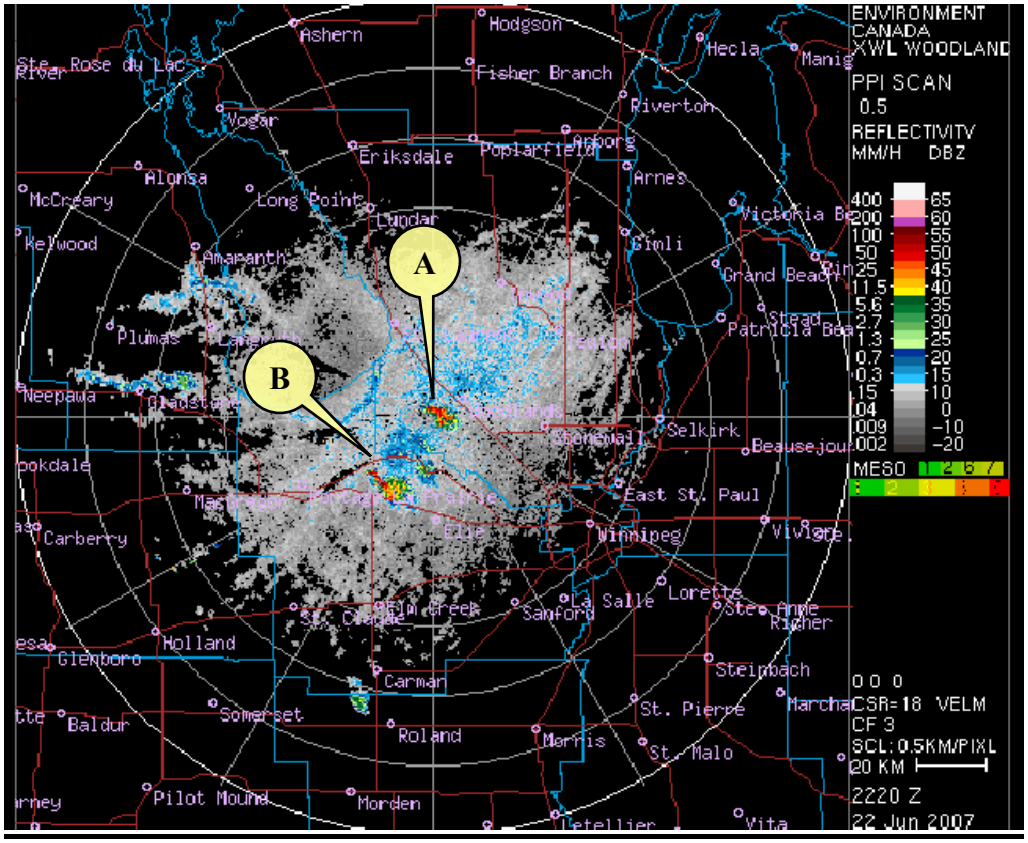

Figure 4.22: 2220 UTC 0.5 km CLOGZ LOLAA imagery (Yellow circles showing Storm A and Storm B).

At 2240 UTC, the boundaries that aided in triggering convection in the vicinity of the GBE were starting to become washed out on radar with two severe thunderstorms located near the Woodlands radar site. From this point, storm B was detected as a cell on URP software (every 10 minutes) but was analyzed every 20 minutes for this thesis unless a significant change occurred and more analysis was required. Storm A and C were also detected using URP but for this analysis they will be discussed in relation to Storm B.

At 2300 UTC, **Storm B** was the dominant storm 13 km north-northwest of Elie moving to the southeast at 6 m s^{-1}. The actual storm motion was similar to the RAOB estimated storm motions on the 1800 UTC XWI (7 m s^{-1}) and VAD (5 m s^{-1}) hodographs in section 4.1.4. A wall cloud was observed on **Storm B** (Figure 4.23). The storm was a classic supercell in terms of its visual structure exhibiting a mesocyclone with tilted updraft, and a separated hail/rain core. **Storm B** had a distinct couplet with inbound/outbound values approaching 20 m s^{-1} gate-to-gate at low-levels. The BWER height was at 7.6 km indicating that the updraft region of the storm was becoming better organized and the storm was becoming increasingly severe.

Figure 4.23: 2300 UTC image taken 1.6 km south of Elie looking north-northwest towards Storm B.

At 2320 UTC, **Storm A** moved 21 km east-southeast of Woodlands and was beginning to lose supercell characteristics. It was now moving away from the GBE and was producing large hail near Stonewall, MB. **Storm B** continued as the dominant storm with an inflow notch and hook appendage anchored near the GBE; 10 km northwest of Elie. **Storm B** had a very organized couplet with low-level gate-to-gate velocities approaching 36 m s^{-1} (Figure 4.24). The BWER height was not analyzed by URP at this time. A rapidly rotating wall cloud with a funnel ¾ of the way to the ground could be seen at this time as the storm continued to move to the southeast at 4 m s^{-1} (Figure 4.25).

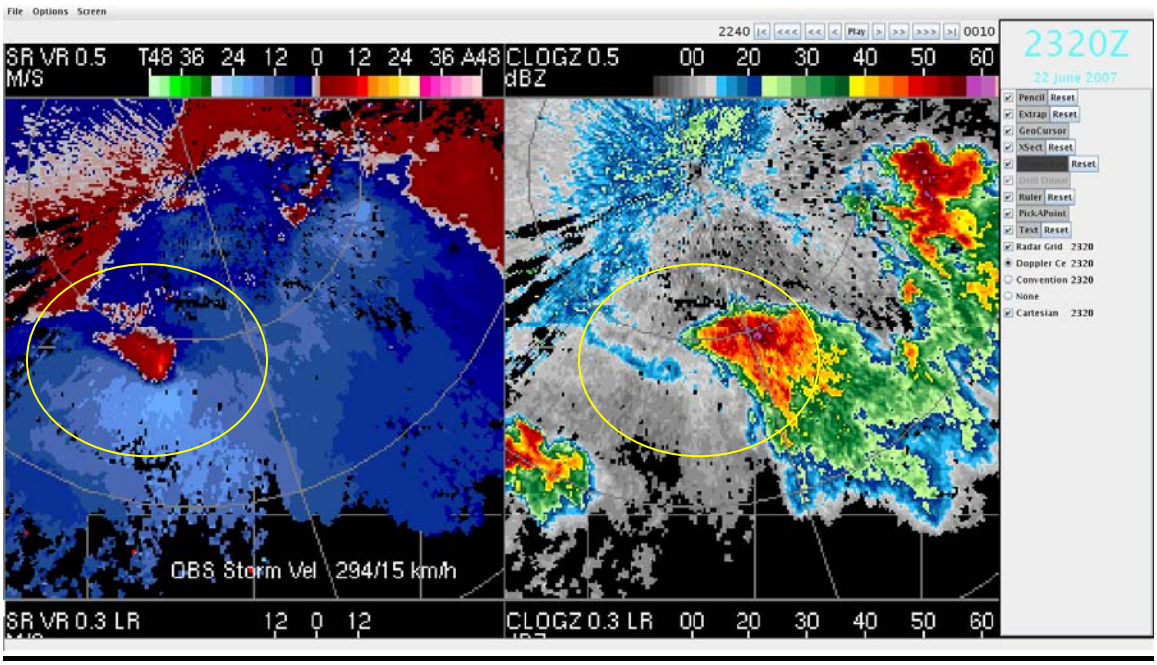

Figure 4.24: 2320 UTC URP CLOGZ LOLAA velocity/reflectivity imagery showing Storm B with yellow circle.

Figure 4.25: 2320 UTC image taken 1.6 km south of Elie looking north-northwest towards Storm B.

At 2330 UTC, **Storm B** had a tornado on the ground 7 km northwest of Elie (Figure 4.26) and low-level gate-to-gate velocities exceeded 32 m s^{-1} (Figure 4.27). The storm was moving at 5 m s^{-1} to the southeast and was moving closer to the town of Elie. The radar scan showed a very distinct inflow notch/hook appendage that was still rooted

near the GBE. The rear flank downdraft (RFD) was beginning to tighten and coil inwards towards the updraft and could be seen on the radar imagery (Figure 4.27). This RFD interaction possibly increased the rotation at low-levels allowing for tornadogenesis to occur as Lemon and Doswell (1979) suggested (chapter 1). BWER heights had increased to 8.1 km. **Storm C** had a small velocity couplet starting to develop about 20 km west-southwest of Elie (not shown).

Figure 4.26: 2330 UTC image taken 1.6 km south of Elie looking north-northwest towards Storm B with a tornado on the ground.

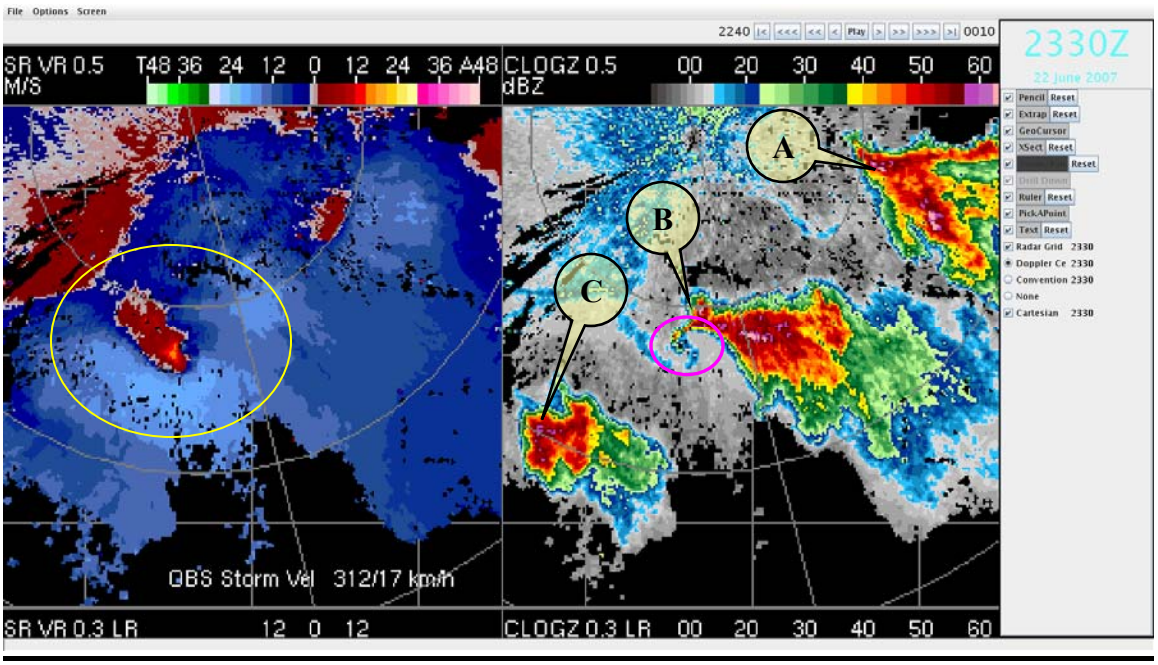

Figure 4.27: 2330 UTC URP CLOGZ LOLAA velocity/reflectivity imagery showing Storm A, B, and C with yellow circle showing storm B's velocity couplet. Pink circle highlights area where rear flank downdraft was beginning to wrap inward towards the updraft.

At 2340 UTC, **Storm B** still had a tornado on the ground 5 km northwest of Elie that was increasing in size and getting closer to the town (Figure 4.28). A tornado warning was issued at this time for Elie and surrounding municipalities. The velocity couplet expanded in terms of size with gate-to-gate values decreasing to 30 m s^{-1}. **Storm B's** mesocyclone remained in approximately the same location as the previous scan however the storm motion shifted towards the south at 4 m s^{-1} as it pivoted over the same area. The BWER height was at 7.8 km. **Storm C** was 16 km west-southwest of Elie.

Figure 4.28: 2340 UTC image taken 1.6 km south of Elie looking north-northwest towards Storm B.

At 0000 UTC, **storm A** was beginning to weaken on radar (Figure 4.29). The storm was starting to collapse with outflow winds arriving in Winnipeg from the west-northwest. **Storm B** had a violent tornado on the ground that was impacting the western side of Elie (Figure 4.30). Multiple power flashes could be seen which were quickly followed by large objects being thrown and wrapped around the tornado. There was a tight velocity couplet with low-level gate-to-gate values of 44 m s^{-1}. Reflectivity returns were increasing within the hook region of the storm, showing signs that the storm may have been starting to become overloaded with heavy precipitation near the updraft region of the storm. BWER heights were at their highest at this time valued at 10.8. **Storm C** had a tornado on the ground near the town of Oakville, MB or 15 km west-southwest of Elie (Figure 4.29). The tornado was large and it was damaging a farmstead. On radar, the hook appendage had bright reflectivity returns indicating that precipitation was

beginning to wrap around the main updraft core (Figure 4.29). Low-level gate-to-gate velocities associated with **Storm C** were near 42 m s^{-1}.

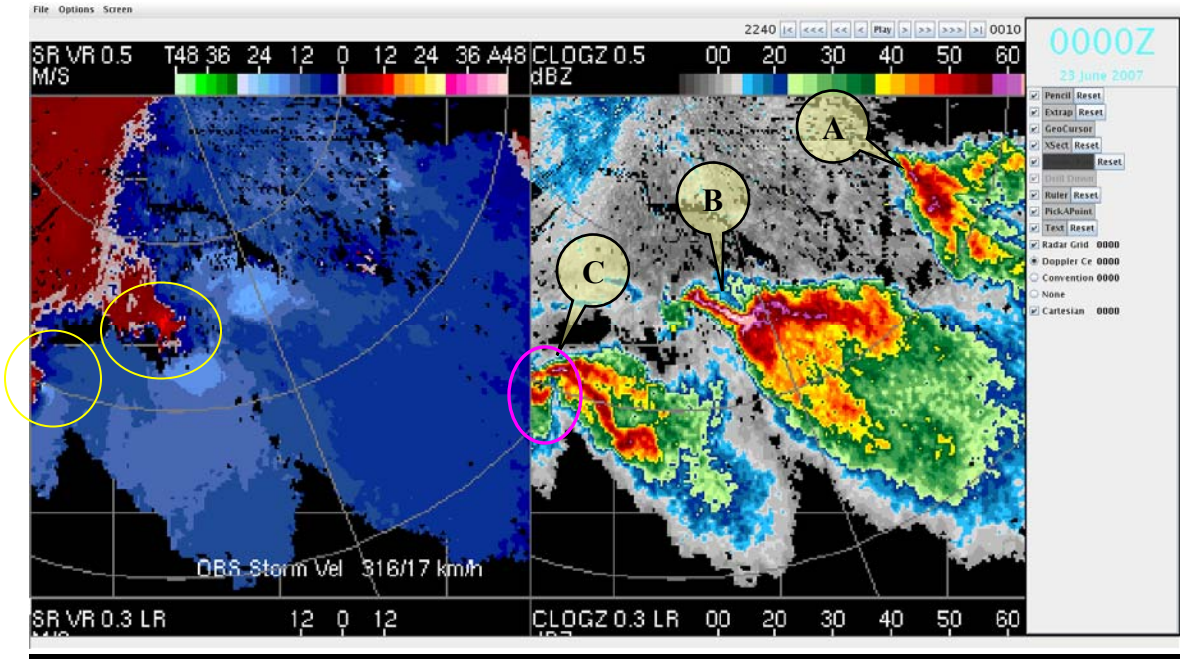

Figure 4.29: 0000 UTC URP CLOGZ LOLAA velocity/reflectivity imagery showing Storm A, B, and C labelled with yellow circles showing Storm B and C velocity couplets. Pink circle indicates location where precipitation was wrapping into the main updraft of storm C.

Figure 4.30: 0000 UTC image taken 1.6 km south of Elie looking north-northwest towards Storm B with a tornado impacting Elie, MB.

At 0010 UTC, **Storm A** was 13 km north-northwest of Winnipeg and was not as intense in terms of reflectivity on the radar as previous scans (Figure 4.31). Thunderstorms near Lake Winnipeg were also weakening as they moved to the southeast (not shown). **Storm B** no longer had a tornado on the ground. It rapidly dissipated between radar scans after impacting the western side of Elie. It still had a rotating wall cloud but was becoming less organized as the velocity couplet was weakening. **Storm C** still had a large tornado on the ground; however, it was quickly being wrapped in rain as heavy precipitation likely started to pollute the updraft region of the storm due to cell contamination from the northwest. The gate-to-gate velocities decreased to 30 m s^{-1}. Visually this could be confirmed because the tornado was becoming shrouded with rain.

After 0010 UTC, **Storm C** supercell features were lost as cells began to merge with one another. The cells then continued to move quickly to the southeast where the severe weather threats consisted of heavy rain, small to large hail, and strong winds (Figure 4.32). The resulting cluster of storms continued into the overnight hours producing severe straight line wind damage in the Whiteshell, MB area.

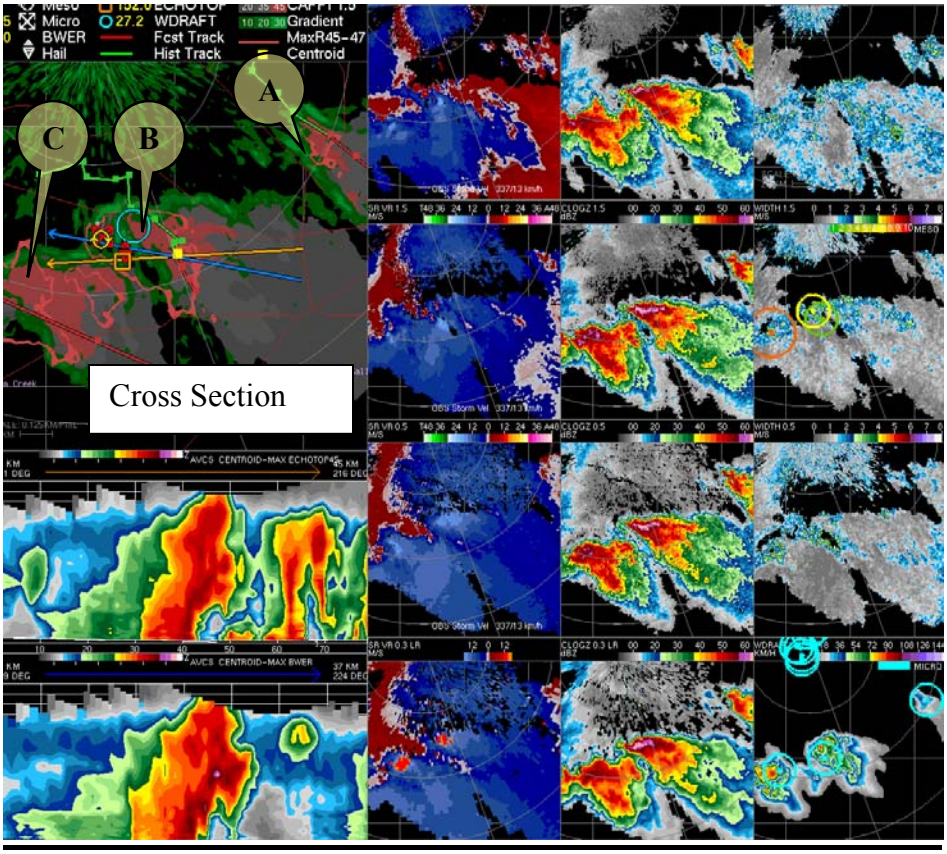

Figure 4.31: 0010 UTC URP Cell view velocity/reflectivity imagery showing Storm A, B and C labelled.

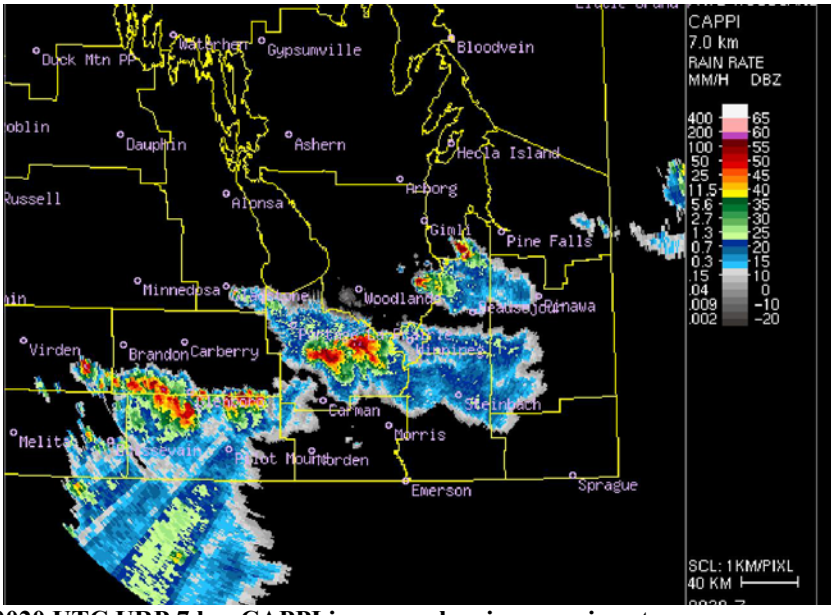

Figure 4.32: 0020 UTC URP 7 km CAPPI imagery showing merging storms.

4.3 - Tornado Path and Width Analysis

The Elie tornado remained situated over a small area for its entire lifetime. The tornado path was determined by examining video and photo evidence that was provided to Environment Canada (Figure 4.33). The tornado looped in and around itself two (third smaller loop identified with aerial imagery later) times under the main mesocyclone impacting an area more than once on a few occasions. The tornadic circulation on the ground via visual evidence was used to estimate the width based on the condensation funnel without the debris circulation being incorporated into the tornado width. The track width could only be estimated using appropriate reference markers and measurement tools using map software.

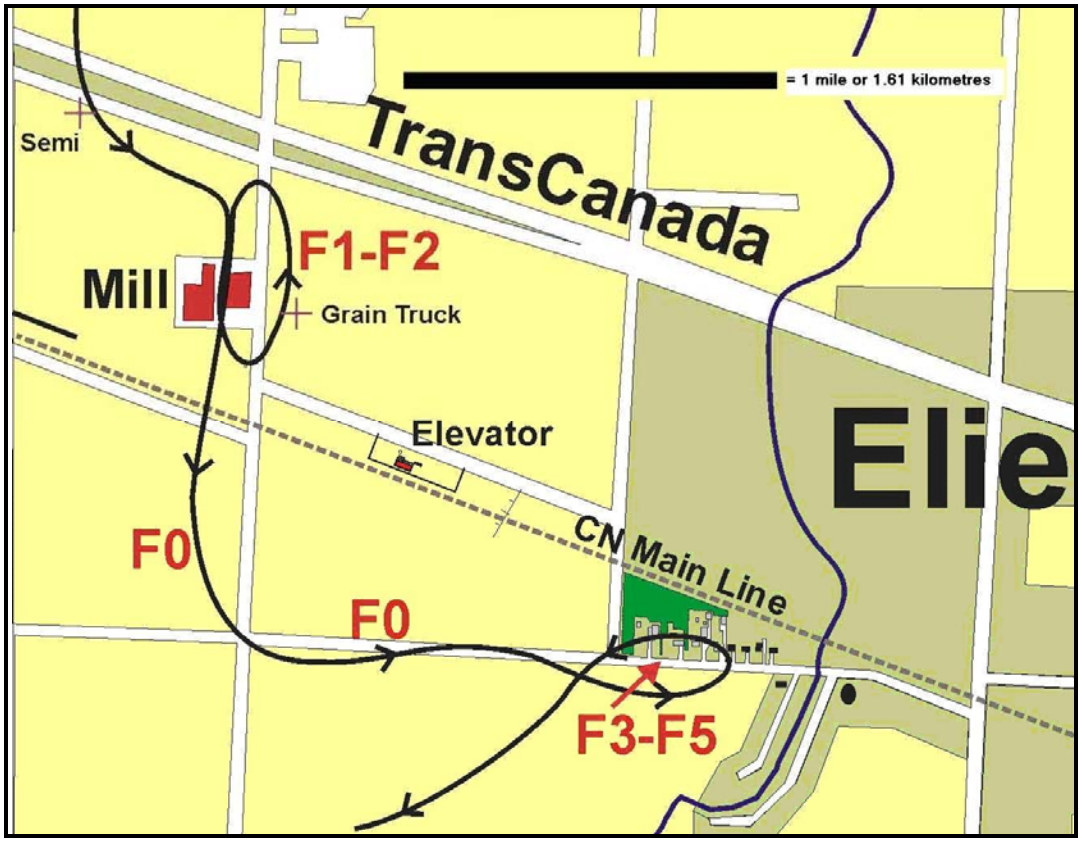

Figure 4.33 : Map of Elie tornado track - black bar at top denotes 1mi/1.61 km reference (McCarthy, 2008).

As mentioned earlier, multiple funnel clouds could be seen at approximately 2320 UTC that were briefly touching down northwest of Elie causing minor damage to farmsteads north of the Trans Canada Highway. A condensation funnel was visible at the surface between 2325-2330 UTC northwest of Elie, north of the Trans-Canada Highway that runs in an East-West direction. The tornado crossed the Trans-Canada highway at 2342 UTC overturning a semi trailer. Highway lanes are 3.6 m in width with a shoulder width of 2.7 m. There are two highway lanes and two shoulders making the total width of the road 12.6 m wide. It can therefore be determined that at this specific time, the condensation funnel was approximately 13 m wide as a storm photo shows the tornado crossing the westbound lane of the Trans Canada highway as it moved to the southeast (Figure 4.34). The circulation with debris was visually larger but the main circulation of the condensation funnel itself is significantly smaller.

Figure 4.34: Tornado image showing tornadic circulation as it crosses over the Trans-Canada highway at 2342 UTC. Tornado is crossing from North to South (right to left) across the westbound lane (PASPC Image Archive, 2007).

The tornado continued southeast and began its initial loop at approximately 2346 UTC as it hit the flour mill to the northwest of the town of Elie. After hitting the flour mill, it continued to the south where it suddenly shifted east, and then north, and then south again impacting the same area of the mill at 2348 UTC. At this time it was determined based on video/photo evidence and reference markers that the tornado was between 49-58 m wide (Figure 4.35). The reference markers that were used were the width of the flour mill from different angles, the distance from the photographers to the tornado, and the distance from the north/south oriented road to where the flour mill was located.

Figure 4.35: Tornado image at 23:48 UTC. Images on the left show the tornado at the same time from three different angles and where it was located on the map (yellow circle). The blue star indicates the location of the photographer that took the top left photo. The middle photo is from 2.8 km northwest of Elie, and the bottom photo is from 1.6 km south of Elie. The tornado width and location were then overlaid on the map to determine the width of approximately 49-58 meters. Background imagery provided by Google Earth and the tornado imagery is from the PASPC Image Archive.

Semis parked at the flour mill were rolled and their associated trailers were thrown several meters. The flour mill was damaged even further on the second pass with F1-F2 rated damage occurring as the tornado continued slowly moving to the south. At 2355 UTC; after 700 m, it shifted due east and moved over a field and gravel road causing F0 damage. At this time the tornado grew wider. The condensation funnel at the surface was approximately 140 m in width as suggested by video/photo evidence (Figure 4.36). The distance from the photographers to the tornado and the spacing between reference houses was measured and used to estimate the width of the tornado.

Figure 4.36: Tornado location at 2355 UTC (yellow circle). Image on left taken from point A in the neighbourhood and image on right taken 1.6 km south of Elie. Using appropriate scales and distances between houses using map software and storm photographs/videos, the width could be estimated by extrapolating and solving for the width using the determined track (red dashed line) the tornado took at a specific time. At this time the estimated tornado width was approximately 140 meters. Background imagery provided by Google Earth and the tornado imagery is from the PASPC Image Archive.

The eastward shift could be seen as the tornado in the video (from the fixed location 1.6 km south of Elie viewing North) started moving to the right. A more detailed tornado track could be determined and a track width could be estimated by using

the damage noted on the ground from the aerial imagery that was analyzed in combination with a vehicle reference marker. The vehicle reference was a ¾ tonne GMC van that was approximately 5.6 m in length. This same vehicle reference was also used to estimate the width using video evidence as the same van was lofted into the tornado and used to estimate its width of 50 m (Figure 4.37).

As the tornado continued east, it decreased in width from 140 m to approximately 50 m as it began to impact the town at 2359 UTC. From here onward, it moved past the houses over a field to the south causing F1-F2 rated damage. The tornado was now smaller in size; so on the first pass made over the field to the south of the houses, the worst of the tornadic winds did not impact the houses greatly at this time as the tornado moved to the east. Upon grazing the houses, at 0000 UTC, it shifted north and then west and this is where the F5 rated damage occurred (Figure 4.38). Video evidence shows power flashes occurring as the tornado started moving to the left (west) in the video. The houses were being impacted directly by the tornado as it moved to the west. Upon devastating the houses, the tornado continued to decrease in width to approximately 18 m based on examining the damage swath on the aerial imagery (Figure 4.37). It moved to the southwest and dissipated in a field 500 m to the southwest of the town after doing a third and final loop at 0003 UTC.

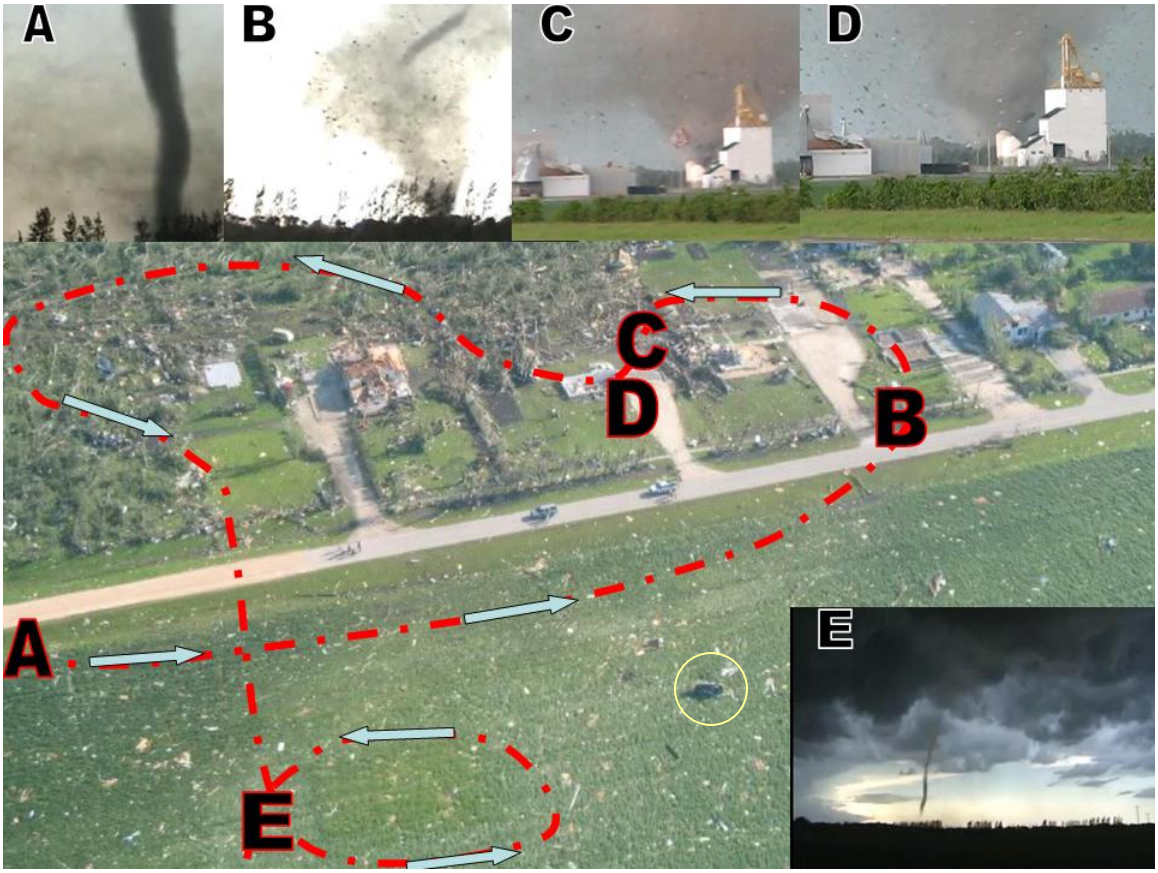

Figure 4.37: Track of tornado as it impacted Elie. Scale not given for aerial imagery but vehicle reference length for GMC Van of 5.6 m is used (yellow circle). Points A through E show where tornado was at each specific time with red dashed line and blue arrows showing the tornado track and direction. Point A: 2359 UTC, Point B: 0000 UTC, Point C: 0001 UTC, Point D: 0001 UTC (few seconds later), Point E: 0003 UTC. Points A, B, and E were from the fixed video position 1.6 km south of Elie and points C and D were from the fixed video position 2.8 km northwest of Elie (PASPC Image Archive, 2007).

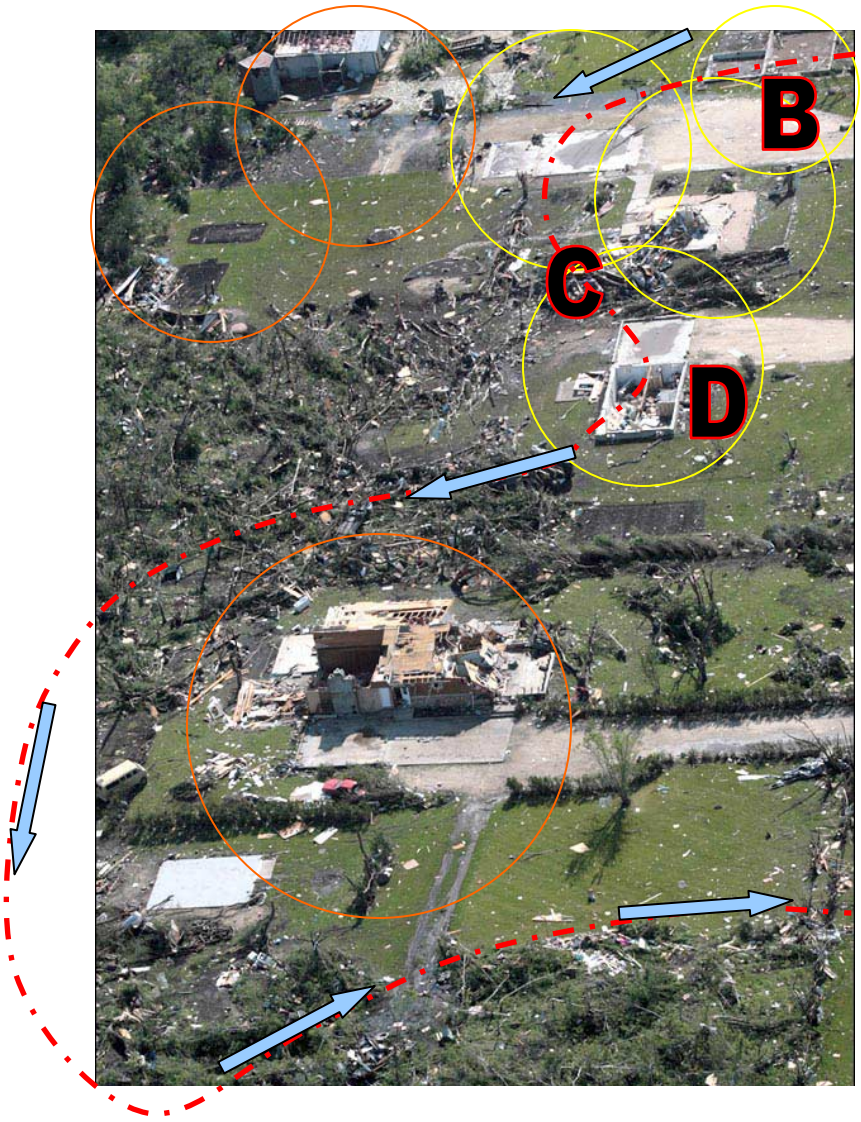

Figure 4.38: Elie aerial image (zoomed in) showing F5 damage in yellow circles and F3-F4 damage in orange circles. Tornado track (red dashed line), direction (blue arrows), Points B (0000 UTC), C (0001 UTC), and D (0001 UTC) also included to relate to previous figure (PASPC Image Archive, 2007).

CHAPTER 5 - COMPARISON TO OTHER MAJOR TORNADO EVENTS IN NORTH AMERICA

5.1 - Summary of Events

The F5 Elie tornado touched down at 6:25 pm local time on 22 June 2007 and was one of two significant tornadoes that occurred that day. Although it produced F5 damage, there were zero fatalities and a few minor injuries. This chapter focuses on comparing the large scale meteorological conditions of the Elie event to a few other significant events in North America with the primary purpose of illustrating the similarities and differences of these major tornado events. The events that were compared to the Elie tornado were the Edmonton, Alberta (F4) tornado on 31 July 1987, Oklahoma City, Oklahoma (F5) tornado on 3 May 1999, Gull Lake, Manitoba (F2) tornado on 5 August 2006, and the Pipestone, Manitoba (F3) tornado on 23 June 2007. A brief introduction to each event is provided next, followed by a summary of the event comparisons.

- On 31 July 1987, a tornado impacted Edmonton, Alberta at the end of a period of hot and unusually humid weather when a cold front acted to trigger a tornado that produced F4 damage causing 27 fatalities and over 300 injuries. To this day after combining the loss of life, injuries and damage ($330 million estimated), the Edmonton tornado ranks as Alberta's worst natural disaster and one of Canada's worst weather disasters (Heidorn, 2008).
- On 3 May 1999, several supercell thunderstorms produced several large and damaging tornadoes in central Oklahoma during the afternoon/evening hours. The largest tornado was a F5 rated tornado that tore through the Moore and

southern Oklahoma City metro areas. The tornadoes on 3 May 1999 caused a total of 44 fatalities and 675 injuries in Dover, Shawnee, Perry, Bridge Creek, Moore, and the southern Oklahoma City metro areas (Lugo, 2002). Additional tornadoes also hit areas in south central Kansas, and northern Texas with over 70 being reported across the region (Lugo, 2002). The tornado count makes the May 3rd outbreak the largest ever recorded in Oklahoma and it was the most costly outbreak in history for the state ($1.2 billion in damage) (Lugo, 2002).

- During the afternoon of 5 August 2006, an F2 tornado struck a Manitoba campground 80 km northeast of Winnipeg killing a woman and injuring three others. The tornado hit the Gull Lake campground, wrecking boats, uprooting trees, flipping cabins and destroying trailers.
- Conditions were favourable for tornadic storms on 23 June 2007; the day after the Elie tornado. A cyclic tornadic supercell initiated over south-eastern Saskatchewan during the late afternoon resulting in multiple tornado touchdowns with the strongest being rated F3.

5.2 - Summary of Event Comparisons

Table 5.1 summarizes some of the critical parameters for each of the five tornadic events to highlight the key differences and similarities. A more detailed explanation is then given about a few of the critical parameters that were compared.

Event	Edmonton	Oklahoma City	Gull Lake	Pipestone	Elie
F-Rating	F4	F5	F2	F3	F5
Estimated Tornado Width (m)	1000	340-1200	unknown	1800	50-140
Estimated Path Length (km)	40	61	13	15	5
Temperatures (°C)	24	30	23-29	25-30	30
Dewpoints (°C)	17-19	18-20	17-22	19-25	20-25
Max CAPE (J kg^{-1})	2370	5000	2000	3100	6330
Max Vertical Velocity (m s^{-1})	68	100	63	79	112
0-3 km SRH m^2 s^{-2})	241	403	n/a	210	178
0-1 km SRH (m^2 s^{-2})	30	321	n/a	115	150
0-6 km Shear (m s^{-1})	26	23	20	18	15
0-1 km Shear (m s^{-1})	11	15	10	13	10
850 hPa low level jet maximum (m s^{-1})	16	18	18	14	11
Max Gate to Gate Velocities (m s^{-1})	n/a	57	65	62	44
Trigger	Cold Front	Dry Line	Surface Trough	Warm Front	Local Mesoscale Forcing

Table 5.1: Event summary table highlighting important parameters that were analyzed and compared to the Elie tornado event.

The 5 km Elie tornado track was not extensive like the 13 km Gull lake tornado track, 40 km Edmonton tornado track or the 64 km Oklahoma tornado. What made the Elie event different was that the tornado moved approximately 5 km for the 40 minutes it was on the ground while looping and double backing on itself three times whereas the other significant events did not have looping tracks. The looping track can possibly be attributed to the fact that the tornado developed out ahead of the main synoptic forcing along mesoscale boundaries which allowed the storm to move slowly before the stronger winds aloft moved into the region to finally steer the storm. The tornado itself just moved within the main mesocyclone that existed above it. The Gull Lake and Edmonton

events took place ahead of a well-defined cold front and moved rapidly along with the upper level flow. The Pipestone tornado developed along a warm front then moved south-eastward with a stronger mid and upper level flow as compared to the Elie event. The Oklahoma event also had strong mid and upper level flows that carried storms rapidly toward the north-east.

The main upper level flow for the Elie and Pipestone events was from the northwest and this orientation of the upper flow is notorious for producing tornadic events in Southern Manitoba by enhancing the overall shear, given the fact that there is a southerly low-level flow present. The upper level flows for the Edmonton, Gull Lake, and Oklahoma events were from the southwest which is common for severe weather outbreaks.

Another interesting fact was that these tornadic events occurred during the time of the year in which the rate of evapotranspiration was optimal; allowing for higher dewpoints.

At lower levels, there were similarities between the four cases when compared to Elie. The low-level jet identified was 18 m s^{-1} for Gull Lake, 16 m s^{-1} for Edmonton, 18 m s^{-1} for the Oklahoma event, and 14 m s^{-1} for the Pipestone event. For Elie it was approximately 11 m s^{-1}, but the main difference is that the 0-6 km shear for the other cases ranged from 18-26 m s^{-1} with sufficient speed and directional changes with height, and the Elie 0-6 km shear was lower at approximately 15 m s^{-1}. There was good directional and speed shear with height up to 1 km for the Elie event but above that, the shear became more directional and speeds did not change significantly above 1 km when compared to the other events. The Oklahoma and Edmonton events had significant speed

and directional changes at the lower levels and the hodograph kink, as mentioned earlier. The Elie 2210 UTC hodograph prior to CI also exhibited a kink between the surface and 1 km.

Large CAPE values (2000 J kg^{-1} – 5000 J kg^{-1}) and corresponding vertical velocities (63 m s^{-1} – 100 m s^{-1}) were also present (based on the assumptions introduced in chapter 1) for the significant events but the exceptionally large values of CAPE (estimated 6330 J kg^{-1}) on 22 June 2007 meant that higher vertical velocities (112 m s^{-1}) were present.

In terms of the tornado width, the F5 damage associated with the Elie tornado occurred when the tornado was small in width (50 m) whereas the other tornadoes were larger in size (340 m – 1800 m). Large tornadoes tend to be stronger because they are able to impact the same area for an extended period of time. That doesn't mean that due to the smaller size of the Elie tornado (50 m - 140 m) that it should not have been rated as high. Tornadoes change in size as they enter different stages of their life cycle and public reports may exaggerate the size of the tornado. It can only be determined based on photogrammetric analysis with proper fixed references or damage surveys to estimate how wide the tornado actually is. A number of factors can limit the knowledge of the four-dimensional tornado wind field that can be gained through tornado video photogrammetry (Forbes and Bluestein, 2001). One limitation is that only wind components normal to the line of sight can be measured correctly. A second limitation is that, in most cases, a thick dust debris cloud obscures the inner core of the tornado circulation, making it impossible to construct cross sections of tornado wind components (Forbes and Bluestein, 2001). A large limitation is that references may be sizable objects

that do not travel with the velocity of the wind. Horizontal and vertical velocities should be less than that of the true tornado wind and have an outward component (Forbes and Bluestein, 2001). How to determine tornado width can also be a challenge since the funnel itself may be used to estimate the width or the debris pattern may be used to estimate the width which can result in two different width values. As mentioned earlier, the condensation funnel width at the ground was used to estimate the tornado width while discounting the debris being wrapped around the main circulation. The Elie tornado had a very concentrated wind field over a small area and this is when the F5 damage occurred whereas the Edmonton, Pipestone, Oklahoma tornadoes were larger in size based on photographic and video evidence (not shown).

Finally, another interesting fact about the Elie event (not highlighted in table) was that it occurred roughly 20 km to the east of another F3 tornado that devastated a farmstead near Oakville, MB. None of the other major tornado events occurred with other significant (F2 or greater) tornadoes being reported on the ground at the same time from different storms while in close proximity of one another, except for the Oklahoma city event in which supercells had tornadoes on the ground great distances away. What made the Oklahoma event different than the Elie/Oakville event was that the trigger for the Elie and Oakville tornadoes was due to the local forcing of the HCRs, gravity waves, and moisture convergence, whereas the trigger for the Oklahoma City event was attributed to a larger scale feature (dryline). This allowed for several storms to become tornadic over a greater area in Oklahoma on that day.

CHAPTER 6 - SUMMARY AND RECOMMENDATIONS

6.1 - Summary

The three main research questions of this thesis are:

1. **Meteorologically, what were the pre-storm environment conditions on June 22nd, 2007?**
2. **How did the storm and associated tornado evolve?**
3. **How does this event compare to other major tornadic events in Canada and the U.S.?**

The initial objective involved assessing the pre-storm environment conditions on 22 June 2007. The conditions were assessed by performing detailed analyses and monitoring real-time data provided by Doppler radar, surface observations, and local sounding data. One weather balloon was launched at the PASPC (1800 UTC) to assess the potential for severe deep convection. This sounding provided critical data for the operational forecasters leading up to the storm, but also provided key data for analysis within this thesis. The atmospheric sounding showed a large capping inversion that was inhibiting convection (170 J kg^{-1}of CIN) for most of the day due to warming at the mid-levels making it difficult for CI to occur. The hodograph prior to CI exhibited a "kink" similar to analyses performed by Esterheld and Giuliano (2008) and this showed an increased likelihood of strong tornadoes. The question being asked by forecasters was if enough low-level forcing would come into the region to break through the capping inversion. The capping inversion weakened in southwest Manitoba initially as the synoptic cold front was advancing through that area allowing for CI. Further east, low-level mesoscale boundaries (e.g., gravity waves, horizontal convective rolls and sufficient

moisture convergence) likely played a critical role in CI near Elie. CAPE values at the time of convective initiation were large (6330 J kg^{-1}) and this energy was quickly converted to kinetic energy as the storm developed. In VORTEX, two thirds of significant tornadoes have occurred within 20 km of detected boundaries (Markowski et al., 1998). The above mentioned low-level mesoscale boundaries were occurring in an environment with high 0-1 km SRH values (150 m^2 s^{-2}) and could be seen on the low-level radar scans. Davies-Jones et al., (1990) also suggested that 0-1 km SRH values greater then 100 m^2 s^{-2} could lead to strong tornadoes. These high 0-1 km SRH values that were present in combination with the evolution of the RFD associated with the supercell, possibly acted as an increased vorticity source as the RFD intensified on 22 June 2007 resulting in the development of the tornado (Burgess et al., 1977).

The second objective involved performing an analysis of the supercell and its associated tornado that impacted Elie, Manitoba. The supercell thunderstorm that spawned the tornado developed rapidly after 2200 UTC on 22 June 2007 and began producing a series of funnel clouds starting around 2320 UTC (70 minutes later). When the tornado developed at 2325 UTC, it slowly moved to the south east at approximately 5 m s^{-1} lasting nearly 40 minutes. The tornado moved slowly due to the fact that it occurred out ahead of the main synoptic forcing associated with the area of low-pressure that was located over Southern Manitoba, and the upper-level winds did not get stronger to move the storm more quickly until well after the tornado had dissipated. The tornado had a looping track that impacted the western edge of Elie causing F5 damage when it was an estimated 50 m wide. The Elie tornado had a particularly small width for being classified an F5, which is another interesting aspect of this event. From 2330 UTC to

0000 UTC, gate-to-gate couplets were evident in the low-level velocity images with strong winds heading toward and away from the radar (30 – 44 m s^{-1}). This is the classic signature of a well organized mesocyclone and the wind shear and storm motion were such that the Elie storm had significant storm relative streamwise vorticity that led to the prolonged tornado evolution. The low level jet was quite strong that afternoon (11 m s^{-1}), as evident in the upper air sounding, and this enabled the storm inflow region to get a continued influx of warm moist air. During the same time, it could be seen that no cell contamination was occurring as storms that were developing within the range of the radar were not competing with each other by merging or developing on their rear flanks. Precipitation was occurring well downstream of the storm producing the tornado which was effectively allowing the storm to remain severe; i.e. the updraft and downdraft regions were able to remain separated for a prolonged amount of time.

The final objective involved analyzing other significant tornadic events that have occurred in the past in North America with similar meteorological parameters that were present on 22 June 2007. What was remarkable about the Elie tornado was that it was small in size when compared to the other significant events. The tornado had a very tight area of rotation (50 m at times) for an extensive amount of time over nearly the same location without occluding or cycling like the Edmonton, Oklahoma City, Gull Lake, and Pipestone tornadoes. The slow-moving nature of the tornado occurring over a sparsely populated area may have contributed to the small extent of damage despite the tornado being rated F5. The other significant tornado events examined had similar wind profiles including the low-level hodograph "kink" required for tornadogenesis along with strong upper-level flows and the tornadoes/storms were able to propagate more rapidly

impacting a larger area. High vertical velocities were present for the other significant events but the values that were calculated for the Elie event (112 m s^{-1} based on equation assumptions) possibly compensated for what was lacking in the upper-levels allowing the tornado to become strong over a small area.

6.2 - Recommendations for Future Applications and Research

The results from chapter 4 indicate that more surface observations are needed in areas that are deemed important for storm initiation areas such as the Gunton Bedrock Escarpment and the Manitoba Escarpment. If there were more surface observations along or near the Gunton Bedrock Escarpment, it would have been obvious on this day that moisture was moving northward and possibly converging on this area. Other terrain effects can be sampled as well to see if they do in fact affect storm initiation and evolution that may or may not lead to tornadogenesis.

The single sounding launched at the Winnipeg PASPC was critical for real-time operations as well as post-event analysis. Without this data, critical knowledge of the storm environment would not have been available. The southern Prairies (and all of Saskatchewan) do not have any operational upper air sites, and it is these areas that have the highest population densities and where most severe weather occurs. It is therefore highly recommended that, at the very least, targeted upper air observations (thermodynamics and wind) are made available to the operational community (at least one sounding between 1800 – 2100 UTC) on days when severe weather threatens for at least one location within the southern portion of each province. Radar VAD analysis can then be used to supplement balloon data prior to storm initiation. This is especially important given the results of this thesis that have shown the importance of mesoscale processes on storm initiation and evolution.

Analyzing the radar VAD data and clear-air data was absolutely critical in monitoring the pre-storm environment. Fortunately, on this day, radar was able to show the movement of air at low levels. We were able to identify horizontal convective rolls, a

lake breeze boundary, and a gravity wave as it approached the area in which initiation took place. It was also fortunate that these boundaries were able to be identified on radar because clear-air-echoes only clearly appear on the Doppler reflectivity scans with a range of 120 km from the radar site. Unfortunately, our radar coverage is quite sparse in Canada and it is almost impossible to monitor pre-storm environments because it is, for the most part, a rare occurrence to have a tornado threat area occur very close to a radar site. It is therefore suggested that Canada supplement its radar network with smaller, less expensive short-range X-band radars that can detect low level mesoscale phenomena in between the longer-range C-band radars. In addition, for the C-band radars that we do have, a change in scan strategy is needed to allow for five minute updates (similar to the U.S.) versus the current 10 minutes. Having updated radar information every 5 minutes is critical for storm initiation and evolution in order to increase Canada's capacity to issue more timely warnings; this is especially important for quickly evolving weather conditions that occur during severe convective storm days.

Finally, for Southern Manitoba, future studies can be conducted to show how mesoscale boundaries may increase the likelihood of a supercell producing a tornado. Looking at other past tornadic events in Southern Manitoba and how they developed may provide more evidence that highlights and reinforces the fact that the cumulative effect of multiple mesoscale boundaries do play a critical role in convective initiation and tornadogenesis in this region. From this, we can determine what triggers may be more important than others and what synoptic conditions are more conducive for significant tornadoes. This in turn can assist forecasters in issuing better warnings. This is because if

a storm were to develop in an area favourable for tornadogenesis, the appropriate warning could be issued, as a greater confidence in tornado development is achieved.

REFERENCES

Aguado, E., Burt, J.E. (2004). Understanding Weather and Climate. *Pearson Educ*. 608 pages.

Balaji, V., Clark, T.L. (1988). Scale selection in locally forced convective fields and the initiation of deep cumulus. *J. Atmos Sci*, vol. 45, 3188-3211.

Bone, R.M. (2005). The Regional Geography of Canada. (3rd ed.). *Oxford University Press*. USA, 592 pages.

Brandes, E.B. (1984). Relationships between Radar-Derived Thermodynamic Variables and Tornadogenesis. *Earth Sciences*, vol. 112, 1033-1052.

Brooks, H.E., Doswell, C.A. (2000). Normalized Damage from Major Tornadoes in the United States: 1890-1999. *Weather and Forecasting,* vol. 16, 168-176.

Brooks, H.E. (2003). On the relationship of Tornado Path Length and Width to Intensity. *Weather and Forecasting,* vol 19, 310-319.

Browning, W.D., Bookbinder, E.M. (2004). A mesoscale re-analysis of anticipated severe weather threats in the Ozarks during the week of May 4-10th, 2003. *AMS, 1-7.*

Bunkers, M.J., Klimowski, B.A., Zeitler, J.W., Thompson R.L., Weisman, M.L. (2000). Predicting supercell motion using a new hodograph technique. *Weather and Forecasting*, vol. 15, 61-79.

Bureau of Meteorology (2011). Air Services Australia. Commonwealth of Australia.

Burgess, D.W., R. A. Brown, L. R. Lemon, and C.R. Safford. (1977). Evolution of a tornadic thunderstorm. *10th Conference on Severe Local Storms, AMS.* Omaha, NE.

Church, C., Burgess, D., Doswell, C., Davies-Jones., R. (1993). The Tornado: Its Structure, Dynamics, Prediction, and Hazards. *American Geophysical Union*, Washington DC, USA, 637 pages.

Davies-Jones, R.P., D. Burgess, and M. Foster, (1990). Helicity as a tornado forecast parameter. *Preprints. 16th Conf. on Severe Local Storms*, 588-592

Davies, J. (1994). A look at hodographs, helicity and supercells. *Storm Track*, 1-5.

Doswell, C.A., Burgess, D.W., (1993). Tornadoes and Tornadic Storms: A Review of Conceptual Models. *NSSL*, 1-14.

Doswell, C.A. (2000). A Primer on Vorticity for Application in Supercells and Tornadoes. *Cooperative Institute for Mesoscale Meteorological Studies*, Norman, Oklahoma, 1-11.

Dunlop, S. (2003). The Weather Identification Handbook: The Ultimate Guide for Weather Watchers (1st ed.). *The Lyons Press,* 192 pages.

Esterheld, J.M., Giuliano, D.J. (2008). Discriminating between Tornadic and Non-Tornadic Supercells: A New Hodograph Technique. *EJSSM,* vol. 3, no 2.

Etkin, D.A., (1995). Beyond the Year 2000, More Tornadoes in Western Canada? Implications from the Historical Record. *Natural Hazards*, vol. 12, 19-27.

Evans, J.S., Doswell, C.A., (2002). Investigating Derecho and Supercell Proximity Soundings, *AMS*, 635-638.

Fabry, F. (2005). The spatial variability of moisture in the boundary layer and its effect on convection initiation: Project-long characterization. *AMS*. 79-91.

Forbes, G.S., Bluestein, H.B. (2001). Tornadoes, Tornadic Thunderstorms, and Photogrammetry : A Review of the Contributions by T.T. Fujita. *AMS*, vol. 82, 79-96.

Fujita, T.T., (1975). New evidence from the April 3-4, 1974 tornadoes, *AMS,* 248-255.

Grazulis, T.P. (2001). The Tornado: Nature's Ultimate Windstorm. *University of Oklahoma Press.* 324 pages.

Hanesiak, J.M., Melsness, M., Raddatz, R.L. (2009). Observed and Modeled Growing Season Diurnal Precipitable Water Vapor in South-Central Canada. *J. Atmos. Sci.,* 1-14.

Holton, J.R (2004). An introduction to dynamic meteorology. *Academic Press*, 535 pages.

Kellenbenz, D.J., Grafenauer, T.J. (2007). The North Dakota Tornadic Supercells of 18 July 2004: Issues Concerning High LCL Heights and Evapotranspiration. *AMS*, vol. 22, 1200-1213.

King, P. (1997). On the Absence of Population Bias in the Tornado Climatology of Southwestern Ontario. *Environment Canada,* vol. *12, 939-946.*

King, P., Leduc, M.J., Sills, D.M., Donaldson, N.R., Hudak, D.R., Joe, P., Murphy, B.P. (2003). Lake Breezes in Southern Ontario and Their Relation to Tornado Climatology. *MSC*, 795-807.

Klemp, J.B., Rotunno, R. (1983). A study of the tornadic region within a supercell thunderstorm. *J Atmos Sci*, vol. 40, 359-377.

Lemon, L.R. (1977). New severe thunderstorm radar identification techniques and warning criteria. *NOAA Tech*, 1-60.

Lemon, L. R., and C. A. Doswell. (1979). Severe thunderstorm evolution and mesocyclone structure as related to tornadogenesis. *Monthly Weather Review,* vol. 107, 1184-1197.

Markowski, P.M., Rasmussen, E.N., Straka, J.M. (1998). The Occurrence of Tornadoes in Supercells Interacting with Boundaries during VORTEX-95. *Weather and Forecasting*, vol. 13, 852-859.

Markowski, P.M. (2001). Hook Echoes and Rear-Flank Downdrafts: A Review. *J. Atmos. Sci.*, vol. 130, 852-874.

Markowski, P.M., Straka, J.M., Rasmussen, E.N. (2002). Direct Surface Thermodynamic Observations within the Rear-Flank Downdrafts of Nontornadic and Tornadic Supercells. *AMS*, vol. 130, 1692-1721.

Markowski, P.M., Hannon, C. (2006). Multiple-Doppler Radar Observations of the Evolution of Vorticity Extrema in a Convective Boundary Layer. *Monthly Weather Review,* vol. *134, 355-374*

Markowski, P.M., Richardson, Y., Rasmussen, E., Straka, J., Davies-Jones, R., Trapp, R.J. (2008). Vortex Lines within Low-Level Mesocyclones Obtained from Pseudo-Dual-Doppler Radar Observations. *J. Atmos. Sci*., vol. 136, 3513-3535.

Markowski, P.M., Richardson, Y. (2010). Mesoscale Meteorology in Midlatitudes. *John Wiley & Sons, Ltd*. West Sussex, UK.

Marshall, T.P., McDonald, J.R., Forbes, G.S. (2004). Then enhanced Fujita (EF) Scale. *AMS 22nd Conf. of Severe Storms*, 1-7.

McCarthy, P.J., Carlsen, D., Slipec, J. (2008). Elie, Manitoba, Canada, June 22, 2007: Canada's first F5 Tornado. *Environment Canada*, 1-7.

Miller, R.C., (1972). Notes on the Analysis and Severe-Storm Forecasting Procedures of the Air Force Global Weather Central. *Air Weather Service Tech*. Rept. 200,

Miller, D.J., (2006). Observations of Low Level Thermodynamic and Wind Shear Profiles on Significant Tornado Days, *NOAA*, 1-6.

Mitchell E.D., Vasiloff, S.V., Stumpf, G.J., Witt, A., Eilts, M.D., Johnson, J.T., Thomas, K.W. (1997). The National Severe Storms Laboratory Tornado Detection Algorithm. *Weather and Forecasting*, vol. 13, 352-366.

Mogil, H.M., Groper, H.S. (1977). NWS Severe Local Storm Warning and Disaster Preparedness Programs. *AMS,* vol. 58, 318-324.

Moller, A.R. (1978). The improved NWS storm spotter's training program. *NWS*, vol. 59, 1574-1582.

Patrick, D., McCarthy, P.J. (2008). Improved Thunderstorm Detection, Tracking and Assessment Products for Environment Canada Radars. *Environment Canada*, 1-10.

Potter, T., Colman, B.R. (2003). Handbook of Weather, Climate and Water. *John Wiley & Sons*

Raddatz, R.L., Hanesiak, J.M. (1991). Climatology of Tornado Days 1960-1989 for Manitoba and Saskatchewan. *Climat. Bull.*, 25, 47-59.

Raddatz, R.L. (1998). Anthropogenic vegetation transformation and the potential for deep convection on the Canadian prairies. *Canadian Journal of Soil Science,* vol. 78, 657-666.

Raddatz, R.L., Cummine, J.D. (2003). Inter-Annual Variability of Moisture Flux from the Prairie Agro-Ecosystem: Impact of Crop Phenology on the Seasonal Pattern of Tornado Days. *Boundary Layer Meteorology,* vol. 106, 283-295.

Rasmussen E.N., Blanchard, D.O. (1998). A Baseline Climatology of Sounding-Derived Supercell and Tornado Forecast Parameters. *Weather and Forecasting*, vol. 13, 1148-1164.

Rinehart, R.E., (1997). Radar for Meteorologists. Rinehart Publications. *University of North Dakota,* Chapter 9. 169-178.

Source: "Elie, Manitoba Map." Google Earth. September 8th, 2011.

Stull, R. (2000). Meteorology for Scientists and Engineers. *Brooks/Cole*, 502 pages.

Trapp, R.J., (1999). A Clarification of Vortex Breakdown and Tornadogenesis. .*NSSL: Monthly Weather Review*, vol. 128, 888-895

Trapp, R.J., Davies-Jones, R. (1997). Tornadogenesis with and without a Dynamic Pipe Effect. *J. Atmos. Sci.,* 113-133.

Vasquez, T. (2002). Weather forecasting handbook (5th ed.). *Weather graphics technologies*. Norman, Oklahoma

Wang, L., Geller, M. (2003). Morphology of gravity-wave energy as observed from 4 years (1998-2001) of high vertical resolution U.S. radiosonde data. *Journal of Geophysical Research*, vol. 108. 1-12.

Weckwerth, T.M., Parsons, D.B. (2005). A Review of Convection Initiation and Motivation for IHOP 2002. *AMS*, vol. 134. 5-22

Wilson, J.W., Roesli, H.P. (1985). Applications of Doppler Weather Radar. *Academic Press* vol. 9, 125-145.

Yang, W., Geerts, B. (2006). Horizontal Convective Rolls in Cold Air over Water: Buoyancy Characteristics of Coherent Plumes Detected by an Airborne Radar. *J. Atmos. Sci,* vol. 45, 1-24.